UNIVERSITÀ DEGLI STUDI DI PADOVA

UNIVERSITA' DEGLI STUDI DI PADOVA

Dipartimento di Ingegneria Industriale DII

Corso di laurea magistrale in Energy Engineering

Integration of a cold thermal energy storage for air conditioning demand in a CO_2 refrigeration system of a supermarket

Relatore: Prof.ssa Anna Stoppato

Correlatore: Prof. Armin Hafner

Studente: Davide Tommasini

Matricola: 2038170

Anno accademico 2022-23

Preface

This master's thesis was carried out in the Department of Energy and Process Engineering at the Norwegian University of Science and Technology (NTNU) in Trondheim, from February until July 2023, thanks to the Erasmus+ exchange program between the University of Padua and NTNU. This research project was conducted under the supervision of Prof. Armin Hafner and Prof. Anna Stoppato.

Readers are assumed to have a basic knowledge of thermodynamic and heat transfer to facilitate better comprehension of the topics covered and the results presented in this thesis.

Abstract

There is a significant transition in supermarket refrigeration, with a strong focus on reducing energy demand and installation costs. Generally, industry processes require cooling the most for short periods every day. The rest of the time, the cooling system runs at partial load with lower efficiency, but it is still designed for the highest capacity.

Applying cold thermal energy storage (CTES) technologies, which can deliver some of the cooling during peak times, will reduce peak load demand and will allow for load shifting to periods with low electricity cost, free cooling capacity from the rack or high electricity production from renewable energy sources (e.g. photovoltaic panels). This will also contribute to a more flexible power system, and allow for an increased proportion of power production with variable renewable energy sources. Additionally, these units can also lead to a significant downsizing of the compressor pack, reducing the cooling system capacity.

Currently, the air conditioning (AC) in REMA 1000 supermarkets, a leading supermarket chain in Norway, is supplied by a glycol circuit which is cooled by the CO_2 (R744) booster refrigeration system. The design capacity of the refrigeration unit must handle all the refrigeration loads and the AC load during the warmest summer day, which results in overcapacity and part load operation for most of the year.

This master's thesis describes and investigates a proposed design for the implementation of a CTES dedicated to AC demand in a supermarket located in the Oslo region. This system aims to substitute the existing glycol circuit towards the air handling unit (AHU). Simulation results demonstrate that CTES offers substantial potential for reducing electrical peak power consumption during the warmest periods. The functioning of the CTES and its impact on the existing refrigeration system were simulated, revealing a peak reduction of up to $32,33\%$. The load shifting capability is demonstrated, absorbing $31,53\%$ of the daily electricity consumption during the night, when the supermarket

is closed, compared to $16,14\%$ considering the instantaneous production of AC with the existing system. Consequently, electricity consumption can be increased by up to $74,8\%$ during the night and decreased by up to 28% during the day. Even though energy savings are not the primary objective of this project, they are achieved by producing and storing energy required for AC during periods when the outdoor temperature is lower, and the coefficient of performance (COP) of the system is higher. The energy savings can reach up to $11,8\%$ during the hottest day. Finally, the economic benefits of the system are assessed under spot pricing and tariff pricing systems, revealing potential electricity cost savings of up to $12,56\%$ and $16,45\%$, respectively.
The main big challenges of this system still remain its economical viability, in terms of payback time, and expanding its utilization during the winter period.

Riassunto

In questi anni, c'è una significativa transizione nella refrigerazione dei supermercati, incentrata principalmente sulla riduzione della domanda energetica e dei costi. Generalmente, i processi di refrigerazione richiedono la potenza massima per brevi periodi ogni giorno. Per il resto del tempo, l'impianto di refrigerazione funziona a carico parziale con una minore efficienza, ma è comunque progettato per fornire la richiesta di potenza massima.

L'utilizzo di sistemi di accumulo del freddo (cold thermal energy storage - CTES), che possono fornire parte del raffreddamento durante i periodi di picco, ridurrà la richiesta di carico di picco e consentirà di spostare il carico verso periodi con minori costi dell'elettricità, capacità di raffreddamento gratuita dai compressori o elevata produzione di elettricità da fonti di energia rinnovabile (ad esempio, pannelli fotovoltaici). Ciò contribuirà anche a rendere più flessibile il sistema elettrico e permetterà di aumentare la percentuale di produzione di energia elettrica da fonti rinnovabili non programmabili. Inoltre, queste unità possono portare anche a una significativa riduzione del gruppo compressori, riducendo la potenza del sistema di refrigerazione.

Attualmente, il condizionamento dell'aria nei supermercati REMA 1000, una delle principali catene di supermercati in Norvegia, è fornito dall'unità di trattamento aria tramite un circuito acqua-glicole raffreddato dal sistema di refrigerazione. L'impianto installato è un sistema booster a CO_2 (R744), ed è progettato per riuscire a fornire tutti i carichi di refrigerazione e aria condizionata durante il giorno più caldo dell'estate. Questo comporta un sovradimensionamento e un funzionamento a carico parziale per la maggior parte dell'anno.

Questa tesi magistrale descrive e indaga un design proposto per l'integrazione, tramite un circuito a CO_2, di un CTES dedicato alla domanda di aria condizionata (TES-AC) nel sistema di refrigerazione in un supermercato situato nella regione di Oslo. Questo sistema punta a sostituire il circuito acqua-glicole esistente verso l'unità di trattamento dell'aria (AHU).

Parte del progetto ha previsto anche di seguire la progettazione di un'installazione dimostrativa di questo sistema. Il supermercato scelto per l'installazione è dotato di congelatori plug-in, con conseguente bassa potenza frigorifera per il livello LT (bassa temperatura - congelatori), necessaria solo per la cella frigorifera principale, e un'elevata richiesta di aria condizionata, dovuta ai carichi interni di questi congelatori. La costruzione del sistema dimostrativo è prevista per il prossimo autunno a Orkidehøgda, Mjøndalen MØ, mentre i test sperimentali sono previsti per l'estate 2024.
Lo studio di simulazione è stato effettuato utilizzando il software Dymola 2022x1 (Dassault Systems, Vélizy-Villacoublay, France), sfruttando la libreria TIL 3.11.0 (TLK-Thermo GmbH, Braunschweig, Germany) per i componenti e le proprietà dei fluidi. Due modelli di simulazione dinamici sono stati sviluppati per il sistema TES-AC e per il sistema di refrigerazione.
I risultati dimostrano che il CTES offre un significativo potenziale per la riduzione del picco di assorbimento di energia elettrica durante i periodi più caldi. Il funzionamento del CTES e il suo impatto sul sistema di refrigerazione esistente sono stati simulati, rivelando una riduzione del picco fino al $32,33\%$. La capacità di spostamento del carico è dimostrata, assorbendo il $31,53\%$ del consumo giornaliero di energia durante la notte, quando il supermercato è chiuso, rispetto al $16,14\%$ considerando la produzione istantanea di aria condizionata con il sistema esistente. Di conseguenza, il consumo di energia può aumentare fino al $74,8\%$ durante la notte e diminuire fino al 28% durante il giorno.
Anche se il risparmio energetico non è l'obiettivo primario di questo progetto, esso è ottenuto producendo e accumulando l'energia necessaria per l'AC durante i periodi in cui la temperatura esterna è più bassa e, di conseguenza, il coefficiente di prestazione (COP) del sistema è più elevato. Il risparmio energetico può arrivare fino all' $11,8\%$ durante i giorni più caldi.
Infine, i vantaggi economici del sistema sono valutati considerando un sistema di tariffazione al prezzo di mercato e un sistema tariffario orario, rivelando potenziali risparmi sui costi dell'elettricità fino al $12,56\%$ e al $16,45\%$, rispettivamente.
Le principali sfide di questo sistema rimangono ancora la sua fattibilità economica, in termini di tempo di ritorno (payback time), e il prolungamento del suo utilizzo durante il periodo invernale.

Acknowledgments

I would like to start the acknowledgments from the people I met during my Erasmus period, ended in this thesis.

First, my gratitude goes to Armin for his invaluable guidance and continuous encouragement. His mentorship has been helpful in shaping this research. Thanks also to made me discovered how to prevent the chocolate melting. I will always remember his words "no stress guys, we are in Norway".

My appreciation goes also to Prof. Anna Stoppato for her support and for giving me the opportunity to live this unforgettable experience at NTNU.

I would also like to thank Engin and Mihir for their continued presence and suggestions, and for all the coffees and lunches at the 6^{th} floor canteen.

I express my heartfelt gratitude to the "Tribù" consisting of Daniele, Davide, Giovanna, Pietro, and Riccardo, for all the cabin trips and adventures in Norway. A special thanks goes to Davide for being with me in this incredible experience and making it truly exceptional. Without him, this experience would not have been the same. Additionally, I would love to thank each of them for the trip to the Ålesund/Geirangerfjord region.

Thanks Camillo for the adventures in July and for all the rain he brought during our tent trip to the Bergen/Stavanger region.

Moreover, I am thankful to Mattia for the countless table soccer matches and conversations at Loftet.

My sincere appreciation goes to all my flatmates at Moholt Allmenning 2 - floor 9. Special greetings to Pauline and Lara for the memorable "girls night", and to Matteo and Giacomo for making me feel in Italy even in Norway.

Furthermore, I would like to thank my family for their unwavering support in every choice I've made.

A heartfelt thank you to Valentina for understanding me and for being there in every moment. I would also love to thank her for coming to Lofoten in June.

I extend my gratitude to Diego for all the time that we spent together during our teenage.

Finally, many thanks to Enrico, Jacopo, Matteo, Paolo, Riccardo, Samuele, Stefano, and especially Giacomo and Nicolò, who have been studying with me since our high school. They all made my days at the university much more enjoyable.
In conclusion, the completion of this master's degree would not have been possible without the support of all those mentioned above. Thank you for being part of this journey. I dedicate this thesis to all of them.
Tusen takk! - Grazie mille!

Contents

List of Figures

List of Tables

Nomenclature

c_p	specific heat capacity
f	correction factor
h	enthalpy
m	mass
$\dot{m}$	mass flow rate
P	power, capacity
p	pressure
Q	thermal energy
$\dot{Q}$	heat flow rate
T	temperature
TC	transcritical correlation factor
V	volume
$\dot{V}$	volume flow rate, displacement
W	work energy

Subscripts

AC	air conditioning
amb	outdoor ambient
Ca	Carnot
C	cold, cooling
$cond$	condensation
$disch$	discharge
el	electrical
$evap$	evaporation
fus	fusion
H	hot, heating
in	inlet
is	isentropic
nom	nominal

out	outlet
PCM	phase change material
ref	refrigerant
$subcr$	subcritical
$suct$	suction
th	theoretical
$transcr$	transcritical
vol	volumetric

Abbreviations

AC	air conditioning
AHU	air handling unit
CFC	chlorofluorocarbon
CO_2	carbon dioxide, R744
COP	coefficient of performance
CTES	cold thermal energy storage
DHW	domestic hot water
EJ	ejector
FGBV	flash gas by-pass valve
GC	gas cooler
GWP	global warming potential
HC	hydrocarbon
HCFC	hydrochlorofluorocarbon
HFC	hydrofluorocarbon
HFO	hydrofluroolefin
HP	high pressure
HPV	high pressure valve
HTC	heat transfer coefficient
HX	heat exchanger
HVAC&R	heating, ventilation, air conditioning, and refrigeration
IHX	internal heat exchanger
LHS	latent heat thermal energy storage
LR	liquid receiver
LT	low temperature
MEG	mono-ethylene glycol
MT	medium temperature
NTNU	Norwegian University of Science and Technology

ODP	ozone depletion potential
P&ID	piping and instrumentation diagram
PCM	phase change material
PP	pillow plate
SHS	sensible heat thermal energy storage
TES	thermal energy storage
TES-AC	thermal energy storage for air conditioning

Introduction

This chapter starts with the motivation for this research on the implementation of cold thermal energy storage (CTES) dedicated to the AC demand in a R744 booster refrigeration system of a supermarket. The chapter subsequently outlines the objectives of the master's thesis project and concludes by providing an overview of its structure.

1.1 Motivation

According to the International Energy Agency, the need for cooling will increase significantly over the coming decades [1]. Generally, industry processes require cooling the most for short periods every day. The rest of the time, the cooling system runs at partial load with lower efficiency, but it is still designed for the highest capacity. Applying cold thermal energy storage (CTES) technologies, which can deliver some of the cooling during peak times, will enable to reduce the cooling system capacity, thereby reducing the total energy consumption and associated costs. Furthermore, this will also contribute to a more flexible power system, and allow for an increased proportion of power production with variable renewable energy sources.

On the other hand, climate change and the increasing effect of greenhouse gases have encouraged the research and the industry to go towards natural refrigerants such as R744 (CO_2) as an alternative to the traditional refrigerants widely used in the past, such as chlorofluorocarbons (CFC) and hydrochlorofluorocarbons (HCFC). The ozone-depleting problem together with the greenhouse gases effects brought a new transition in the last 20 years where natural refrigerants play an important role.

Natural refrigerants, like CO_2, are gaining popularity due to their lower global warming potential and ozone depletion potential compared to synthetic refrigerants. Developing more efficient CO_2 systems promotes the widespread

adoption of these units, contributing to mitigating climate change and playing a pivotal role in achieving a greener and more sustainable future.

Currently, CO_2 is regarded as one of the most promising options for supermarket refrigeration, as it has the potential to significantly reduce the environmental impact of this sector. In particular, CO_2 transcritical refrigeration systems have demonstrated reliability and good performance in Northern Europe. However, developing cost and energy-efficient units that can operate effectively in warmer climatic conditions remains a notable challenge.

New technologies and improvements have been developed to enhance the system efficiency, for instance with the use of multi-ejectors, overfed evaporators, parallel compression, pivoting compressor arrangements [2], and the implementation of local CTES. Multi-ejector expansion modules, intended as a substitute for standard high-pressure control valves (HPV), were designed by SINTEF/NTNU/Danfoss and experimentally investigated at the SuperSmart-Rack test facility (Varmeteknisk laboratory EPT/NTNU, Trondheim) [3]. Presently, there is a trend towards integrating heating, ventilation, and air conditioning (HVAC) functions within CO_2 refrigeration systems, referred to as "integrated CO_2 refrigeration systems". The implementation of a multi-ejector block for air conditioning (AC) production has also been tested in the past at NTNU's laboratory, showing its potential for reducing the power consumption of integrated CO_2 refrigeration systems [4]. The "ejector for the world" concept further simplifies ejector supported system architectures and complements these advances, making the solutions cost-effective [5]. It is based on active and passive utilization of the ejector and requires only two compressor stages for the entire supermarket to meet the requirements in the different seasons.

Furthermore, the implementation of CTES in combination with the R744 refrigeration system can have economic benefits which enables an implementation in the market, as CTES devices reduce the peak load demand and allow for load shifting to periods with low electricity cost, high electricity production from renewable energy sources (e.g. photovoltaic panels) or free cooling capacity from the rack. These units can also lead to a radical downsizing of the compressor packs and make it possible to remove the frequency controlling device of the MT compressors. The first approach to thermosyphon-driven versus pump circulation in CTES has been experimentally investigated at NTNU's laboratory [6], but the concept needs to be refined and deeply investigated related to the impact on the total system architecture and costs.

Currently, the air conditioning (AC) in REMA 1000 supermarkets, a leading

supermarket chain in Norway, is supplied by a glycol circuit which is cooled by the CO_2 refrigeration system with booster layout. The design capacity of the refrigeration system must handle all the refrigeration loads (chilling and freezing) and the AC load during the warmest summer day, which results in overcapacity and part load operation for most of the year. An integration, within the refrigeration system, of a CO_2 circuit coupled with a CTES dedicated to meet the AC demand, is proposed for a demonstration supermarket in the Oslo region.
The demo system is slated for construction in the upcoming autumn at Orkidehøgda, Mjøndalen MØ, with testing scheduled for the summer of 2024.

1.2 Objective

The primary objective of this master's thesis is to explore the feasibility and benefits of implementing a CTES system dedicated to meeting the air conditioning (AC) demand of a supermarket located in the Oslo region. The investigation will focus on the operation of the proposed CTES implementation. Its impact on the existing refrigeration system within the supermarket will be analyzed, assessing the potential reduction in peak electrical power consumption during warmer periods. Moreover, the thesis will investigate the CTES capability for load shifting, aiming to absorb a substantial portion of the daily electricity consumption during off-peak hours, especially when the supermarket is closed. Finally, an essential aspect of the research involves conducting an economic analysis to determine the potential cost savings in electricity consumption achievable through the adoption of the CTES system.

1.3 Structure of the thesis

This thesis is organized as follows:

1. Introduction: provides an introduction to the research background motivation, objectives, scope, and limitations.
2. Literature review and theory: provides a research background on CTES technology, R744 refrigeration systems, and their integration in supermarket applications.
3. Method: presents the methodology adopted for simulating the CTES system and evaluating its performance and economic benefits.

4. Results: presents the simulation results and briefly discusses them.
5. Discussion: draws conclusions regarding the effectiveness of the proposed implementation of CTES within supermarket CO_2 booster refrigeration system.
6. Conclusions: summarizes the key outcomes of this thesis, along with recommendations for future work.
7. Appendix: provides additional results and supporting information related to the simulation models.

Overall, this thesis aims to contribute valuable insights into the integration of CTES within R744 refrigeration systems in supermarkets and demonstrate its potential economic benefits.

Literature review and theory

This chapter gives a theoretical background and a view regarding the actual state-of-art. The focus is on the CO_2 industrial refrigeration systems and on the cold thermal energy storages (CTES) with phase change materials (PCM).

2.1 Refrigeration

2.1.1 Vapour compression cycles

The goal of a refrigeration cycle is to transfer heat from a source at low temperature (cold heat source) to a sink at high temperature (hot heat sink). This process requires energy in the form of mechanical work to run the compressor that drives the cycle as shown in Figure 2.1.

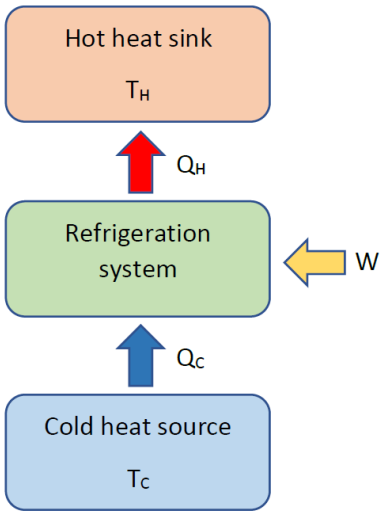

Figure 2.1: Illustration of a refrigeration system working between two temperature levels

Its theoretical efficiency for the cooling production is expressed by the Carnot Coefficient of Performance (COP_{Ca}) with the Equation[1] 2.1.

[1] In the Equation 2.1 the temperatures are expressed in Kelvin

$$COP_{Ca} = \frac{T_C}{T_H - T_C} \tag{2.1}$$

The simplest refrigeration system configuration is made of 4 components: a compressor, a condenser, an expansion device and an evaporator. This system is illustrated in Figure 2.2 and its cycle is represented in the p-h diagram as shown in Figure 2.3. The theoretical thermodynamic transformations of a refrigerant cycle are the following: an isentropic compression, an isobaric condensation, an isenthalpic expansion and an isobaric evaporation. The refrigerant saturated vapour (point 1) is compressed to superheated vapour (point 2) by the compressor that uses electricity to run the motor. In the condenser, the vapour rejects heat to the hot heat sink condensing to saturated liquid (point 3). Then it is throttled by the expansion device decreasing its pressure and becoming a liquid-vapour mixture (point 4). In the evaporator, the refrigerant mixture absorbs heat from the cold heat source evaporating to saturated vapour (point 1). The cycle is finally closed returning to point 1.

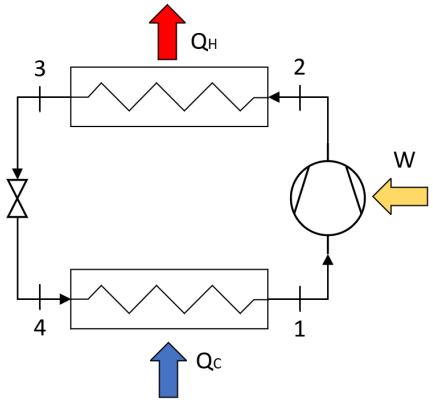

Figure 2.2: Illustration of a simple refrigeration system

In a real cycle, pressure losses in the pipes, in the condenser and in the evaporator are present. There are also compression losses leading a non-isentropic compression. This increases the compressor work and decreases the COP of the cycle. The real performances of the refrigeration system are expressed as the heat produced (extracted form the cold source) divided by the electrical consumption of the compressors, as in Equation 2.2.

$$COP = \frac{Q_C}{W_{el}} \tag{2.2}$$

The efficiency can be written as the real performance divided the Carnot performance, which is the maximum achievable, as in Equation 2.3.

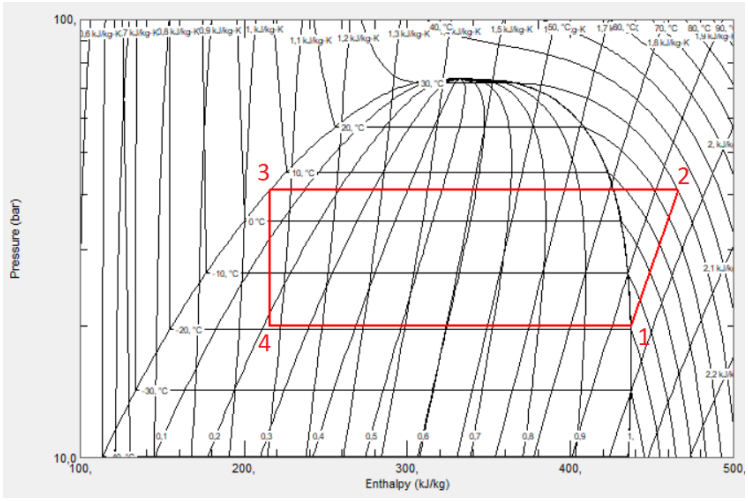

Figure 2.3: Refrigeration cycle on the logarithmic pressure-enthalpy diagram for CO_2 related to the system in Figure 2.2. Plotted using REFPROP

$$\eta = \frac{COP}{COP_{Ca}} \tag{2.3}$$

When the cycle is transcritical it is not possible to define a unique temperature for hot side since during condensation there is a temperature variation as explained in Section 2.1.4. In this case the Carnot's COP ($\mathrm{COP_{Ca}}$) has no more sense, instead the Lorenz's COP ($\mathrm{COP_{Lorenz}}$) has to be used, which considers the mean logarithmic temperature as shown in Equations [2] 2.4, 2.5, 2.6, 2.7.

$$COP_{Lorenz} = \frac{\overline{T}_C}{\overline{T}_H - \overline{T}_C} \tag{2.4}$$

$$\overline{T}_H = \frac{T_{H,in} - T_{H,out}}{\ln\left(\frac{T_{H,in}}{T_{H,out}}\right)} \tag{2.5}$$

$$\overline{T}_C = \frac{T_{C,in} - T_{C,out}}{\ln\left(\frac{T_{C,in}}{T_{C,out}}\right)} \tag{2.6}$$

$$\eta = \frac{COP}{COP_{Lorenz}} \tag{2.7}$$

2.1.2 History of refrigerants

In 1803 Thomas Moore received the first US patent for refrigerator. In 1805 Oliver Evans proposed a closed cycle vapor compression refrigeration system in "The Young Steam Engineer's Guide" [7]. In the following years a lot of inventions and improvements were made in the refrigeration sector.

[2] In the Equations 2.5, 2.6 the temperatures are expressed in Kelvin

In the time period between 1830 and 1930, when the refrigeration system was evolving, ammonia (NH_3, R717), carbon dioxide (CO_2, R744), sulphur dioxide (SO_2, R764), diethyl ether ($C_4H_{10}O$, R610), hydrocarbons (HC) and air were used as refrigerants [8]. These were classified as first generation refrigerants. Unfortunately they had high flammability, toxicity and reactivity, except for CO_2.

In 1928, chlorofluorocarbon refrigerants (CFC) were first synthesized by General Motors Research Lab [7]. A second generation of refrigerants, comprised of chlorofluorocarbons (CFC) and hydrochlorofluorocarbons (HCFC), was developed in the following years. The focus of these refrigerants was on reduced toxicity and flammability.

In 1987, with the Montreal Protocol, these refrigerants were began to phaseout due to their high ozone depletion potential (ODP): it was discovered that they were damaging the ozone layer into the atmosphere. CFCs were phaseout to the end of 1995, instead HCFCs has to be phased out in steps by 2030. A third generation of refrigerants consists of hydrofluorocarbons (HFC) and HCFCs, but they have an high GWP (global warming potential).

In 1997 with the Kyoto Protocol, the problem of the global warming, due to the greenhouse gasses emissions, was highlighted. In 2014 European Commission has introduced the F-gas Regulation to control emissions from fluorinated greenhouse gases [9].

Nowadays we are moving towards the fourth generation of refrigerants focused on zero ODP and low GWP. Hydrofluroolefins (HFO) are part of this generation with two types of refrigerants: R1234yf and R1234ze [9]. Atmospheric oxidation of R1234yf gives TFA (trifluoroacetic acid), a very persistent pollutant which effect is being studied, and PFAS (polyfluoroalkyl substances) [10].

Natural refrigerants have begun to be revive nowadays and a lot of technologies are being developed. In the early 1990s professor Gustav Lorentez at NTNU proposed to re-use CO_2 as a refrigerant [11]. Since then, a lot of efforts and researches on natural refrigerants have been carried out. In 2001 the first transcritical CO_2 domestic heat pump, called EcoCute, was marketed in Japan in 2001. At the beginning of the 2000s, the first transcritical system was installed in a supermarket, marking the rise of their popularity in Northern Europe. Starting from around 2008, the introduction of parallel compression and subsequently ejectors led to a much higher adaptability of transcritical CO_2 in warmer regions. In 2020 there were more than 35500 installations

globally, 29000 of which only in Europe, with an 74% increase between 2018 and 2020 [12].

2.1.3 R744 properties

The main properties of the CO_2 as a refrigerant (R744) are [13]:

- low critical temperature: $31,1°C$
- higher pressures than other refrigerants at similar temperatures
- triple point above atmospheric pressure: $5,18$ *bar*
- good heat transfer properties
- high thermal expansion coefficient in the liquid phase
- ODP=0
- GWP=1
- safety class A1: low flammability and low toxicity

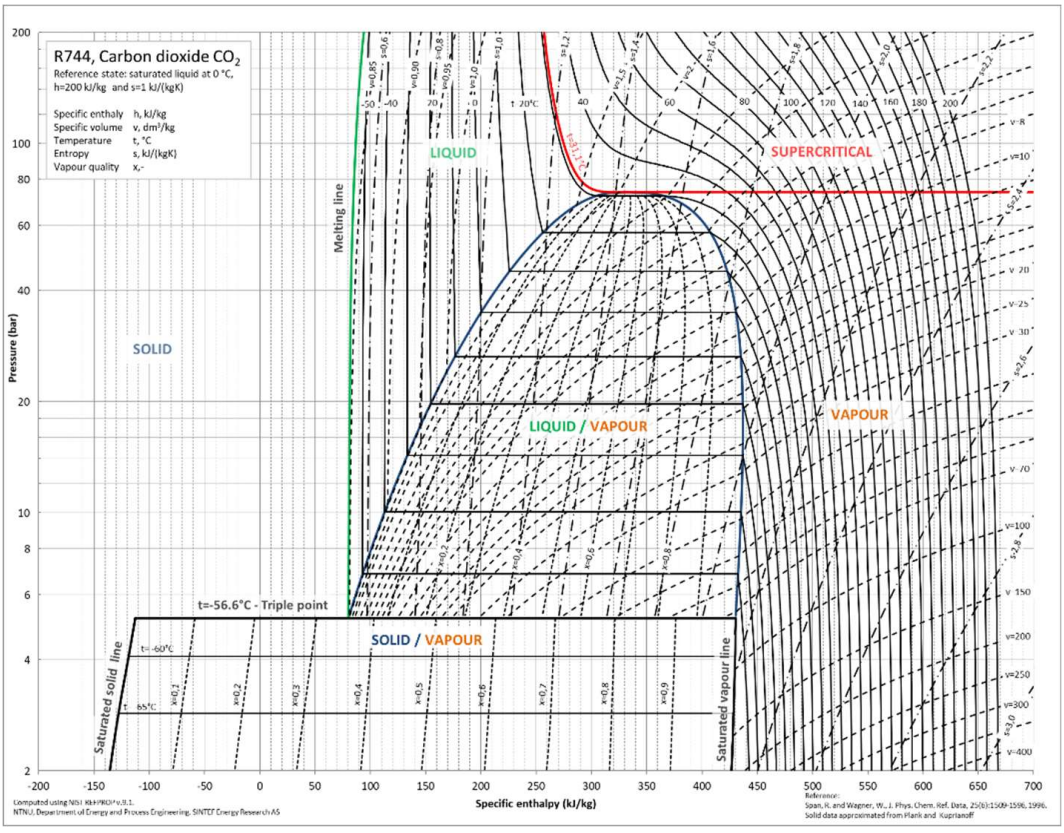

Figure 2.4: Logarithmic pressure-enthalpy diagram for CO_2 including phase regions [13]

R744 is a natural refrigerant that does not have ozone-depleting characteristics and therefore has an ODP equal to 0. It is used as a reference when determining the GWP of other gases. Hence, CO_2 has a GWP of 1.

It has a critical temperature of $31,1°C$ and a critical pressure of $73,8\ bar$, and above this point,in the transcritical region, only the gas phase exists.
The triple point ($-56,6°C$; $5,18\ bar$) is above atmospheric pressure and this means that in case of leakages or if a safety valve is opened, CO_2 expands rapidly forming dry ice (solid CO_2), attention has to be paid during installation and maintenance.
The components of the system must standstill a higher pressure compared to other refrigerants. Saturation pressures for different refrigerants are compared in Table 2.1. CO_2 has also a higher density with respect to other fluids, as shown in Figure 2.5. Due to the high pressure and high density, the pipes have to be smaller and thicker.

		$p_{sat}\ [bar]$						
		R744 (CO_2)	R717 (ammonia)	R290 (propane)	R410A	R32	R134a	R1234yf
$T_{sat}\ [°C]$	30	72,14	11,67	10,79	18,89	19,28	7,70	7,84
	0	34,85	4,29	4,75	8,01	8,13	2,93	3,16
	-10	26,49	2,91	3,45	5,75	5,83	2,01	2,22
	-30	14,28	1,19	1,68	2,70	2,73	0,84	0,99

Table 2.1: Saturation pressures of different refrigerants. Data obtained from REFPROP

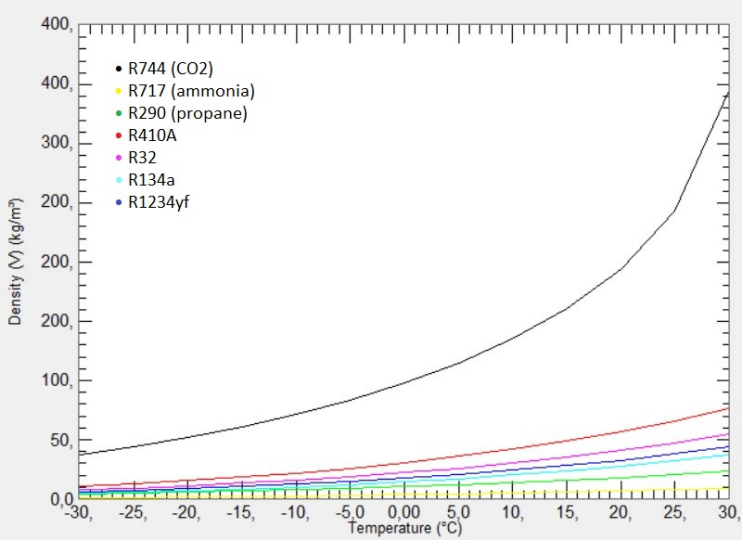

Figure 2.5: Saturated vapor density of different refrigerants vs saturation temperature. Plotted using REFPROP

The compressor requires a lower swept volume, thanks to the high density, thus it is smaller. The pressure ratio in the circuit is much lower than compared to other refrigerants. This contributes significantly to a higher efficiency of the compressor.

The temperature loss resultant from a pressure loss, always present inside the circuit especially in the gas cooler/condenser and in the evaporator, is much lower than other refrigerants. The heat exchangers can be designed for large flow velocities, leading to a more effective heat transfer.
Liquid CO_2 has a quite good thermal conductivity, low viscosity and a high specific heat capacity. These properties are favourable for convective heat transfer and the low viscosity minimises friction pressure losses. Liquid CO_2 has a large volume expansion, so it is necessary to check if there is enough space in all the components containing liquid to allow the expansion when the highest operational temperature is reached.
The specific heat capacity varies with the temperatures and with the pressure. Approaching the critical point the c_p increases rapidly as shown in Figure 2.6. Another challenge is the use of organic sealing materials because CO_2 at high pressure can diffuse into them and can cause swelling [13], [14].

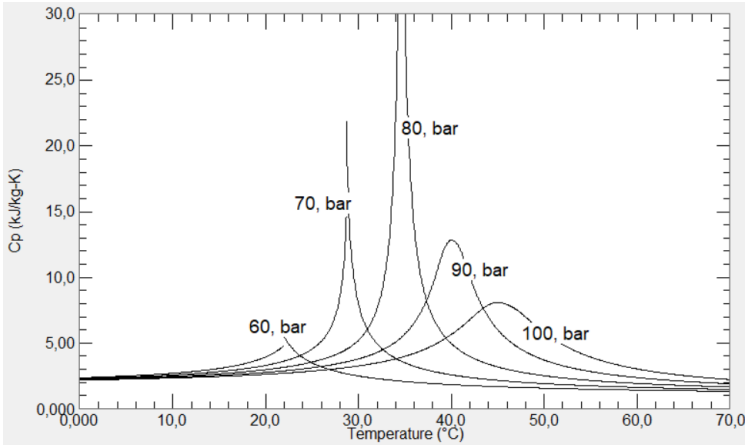

Figure 2.6: Specific heat capacity (c_p) vs temperature at various pressures for CO_2. Plotted using REFPROP

2.1.4 Industrial refrigeration systems

Industrial refrigeration systems refer to large-scale refrigeration systems with high capacities and CO_2 has become very popular in this systems.
CO_2 is used in practice in three different refrigeration cycles [14]:

- Subcritical (cascade systems)
- Transcritical (CO_2 - only systems)
- Secondary fluid (CO_2 used as a volatile brine)

There are a several applications where CO_2 is attractive and already widely used today:

- Industrial refrigeration. CO_2 is generally used in combination with ammonia, either in cascade systems or as a volatile brine
- Food/retail refrigeration
- Heat pumps
- Transport refrigeration

CO_2 systems can also be extended to cover heat recovery. In many cases the extra investment for gaining the waste heat is negligible and several cases have demonstrated that.

R744 is often coupled with ammonia in cascade systems where the CO_2 works in a subcritical cycle producing the lower temperature level. This is done to avoid the problems related with ammonia at very low temperatures: for evaporation temperatures below $-33,5°C$, the pressure of ammonia is below 1 bar. The vapour density decreases rapidly, and the volume of refrigerant to be compressed by the compressor increases, resulting in a lower efficiency.

In systems using only CO_2, there are some differences compared to normal ones. Due to such a low critical temperature, CO_2 systems normally operates in transcritical conditions, where only gas phase exists. There is not condensation at constant temperature anymore, instead there is a temperature variation along the gas cooler as shown is Figure 2.7. This make it possible to use the heat more effectively, for instance to heat water from $10°C$ to relatively high temperatures (maximum $90°C$) [13].

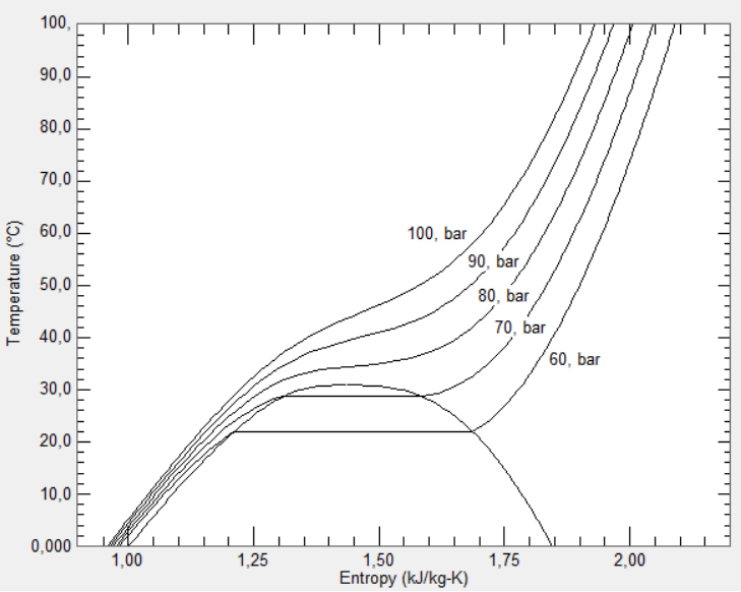

Figure 2.7: Temperature variation on the T-s diagram at various pressures for CO_2. Plotted using REFPROP

If the user demands heating at different temperature levels, for instance by a combination of space heating and domestic hot water production, the gas cooler can be split into different heat exchangers to achieve a more effective heat recovery. An example of gas cooler heat reclaim for the production of DHW and space heating is shown in Figure 2.8 [15].
Due to the change in the specific heat capacity in the transcritical region, the gas cooler (GC) must be divided into several elements to allow a precise calculation.

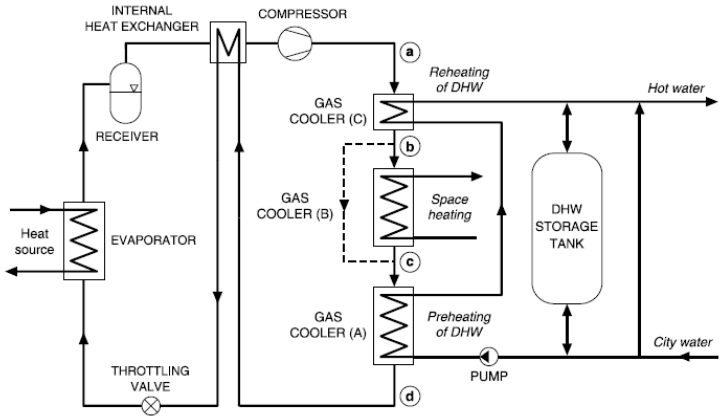

(a) Refrigeration system with heat recovery at the gas cooler

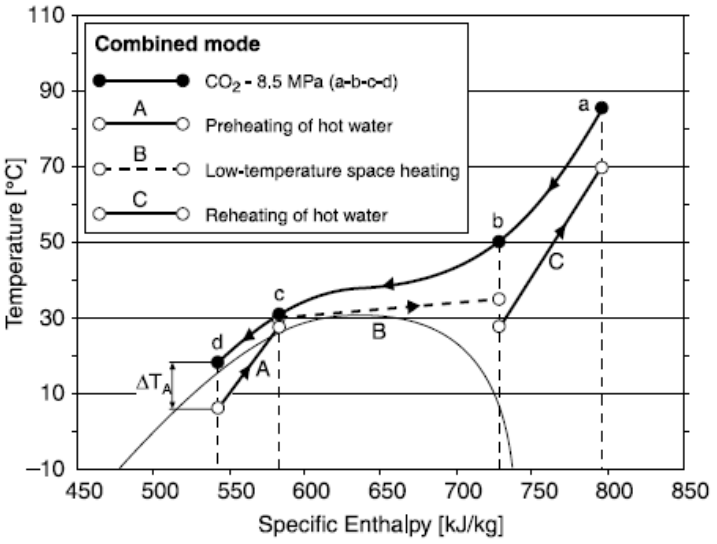

(b) Tripartite gas cooler with heat rejection

Figure 2.8: Illustration of a tripartite gas cooler with heat reclaim at three temperature levels [15]

In the transcritical region, in addiction to the pressure, the outlet temperature of the GC has to be fixed to define the refrigeration cycle. These two parameters affect in a significant way the performances of the overall system. When the gas cooler outlet temperature is fixed, the cooling capacity increases

significantly with the pressure in the area above the critical point, as shown in Figure 2.9. Transcritical cycles have a slightly higher cooling capacity than subcritical cycles with the same temperature before the throttling expansion. Therefore, if the gas cooler outlet temperature is above the critical temperature, the cooling capacity drops rapidly and this can be partially compensated by increasing the pressure.

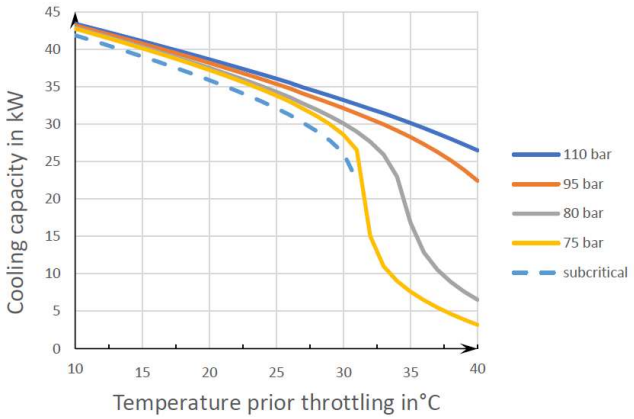

Figure 2.9: Cooling capacity per 10 m^3/h suction volume flow rate dependent on temperature prior to throttling. Evaporating temperature of $-10°C$ [13]

When the gas cooler pressure is fixed, the theoretical COP of the cycle (COP_{th}) increases as the gas cooler outlet temperature decreases as shown in Figure 2.10. In the same figure it is possible to see that, for a fixed gas cooler outlet temperature, the COP_{th} has a maximum depending on the gas cooler pressure. For higher GC outlet temperatures, the maximum COP_{th} is achieved at higher pressure.

For all this reasons, a smart choice of these two parameters is required to achieve a good performing system.

Supermarket refrigeration has been the major application for transcritical CO_2 systems. Due to the necessity of providing cooling at two temperature levels, one for the fridges and one for the freezers, the standard solution has become the booster system. The booster systems are able to provide both medium-temperature (MT) and low-temperature (LT) cooling with the same refrigeration circuit as shown in Figure 2.11. They are usually built with heat recovery at the gas cooler useful for DHW production or for space heating.

To improve the efficiency of the CO_2 refrigeration systems, particularly in warmer climates, alternative solutions have been developed: parallel compressors, overfed or non-superheated evaporators, internal heat exchangers and ejectors.

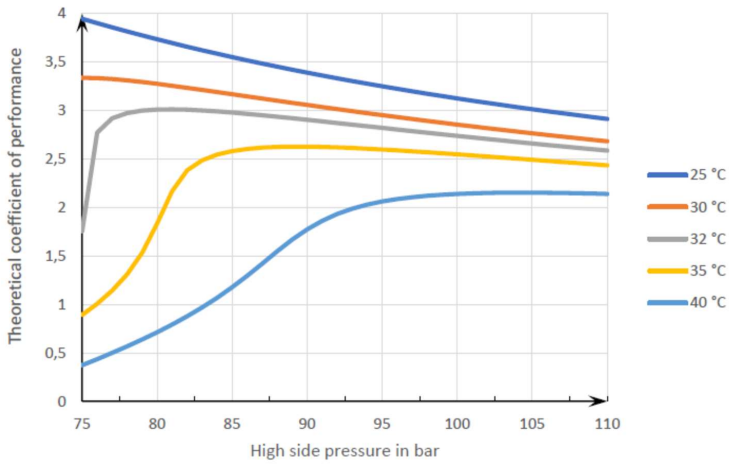

Figure 2.10: Theoretical COP vs gas cooler pressure varying gas cooler outlet temperature. Evaporating temperature of $-10°C$ [13]

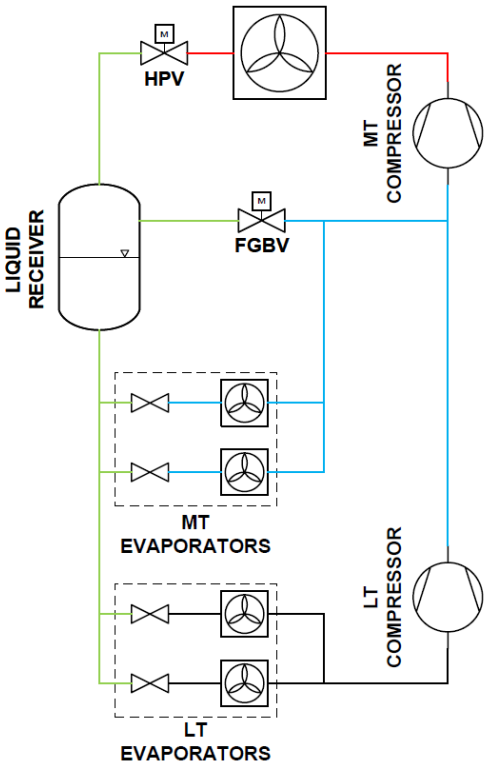

Figure 2.11: Simplified P&ID of a booster system for industrial refrigeration

2.1.4.1 Parallel compressors

In a system with parallel compression, an auxiliary compressor is used to compress the refrigerant vapour that is separated at the liquid receiver. In this way the vapour is not expanded to the MT pressure before recompressing it to the GC pressure, as is typically done in traditional booster systems. Instead, the vapour is compressed directly to the GC pressure as illustrated in Figure 2.12. This reduces the overall work done by the MT compressors, leading to an increase in the COP of the system.

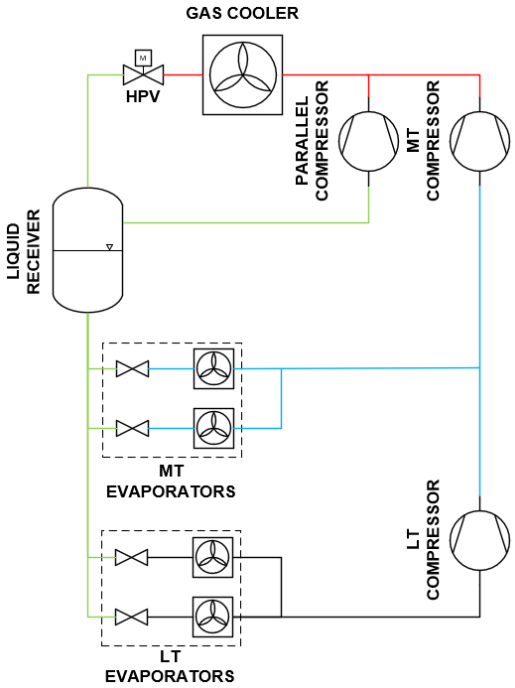

Figure 2.12: Simplified P&ID of a booster system with parallel compressor for industrial refrigeration

2.1.4.2 Overfed evaporators

Overfed evaporators allow to have vapor quality lower than 1 at their exit. In this way the evaporation temperature can be increased compared to a superheated evaporator. Energy savings around 3% per 1 K evaporation temperature increase can be achieved in any location [16]. Azzolin et al. (2021) [17] demonstrated that overfeeding the evaporators in warm climates can improve the performance of the system with an increase in the average COP by 13%, compared to the use of dry evaporators. Recently Pardiñas et al. (2023) [18] proposed and tested a novel two-stage brazed plate evaporator for its use in R744 heat pumps with greywater as a heat source. It splits the evaporation in two levels: one is gravity driven and it is at the same pressure of the liquid

receiver, and the other one is ejector-driven. The researchers shown that splitting the evaporation process in two stages with an ejector allows reducing the evaporation pressure while the compressor suction pressure can be increased. Heat pump COP was 10% higher compared to the same system using a one-stage evaporator.

2.1.4.3 Subcooling methods

Subcooling of CO_2 after the gas cooler can enhance the performance of the system as well as the cooling capacity. The overall performance can be improved up to 12% with internal heat exchangers, 22% with economizers, $25,6\%$ with thermoelectric systems and $30,3\%$ with dedicated mechanical subcooling methods based on the use of an additional vapour compression system with another refrigerant [19]. Internal heat exchangers are mainly used due to their simplicity.

2.1.4.4 Ejectors

An alternative approach to increase the energy efficiency of CO_2 refrigeration systems is the use of ejectors, substituting the high-pressure control valve, after the GC. It can recover part of the expansion work to pre-compress vapour at lower pressure and thereby reduce the work of compression by elevating the suction pressure level. This reduces the work required by the MT compressor, resulting in a decrease in the overall compression work and an increase in the COP of the refrigeration system. An ejector-supported booster system is shown in Figure 2.13.

A fixed geometry ejector is able to work with a good efficiency only in design conditions. To find a solution to this problem two technologies have been developed: variable geometry ejector and multi-ejectors. These two solutions are able to work with a good efficiency even when the pressures are not the ones of the design conditions and can improve significantly the COP of the refrigeration system.

The first one is an ejector equipped with a conical needle that adjust the throat area depending on the working pressures. In most cases, according to a study by Smolka et al. (2016) [20],its efficiency is 25% higher than fixed-geometry ejector when the motive nozzle throat was reduced by approximately 35%, after which the efficiency gradually decreases.

The second one is a module made of more fixed ejectors installed in parallel in the same pack. Hafner et al. (2014) [21] investigated the benefits of a

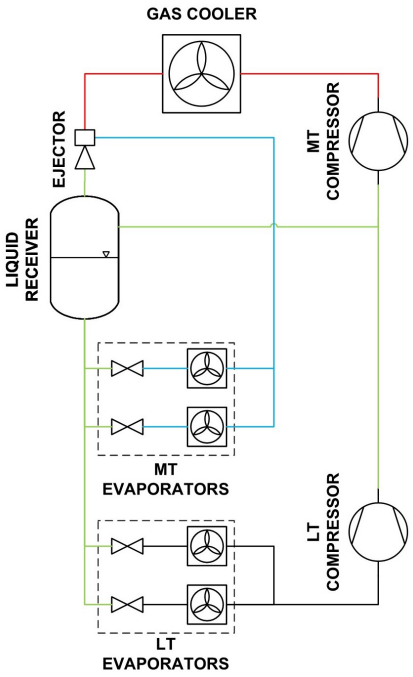

Figure 2.13: Simplified P&ID of a booster system with the MT evaporators driven by an ejector for industrial refrigeration

multi-ejector pack on a R744 supermarket system layout with heat recovery for different climate conditions. Compared to the investigated reference system an COP increase between 10% at $15°C$ and 20% at $45°C$ ambient temperature can be determined. Typical COP increase during the cooling mode of 17% in Athens, 16% in Frankfurt and 5% in Trondheim can be achieved during the summer. In the winter the typical COP increase is between 20% and 30%. Söylemez et al. (2022) [22] recently carried out a performance analysis of an integrated CO_2 refrigeration system with multi-ejectors installed in a supermarket in Portugal. The study aimed to evaluate the energy savings and cooling capacity improvements achieved by incorporating multi-ejectors into the refrigeration system. The researchers found that the total energy saving of the multi-ejector system varied from $7,5\%$ up to 11% compared to a parallel compression system, depending on the outdoor temperatures. This highlights the significant potential of multi-ejector systems in reducing energy consumption and improving the overall efficiency of the refrigeration system. Furthermore, the study showed that the multi-ejectors were capable of enhancing the cooling capacity of the MT stage of the system by $17,4\%$.
Pardiñas et al. (2021) [23] studied an integrated CO_2 refrigeration system able to deliver the entire HVAC&R demand for a supermarket in Porto de Mos, Portugal. A dynamic system model was developed in Modelica and validated against measurement data from the site. By incorporating flooded evaporation

with multi-ejectors and smart regulation of the receiver pressure, the overall efficiency increases of 15%, compared to a system using a high-pressure valve. Recently Pardiñas et al. (2023) [16] suggested an adaptation of an ejector-supported booster system based on: MT and LT compressor suction groups, overfed MT evaporation with increased evaporation temperature, and ejector. The novel configuration proposed in this study outperformed a conventional booster system at all ambient conditions, with enhancements of the COP between 5% and 42% when the gas cooler outlet temperature is $10°C$ and $40°C$ respectively.

2.2 Cold thermal energy storage

TES can be classified based on the mechanism used to store and release the energy. TES technology is divided into three classes: sensible (SHS), latent (LHS) and thermochemical. SHS stores heat by changing the temperature of the material without change of phase. The amount of energy stored depends on the mass m, the specific heat capacity c_p and the temperature difference between the initial temperature T_i and final temperature T_f according to the Equation 2.8.

$$Q_{sens} = \int_{T_i}^{T_f} m \cdot c_p \, dT \tag{2.8}$$

The temperature difference in many SHS is limited by the constrain of the phase change temperature, such as in cold water storage for cooling in AC applications. A common application of SHS is a hot water tank for HVAC systems commonly coupled with a heat pump.

The LHS method involves storing thermal energy in the phase transition of the storage material, typically the transition between solid and liquid (i.e., melting and solidification). This approach offers a significant advantage since the phase transition occurs at a constant temperature, allowing for the storage of large amounts of thermal energy within a narrow temperature range. The amount of thermal energy that can be stored in LHS systems depends on two factors: the mass of the storage material (m) and the latent heat of fusion ($\Delta h_f us$). The relationship between these variables can be expressed using the Equation 2.9.

$$Q_{lat} = m \cdot \Delta h_{fus} \tag{2.9}$$

Due to the huge volumetric expansion of the material during liquid-gas phase change, most LHS are design to utilise the solid-liquid phase change. The storage materials used in solid-liquid latent TES systems are often called phase change materials (PCM) due to their tailored application of storing thermal energy. The most common PCM utilised in refrigeration systems is water/ice for storing thermal energy at $0°C$. Its Δh_{fus} is 80 times greater than the c_p of liquid water. This means that the energy released by melting one kg of ice corresponds to a temperature increase of $80°C$ of one kg of water. For this reason, the LHS systems are generally more compact compared to SHS systems. However, other PCMs are available for both higher temperatures and sub-zero applications.

In LHS there is often a combination of latent and sensible heat: the initial tem-

perature is lower than its phase-change temperature and the final temperature is higher than it. Hence, the total energy stored by the TES is a combination of Equations 2.8 and 2.9 resulting in Equation 2.10.

$$Q_{TES} = \int_{T_i}^{T_{fus}} m \cdot c_p \, dT + m \cdot \Delta h_{fus} + \int_{T_{fus}}^{T_f} m \cdot c_p \, dT \tag{2.10}$$

Today, there are several manufacturers supplying PCMs to the commercial market. The costs per unit storage capacity of latent TES systems are generally higher than for sensible TES systems, but the specific costs are gradually reducing as the technology matures.

In thermochemical energy storage, the thermal energy is stored in the form of reversible chemical reactions between two components. Example of thermochemical TES systems are reversible reaction-based storage (e.g., calcium looping) and sorption-based storage (e.g., hydration/dehydration of salt hydrates). Using the latter case as an example, heat is absorbed to separate two components by removing water vapor from the salt hydrate. To reverse the reaction, the salt hydrates are hydrated with water vapor again, releasing the thermal energy. Thermochemical TES is the least mature TES technology considered here but presents the opportunity for a very compact design and the possibility to store thermal energy for a very long time without considerable losses. The challenges in thermochemical TES are the stability (number of cycles) of the materials used and designing well-functioning reactors. This technology is under research and development due to its potential to store energy for long periods with a high energy density [24]. Due to the low maturity of this technology, the associated cost is high.

The various TES methods are summarised in Figure 2.14 below. We see that the maturity decreases as we move from left to right in the figure, while the compactness, cost and applicable storage time generally increase transitioning from sensible to thermochemical TES.

TES technology applied to temperatures below ambient temperatures is often denoted CTES. In the academic context, latent CTES using PCMs as the storage medium has attracted a lot of attention the latest years due to offering a more compact solution over sensible TES and the possibility to select a PCM with a phase transition temperature well matched with the requirements in the process. A recent review paper has revealed that CTES with PCM has been considered in almost the entire cold chain, spanning from industrial refrigeration in production/processing, to transport refrigeration and packaging,

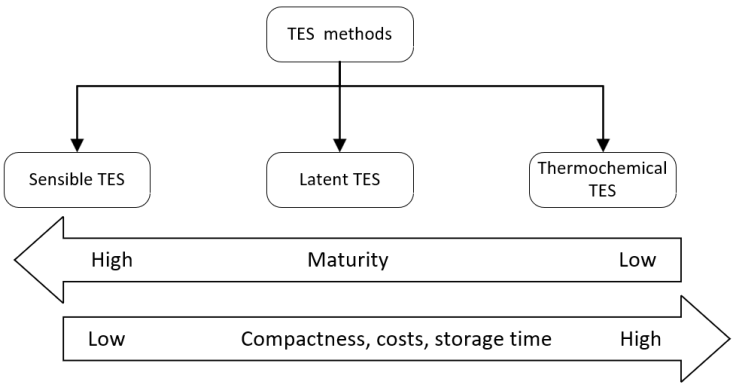

Figure 2.14: TES methods and their characteristics

commercial refrigeration in supermarkets and domestic refrigeration [25]. Key benefits of CTES technology applied to refrigeration systems include:

- Peak shaving and load shifting: CTES enables decoupling of supply and demand between the refrigeration system and the cooling load. By storing the cold thermal energy in periods of low demand and supplying this cold energy in times of high cooling load, the maximum required peak power from the electrical grid is reduced. The electricity consumption is then much more evenly distributed. According to the research of Zehir et al. (2012) [26], about $37,9\%$ of refrigerators have the potential to shift their demand to off-peak hours resulting in about $11,4\%$ reduction in customers' bill. CTES in refrigeration systems can also help the penetration of renewable energy sources. For instance, the CTES can be fulfilled during high photovoltaic production periods, therefore during the daytime. Proper use of control strategy is required [27]. In an attempt to implement this idea, PCM was used in a domestic refrigerator whose control strategy was changed to align to grid supply availability in California [28], [29]. The study found that refrigeration systems could adapt their energy consumption patterns to better match the availability of renewable sources. Additionally, due to the longer OFF periods of PCM-equipped refrigerators, they could be a promising option for use in net zero energy buildings (NZEBs) to compensate for the intermittency of renewable energy sources [27].
- Reduce monetary investment of refrigeration system: refrigeration plants are typically designed to handle the worst-case scenario, which for AC systems corresponds to provide cooling during the warmest day of the year. As a result, the refrigeration plant operates at partial load for most of the time and the excess capacity remains unused. By implementing

CTES to cover the extra load needed during the warmest summer days, the investment costs of the overall system can be reduced.

- Backup: the CTES system can operate as a backup in case of failure of the refrigeration system or electrical blackout.

Various studies have investigated the application of PCM in refrigeration systems for thermal energy storage.
Selvnes et al. (2021) [25] classified CTES units into two categories: those integrated into the secondary refrigerant circuit and those integrated into the primary refrigeration circuit. The latter function as an evaporator during the charging process and a condenser during the discharging process for the refrigeration system. Integrating the CTES unit into the primary refrigerant circuit allows for a higher evaporation temperature during the charging process, leading to increase system efficiency compared to using a secondary refrigerant circuit [30], [31].
Recent studies have focused on the implementation of phase change materials into the walls of refrigerated containers and boxes, as reported by Leungtongkumet et al. (2022) [32]. These studies have shown better quality preservation and energy management in food cold chains. For instance, Gin et al. (2010) [33], [34] studied the effect of PCM panels placed against the internal walls of a freezer during repeated power loss demonstrating that the lower temperature fluctuations achieved through PCM use led to better food quality. Similarly, Ghodrati et al. (2022) [35] evaluated the effect of PCM use in a freezer, showing decreased likelihood of food spoilage, reduced energy consumption, slower temperature rise and better control of energy fluctuations. However, optimal PCM melting temperature should be in the freezer operating range and close to the minimum temperature to achieve better performance.
Elarem et al. (2017) [36] found that incorporating a PCM in a refrigerator resulted in a 12% reduction in power consumption and an 8% increase in COP compared to a refrigerator without PCM. The study conducted by Bista et al. (2018) [37] evaluated the effects of using PCM in various components of refrigerators, including the evaporator, condenser, and compartment. The results showed that using PCMs in these components can have a positive impact on reducing electricity consumption. According to Li et al. (2019) [38], incorporating an ice-cold storage tank into a refrigeration unit can result in an increase in the COP of the chiller by more than 5% and an increase in cold storage capacity by up to 20%. In the investigation presented by Liu et al. (2022) [39], a novel PCM-CTES unit is proposed as a mobile refrigeration unit

for transport refrigerated vehicles to improve their room temperature control performance. The energy cost for the PCM-CTES unit had up to $91,4\%$ reduction compared to conventional mechanical refrigeration units driven by a diesel engine.

In their research, Fragnito et al. (2022) [40] performed both experimental and numerical analyses of a PCM shell-and-tube heat exchanger for CTES. The results showed that only 39% of the PCM mass underwent a complete phase change process, indicating that the current design does not fully utilize the thermal storage potential of the PCM.

Xu et al. (2022) [41] conducted a study on water-ice phase change in CTES developing both experimental and unified mathematical frameworks. They investigated the thermal effects of various factors, including radial positions, geometries, initial temperatures, heat transfer fluid temperature, and heat transfer coefficients on the CTES system. The experimental and mathematical frameworks developed in this study could be used for optimizing the design and operation of CTES systems.

Selvnes et al. (2021-2022) [31], [42] also investigated the use of a water-based PCM in a CTES system coupled with a pillow plate heat exchanger, which was integrated into a CO_2 refrigeration circuit. It was found that the most important parameter affecting the performance of the unit was the temperature difference between the PCM and the refrigerant inside the CTES unit, both for the charging and discharging process. It was also found that the performance of the CTES unit can be manipulated by changing the distance between the pillow plates in the heat exchanger. The study found that using a distance of 30 mm between plates resulted in the highest average discharge rate and total energy discharged during a cycle. The CTES-PCM unit is flexible and can be adapted to suit various refrigeration loads and temperature levels by adjusting the geometry of the PP-HEX and the type of PCM used as a storage medium. A dynamic model of the PCM-CTES unit was developed in the programming language Modelica using the component library TIL-Suite [43]. The model was validated demonstrating good agreement with the experimental data obtained with various heat exchanger configurations, storage medium and refrigerant parameters.

Other research activities about cold thermal energy storage technologies at subzero temperatures have been conducted by several researchers in recent years [44]. Hafner et al. (2011) [45] studied the effect of a CTES with solid CO_2 in a fish-freezing plant. Up to 30% less electricity is required for the equal freezing

capacity compared to the system without CTES. Recently Mastani Joybari et al. (2023) [46] carried out research on a low-temperature CTES system that utilizes CO_2 as the PCM and pillow plate heat exchangers for energy storage at temperatures as low as $-55°C$. Their study focused on identifying the optimal design and operational conditions for the system.

2.2.1 Phase change materials

PCM are materials used in LHS systems due to their great enthalpy of fusion in the solid-liquid transition. They are commonly classified into three categories as shown in the diagram 2.15: organic, inorganic and eutectic [47].

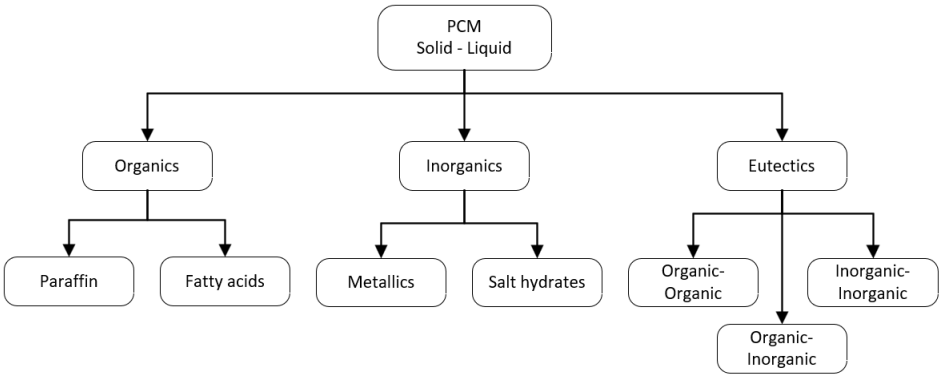

Figure 2.15: PCM classification

Many materials have been studied as PCM, but only a few of them have been commercialized ([37], [48]–[50]), mainly due to problems such as phase separation, supercooling, corrosion, long-term stability, and low heat conductivity [51]. Another important parameter to be taken into account is the volumetric thermal storage density, defined in Equation 2.11.

$$\theta_{PCM} = \Delta h_{fus} \cdot \rho_{PCM} \tag{2.11}$$

The organic classification mainly encompasses fatty acids and paraffins, with the latter garnering increased attention. Paraffins are considered desirable PCM for several reasons, including their wide and variable melting point range, high heat of fusion, lack of supercooling, chemical stability and recyclability, and good compatibility with other materials when used in mixtures. However, paraffins also have certain disadvantages when compared to alternative PCMs. These include their low thermal conductivity (around 0,2 W/m K), relatively large volume change, and flammability risk [52].

To improve heat transfer in PCM and overcome their poor thermal conduc-

tivity, various techniques have been proposed. These include using colloidal suspensions [53], incorporating metal foams [54], [55], and implementing encapsulation methods [56].

Among inorganic materials, hydrated salts have received the most attention as PCMs, particularly in the context of solar heating systems. Inorganic salts are favored for their high heat of fusion, relatively high thermal conductivity (around 0,5 W/m K), low volume change, and low cost. However, they do have drawbacks such as poor nucleation rates leading to super-cooling and their corrosive nature, both of which can compromise the stability of the PCM and its supporting system [52].

Eutectics refer to mixtures of chemical compounds that all undergo phase transition at the same temperature. They also possess a high volumetric thermal storage density defined in Equation 2.11. However, the current challenge with eutectic mixtures is the lack of available thermo-physical data, as pointed out by Zhou et al. (2012) [52].

Method

This chapter elucidates the processes and decisions that lead to the results of this study In the "System information" section, a comprehensive account of the system's components and operational conditions is presented. The "Functional description" section describes the logic governing the components across the different operating conditions. The "AHU evaporator coil design" section, shows the design of the CO_2 evaporator/AHU cooling coil, involving simulations of different geometries. The "Simulation Study" section delineates the development of the simulation models for both the TES-AC system and the refrigeration system. These dynamic models were developed using Dymola 2022x1 [1] (Dassault Systems, Vélizy-Villacoublay, France), leveraging the TIL 3.11.0 library for components and the TIL Media 3.11.0 library for fluid properties [2] (TLK-Thermo GmbH, Braunschweig, Germany). Part of the project entailed also to follow the designing of the demonstrative installation of this system. The demo supermarket has plug-in freezers, resulting in low LT capacity, needed just for the main cold storage room, and high AC load demand. The demo system is slated for construction in the upcoming autumn at Orkidehøgda, Mjøndalen MØ, with testing scheduled for the summer of 2024.

3.1 System description

The actual refrigeration system in REMA 1000 is a traditional CO_2 booster system represented in Figure 3.1. At the inlet of the gas cooler, some heat is recovered and used to do space heating through the AHU. During the summer season, the space cooling requirement is met by the same system utilizing a water-glycol loop. Part of ther refrigerant after the high pressure valve (HPV) is directed to a heat exchanger, in which the CO_2 evaporates cooling down the water-glycol mixture. Subsequently, the refrigerant is sent to the liquid

[1] `https://www.3ds.com/products-services/catia/products/dymola/`
[2] `https://www.tlk-thermo.com/index.php/en/til-suite`

receiver and the formed vapor is flashed to the medium temperature (MT) compressor thanks to the flash gas by-pass valve (FGBV).
Integration of the existing system with a circuit for air conditioning coupled with a CTES (TES-AC) is proposed as shown in Figure 3.2. The TES-AC system is able to store "cold energy" in the PCM-CTES and release it when cooling is required for AC.

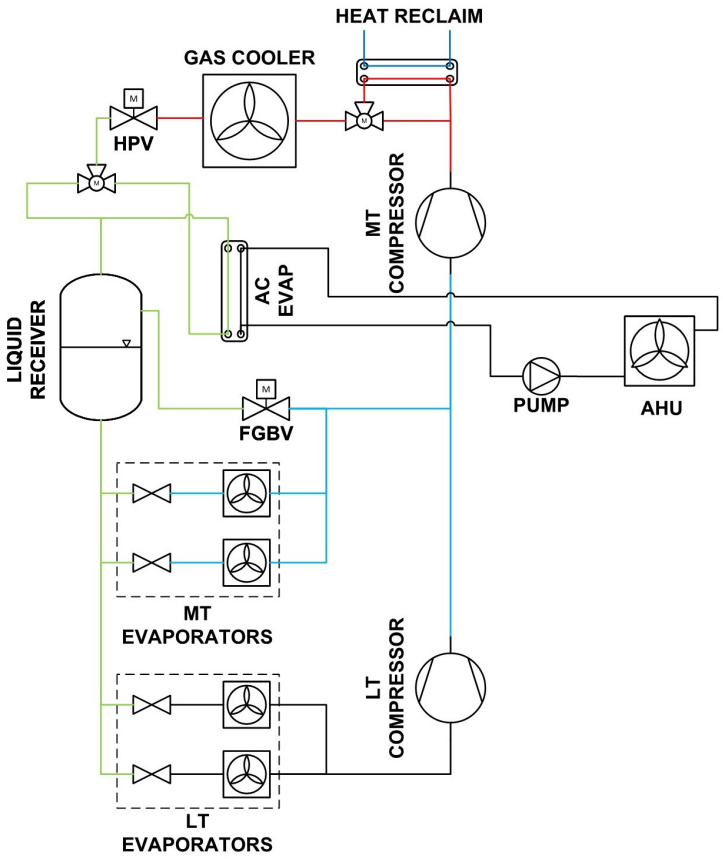

Figure 3.1: P&ID of the actual refrigeration system installed in REMA 1000

3.1.1 Components

In this section, the main components of the TES-AC system, visible in Figure 3.2 and shown in detail in Figure 3.9, are described.

3.1.1.1 PCM-CTES

The cold thermal energy storage (CTES) employs water/ice as phase change material (PCM), resulting in a phase-change temperature of $0°C$. The heat exchanger in the CTES unit consists of a stack of pillow plates (PP-HX) immersed into a stainless-steel container filled with PCM. To minimize the heat losses to the environment, the container's walls are insulated. The charging

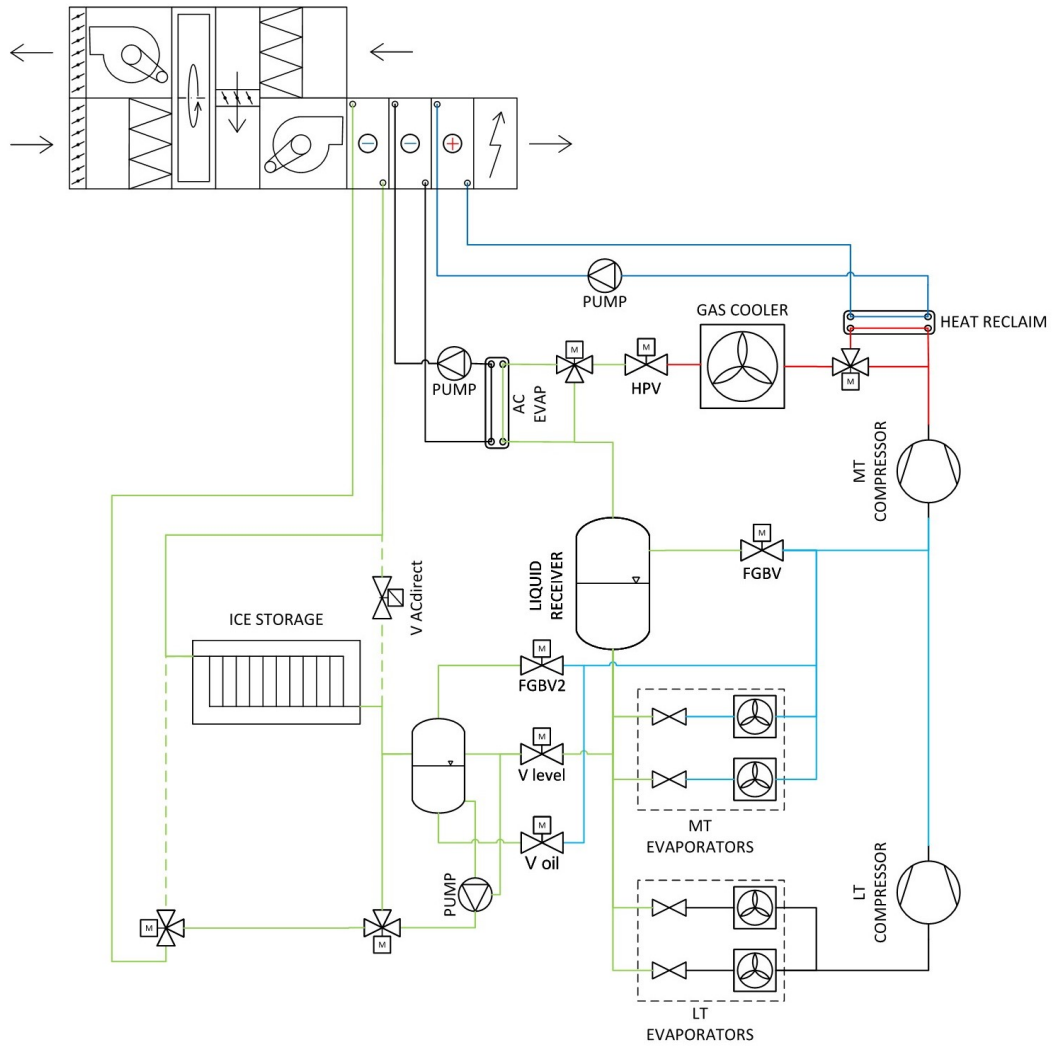

Figure 3.2: P&ID of the proposed system: refrigeration system, CTES and AHU

and discharging processes of the PCM-CTES unit are carried out through evaporation and condensation of the CO_2 circulating inside the plates. The pillow plates are connected together with a specific pitch chosen to optimize the charging/discharging process and to satisfy the requested load. The freezing of water will occur solely between the pillow plates and in the surrounding volume, but it will not extend to the walls of the container. Therefore, around the PP-HX there will be liquid water and there are not problems related to the expansion of water during the freezing process: when water freezes, it expands 9% by volume considering the densities of water ($999,8\ kg/m^3$) and ice ($916,8\ kg/m^3$) at a temperature equal to $0°C$. A sensor is employed to gauge the level of charging and discharging, measuring the distance with the liquid level of the PCM, that changes during the phase change process. Due to its substantial spatial requirements and associated economic considerations, this unit will be placed outdoors, as indoor supermarket floor space holds considerable monetary value.
It has the following geometry:

- 24 plates in parallel
- plate pitch (maximum plates distance) = 40 mm
- metal plate thickness = 1 mm
- pillow plate minimum thickness = 2 mm, because each pillow plate is made of two metal plates welded together
- pillow plate maximum thickness = 6 mm
- maximum duct width = 4 mm
- average duct width = 1,89 mm
- plate dimensions = 2,5 x 1,25 m
- distance between the plates and the wall of the container = 10 cm
- serial hydraulic flows = 6
- welding pattern shown in Figure 3.3

3.1.1.2 AHU evaporator coil

The cooling coil of the air handling unit (AHU) acts as an evaporator for the CO_2. This finned tube heat exchanger is manufactured by FACO S.p.A. (Novara, Italy). Unlike cases where a two-phase fluid enters, this particular evaporator does not incorporate a distributor since only liquid is present

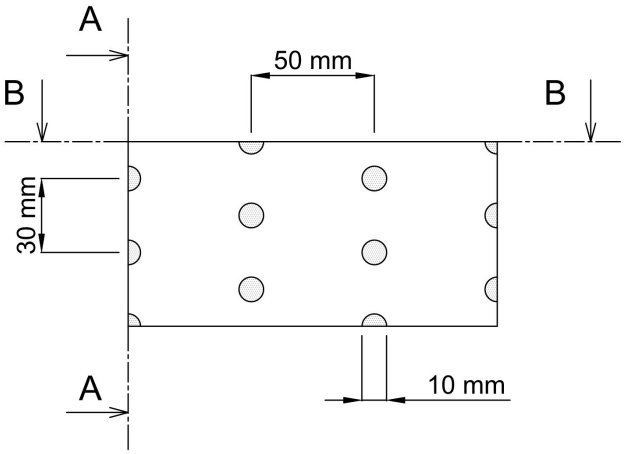

Figure 3.3: Drawing of the welding pattern of the pillow plates

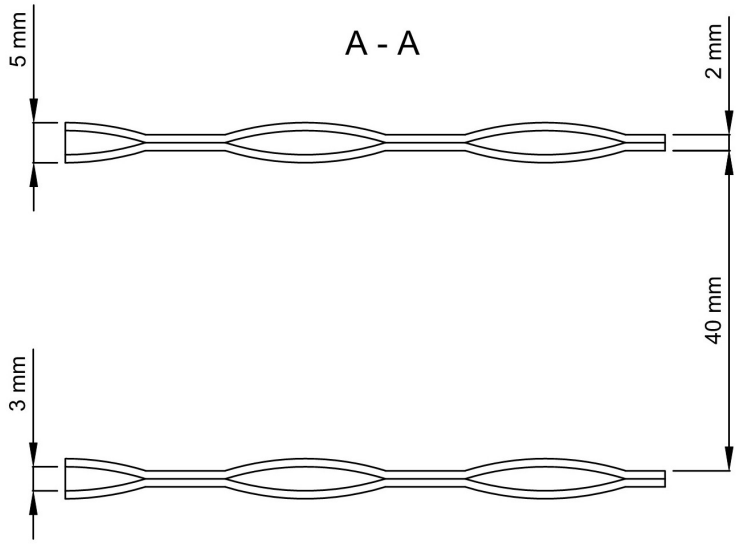

Figure 3.4: Section A-A of the pillow plate

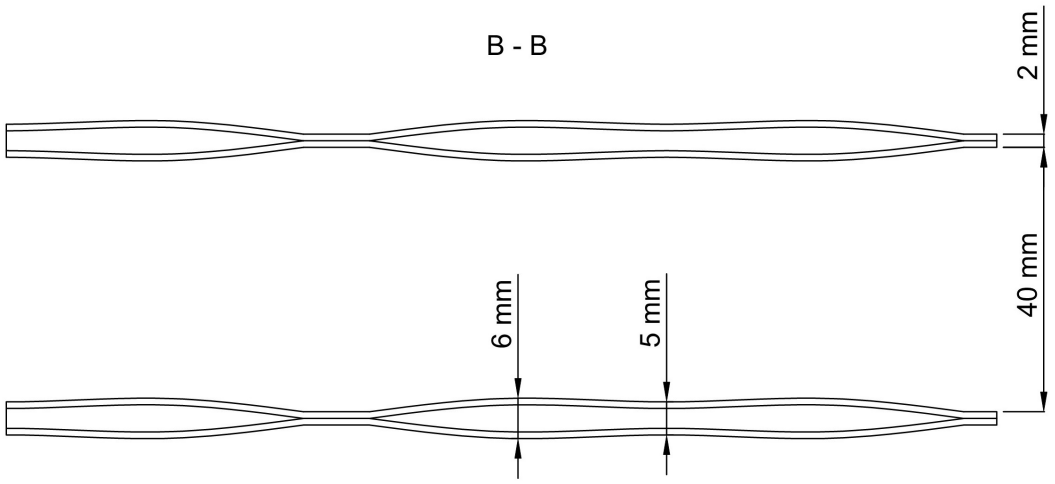

Figure 3.5: Section B-B of the pillow plate

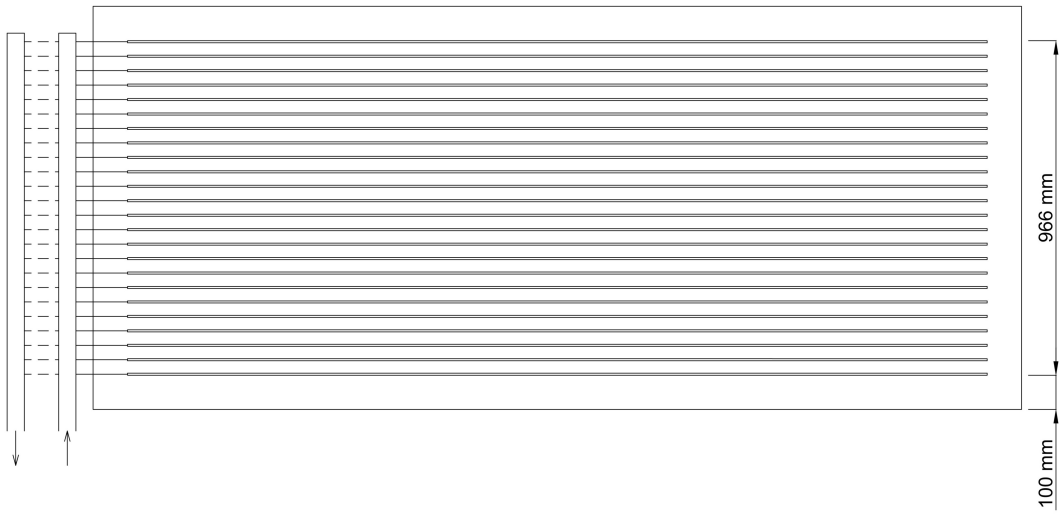

Figure 3.6: Sketch of the stack of pillow plates inside the container

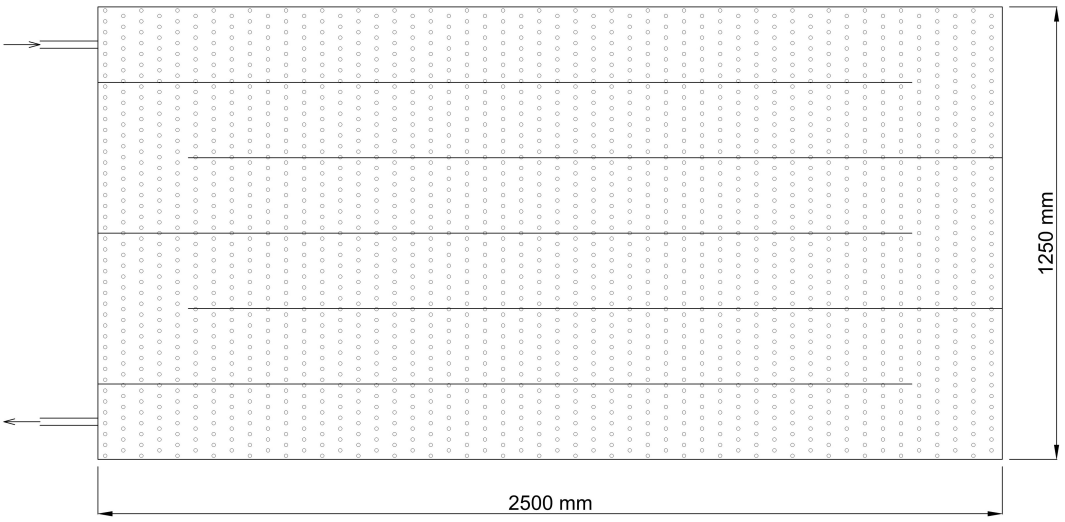

Figure 3.7: Single pillow plate drawing

upon entry. Various geometries have been simulated to determine the optimal configuration, as discussed in the corresponding chapter.

3.1.1.3 Pump

The presence of a liquid separator enables the utilization of a pump for fluid circulation, ensuring that only liquid is pumped through the system. Supplied by WITT (Aachen, Germany), the pump employed is a sealless canned motor pump, larger than required due to the manufacturer's unavailability of smaller pumps designed for CO_2. The specific pump model utilized is HRP3232. To address the necessity of cooling the electric motor, a small part of the refrigerant flows through it for cooling purposes and is subsequently directed back to the receiver. Strategically positioned $0,5\ m$ below the tank, the pump's placement prevents cavitation and reduces the pump's sensibility to system pressure fluctuations. The required diameter of the downleg to the pump is a DN100. The pump is an on-off model, so it is not able to modulate its characteristic curve. The minimum volume flow rate is $0,6\ m^3/h$, while the maximum head is $25\ m$. Incorporating a diverting valve, the system gains the ability to change the flow rate by recirculating part of the flow back to the tank.

3.1.1.4 TES-AC receiver

The primary purpose of the tank is to effectively separate liquid and vapor, ensuring that only liquid enters the pump suction. With a height of $1,7\ m$ and a volume of 188 liters, this relatively tall tank serves to avoid the occurrence of a vortex effect that could lead to vapor entering the pump. To connect the tank to the main CO_2 refrigeration system, two main valves are employed. One regulates the liquid level inside the tank and the other one controls the pressure within the TES-AC circuit. Additionally, another valve is used to allow the oil to return from the bottom of the tank to the MT compressors. Their functioning is described in the chapter "Functional description". A DN100 pipe needs to be welded to enable the connection with the pump's inlet, and another tube for the liquid level sensor requires welding. Supplied by PROFROID (Marseille, France), the tank will undergo modifications by Skala Fabrikk AS (Trondheim, Norway) to fulfill the specific connection requirements. A 3D schematic of the system configuration is shown in Figure 3.8.

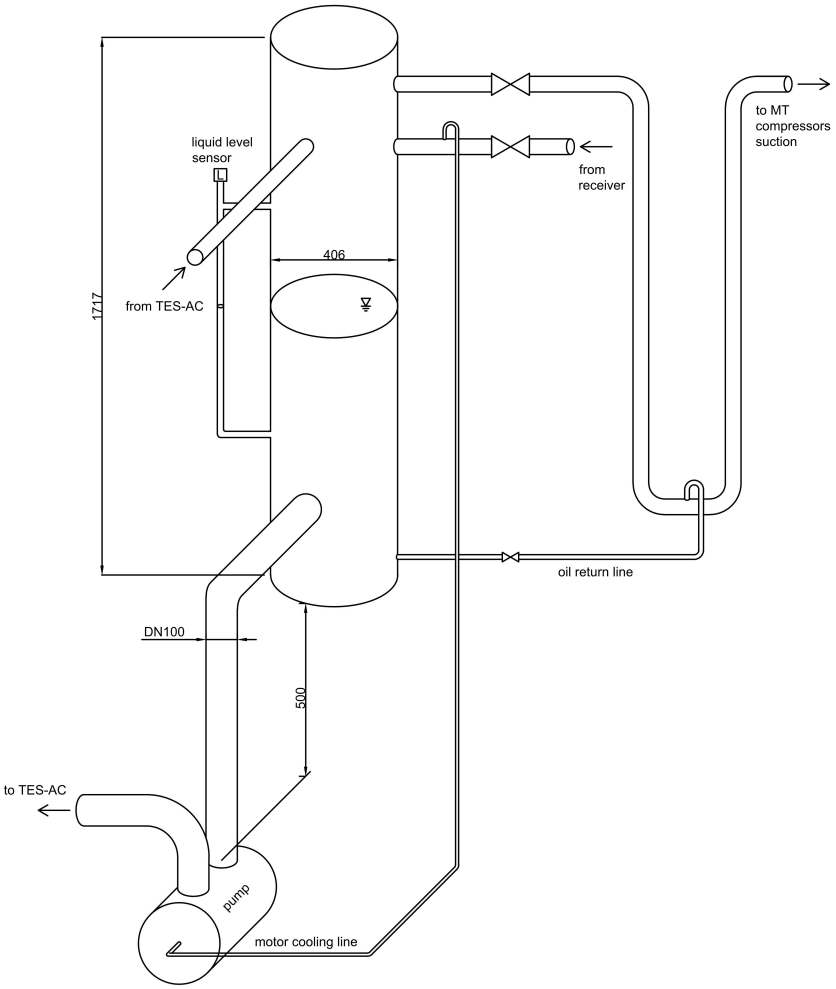

Figure 3.8: 3D sketch of the TES-AC receiver equipped with all connections and the pump. Measures in *mm*

3.1.2 Operating conditions

The system operates in three distinct modes: charging, discharging, and direct air conditioning (AC).
During the charging mode, the system functions at the lowest attainable evaporation temperature to maximize the freezing capacity within the CTES. To achieve this, it operates at the MT pressure level of 28 bar, corresponding approximately to an evaporation temperature of $-7°C$. The evaporation temperature can be adjusted by varying the pressure according to the CTES's discharge level to recharge it over the course of a night. In this process, the refrigerant is directed to the CTES unit, where it evaporates while freezing the water. The formed vapor is then sent to the MT compressors, while new liquid enters to maintain a constant level within the TES-AC receiver.
During discharging, the refrigerant evaporates within the cooling coil of the AHU and subsequently re-condenses within the pillow plates of the CTES. To enable the utilization of latent heat, the system is designed to work with an evaporating temperature above $0°C$. The higher it is, the more capacity can be extracted and the faster the CTES discharges. Additionally, using an evaporation temperature some degrees above $0°C$, prevents frost formation on the AHU cooling coil. To meet all these requirements, the system operates at the pressure level of the receiver (40 bar). Consequently, the evaporation temperature is set approximately at $5°C$.
Once the CTES is fully discharged, the system switches to direct AC mode, effectively bypassing the CTES.

3.1.2.1 Pump vs natural circulation

Initially, a first approach to thermosyphon-driven loop (natural circulation) was investigated to avoid the installation of a pump. In this approach, the CTES would have been situated above the AHU to enable the upward movement of refrigerant vapor generated in the AHU evaporator coil. Then, this vapor would have been re-condensed and flowed downward back towards the AHU. However, for this natural circulation to occur, specific conditions needed to be met. The CTES had to be strategically placed above the AHU, which presented a challenge since the AHU is usually located on the ceiling. To accommodate this arrangement, the CTES would have to be positioned on the rooftop. However, this approach posed several obstacles. Given the weight of the CTES, exceeding 3 tons, the installation would have needed a substantial mechanical structure to ensure stability and safety. This structural re-

quirement would have resulted in significant cost increases, making the option financially unviable. Consequently, this particular approach was disregarded. In contrast, opting for a pump-based solution eliminates the need for CTES placement based on natural circulation criteria, as the pump guarantees consistent flow. Moreover, this approach introduces increased system flexibility due to the pump's capacity for flow rate regulation. By employing a pump, the system design becomes more adaptable and avoids the challenges associated with the thermosyphon-driven approach.

3.2 Functional description of TES-AC system

This section describes the different operational modes of the TES-AC system for supplying air-conditioning (AC) with a cold thermal energy storage (CTES) integrated with the Carrier supermarket CO_2 system. The references to components and numbering are based on the simplified P&ID presented in Figure 3.9. A summary of the control logic is given as a selection tree in Figure 3.10 at the end of the chapter.

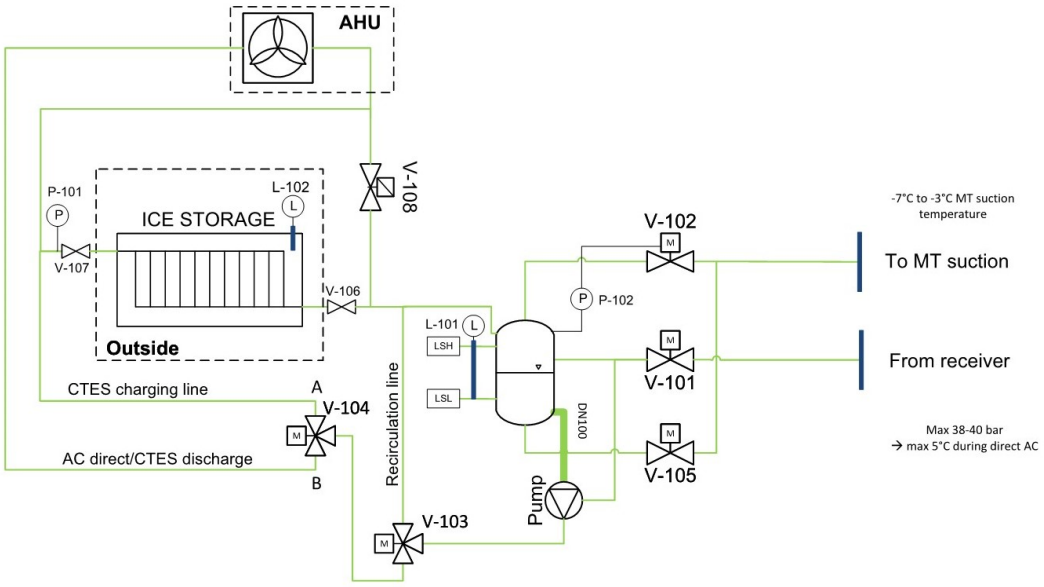

Figure 3.9: Simplified P&ID of the TES-AC system

3.2.1 Activation of TES-AC system

If the ambient temperature is above a certain threshold, then the storage must be charged because the summer period/cooling period has started. This threshold should be selected by the experience of Carrier based on when the existing AC system is activated.

3.2.2 Charging mode

The purpose of the charging mode is to freeze the water in the storage. This is done in off-peak periods (night) or during periods with low refrigeration load. To ensure the freezing of the ice inside the cold thermal energy storage (CTES), the lowest possible MT suction pressure is required. In any case, the CTES controller will send a digital signal to the main controller of the supermarket system and request the lowest suction pressure for charging.

The activation of the charging mode should be possible from:

1. a specific time, e.g. charging from 23:00 (shop closed)
2. other external signals, e.g weather forecast of high temperatures the following day

Signal: Charging=0, No charging=1
Table 3.1 describes the operation of the valves in the TES-AC system during the Charging mode.

Valve	Operation	Mode/position	Input signal
V-101	Controlling	Maintain level of receiver	L-101 (level sensor receiver)
V-102	Controlling	Fully open	None
V-103	Controlling	Control position	Differential pressure set-point between P-102 and P-101 (e.g. 1,5 bar)
V-104	A or B	A	Charging mode active (Digital signal = 0)
V-105	Controlling	Open/close	Timer (oil return valve)
V-106	Manual on-off	Open	None (service valve)
V-107	Manual on-off	Open	None (service valve)
V-108	On-off	Off=closed	Charging

Table 3.1: Valve position during Charging mode

Additional possibility for functionality: If the main system is working in partial load (MT compressor inverter operates between 30 and 45 Hz) and if storage is not full, then activate Charging. The first MT compressor is then able to work at nominal conditions and the efficiency can be improved.

3.2.2.1 State-of-charge, charging mode

Liquid level sensor L-102 measures the water level inside the storage. In other words, it monitors the charging level of the storage. The water level will increase during the charging process due to the expansion of volume when the water solidifies to ice. If the water level, does not change for a certain specified period (to be chosen) it means that the storage is fully frozen. Then the Charging mode can be stopped. The TES-AC controller sends a digital signal to the main controller telling to stop charging (signal No charging = 1).

3.2.3 Control of AC supply mode

Supply of cooling for air-conditioning can be done in two modes: AC direct or CTES discharging (both described in separate sections). The CTES controller asks the liquid level sensor L-102 if the storage is fully or partially charged.

If the storage is fully or partially charged, V-108 must be closed (discharging mode). If the storage is not charged, V-108 must be opened to bypass the storage (direct AC mode).
L-102 must remember the last maximum value as a reference level. The height difference between the fully charged and fully discharged state will be established in the commissioning phase, so the system is able to calculate the minimum water level. The following conditions will apply:

1. If storage is empty (L-102 = minimum value), then AC direct mode is activated
2. If storage is full (L-102 = maximum value or above a certain level), then Discharging mode is activated.

Additional possibility for functionality: If the main system wants to supply cooling to AC and compressor is in part load (MT compressor inverter operates between 30 and 45 Hz), then AC direct. Else, if storage is full then activate discharge mode, else AC direct (see Figure 3.10 at the end of the chapter for clarification).

3.2.4 Discharging mode

The AHU controller sends an analog signal (0 V to 5 V, to be verified) to the CTES controller representing the request to provide cooling. To avoid frost formation on the AHU coil, a temperature higher than $0°C$ is needed on the CO_2 side. Hence, the desired pressure in the TES-AC system is close to the receiver pressure of the main system. Table 3.2 describes the operation of the valves in the TES-AC system during the Discharging mode.

Valve	Operation	Mode/position	Input signal
V-101	Controlling	Maintain level of receiver	L-101 (level sensor receiver)
V-102	Controlling	Maintain pressure	P-102 (CTES receiver pressure)
V-103	Controlling	Control flow rate	AHU request cooling (0-5 V)
V-104	A or B	B	AHU request cooling (>0 V)
V-105	Controlling	Open/close	Timer (oil return valve)
V-106	Manual on-off	Open	None (service valve)
V-107	Manual on-off	Open	None (service valve)
V-108	On-off	Off=closed	L-102

Table 3.2: Valve position during the Discharging mode

3.2.4.1 State-of-charge, discharging mode

L-102 measures the discharging level of the storage. During the discharging mode, the liquid water level will decrease due to the melting of the ice inside the storage. If the water level does not change for a specified period (to be chosen), it means that the storage is fully discharged. The system must switch to Direct AC mode if AHU signals request for cooling.

If AHU request cooling signal is >5 V, then switch to AC direct mode.

3.2.5 AC direct mode

If the liquid level sensor L-102 tells the CTES controller that the storage is empty and there is a request for cooling from the AHU, direct AC mode has to be activated. The same is true if the system is operating in discharging mode the storage become empty (all ice melted) during the process. The CTES controller has to fully open the valve V-108 to bypass the CTES storage and send vapor direct to the receiver in the TES-AC system. Table 3.3 describes the operation of the valves in the TES-AC system during the Direct AC mode.

Valve	Operation	Mode/position	Input signal
V-101	Controlling	Maintain level of receiver	L-101 (level sensor receiver)
V-102	Controlling	Maintain pressure	P-102 (CTES receiver pressure)
V-103	Controlling	Control flow rate	AHU request cooling (5-10 V)
V-104	A or B	B	AHU request cooling (>0 V)
V-105	Controlling	Open/close	Timer (oil return valve)
V-106	Manual on-off	Open	None (service valve)
V-107	Manual on-off	Open	None (service valve)
V-108	On-off	On=open	L-102

Table 3.3: Valve position during the Direct AC mode

3.2.6 Safety mode/Alarm

If L-102 measures a level lower than a certain value (minimum value) it means there has been some leakage of water from the storage, and it must be refilled. A low priority alarm has to activate.

If the liquid level inside the TES-AC receiver is activating the high- or low-level alarm (LSL or LSH), the pump must be stopped. A manual reset is proposed. The main unit must activate glycol-based cooling loop towards AHU.

3.2.7 Component descriprion

3.2.7.1 Valves

1. V-101
   Maintain the liquid level in the separator. Controlled by the sensor L-101.

2. V-102
   Controlling. Maintain the pressure in TES-AC receiver. Controlled by the sensor P-102.

3. V-103
   Controlling. Regulate the flow rate that goes to AHU and to recirculation back to TES-AC receiver. In AC demand mode (Discharging mode/Direct AC mode), it is controlled by the request of the AHU (signal from 0 to 10 volts). In Charging mode, it is controlled by the pressure difference between P-101 and P-102 (ex: 1-2 bar). It must be paid attention to the evaporating pressure (and so the temperature) in the CTES unit. A higher flow rate leads to higher pressure losses in the circuit and so, higher pressure in P-101. A lower flow rate leads to lower pressure losses but has to be verified that the temperature difference is enough to allow ice formation.

4. V-104
   Position A or B. Selection between applying Charging mode or AC demand mode (Discharging mode/Direct AC mode). See the logic scheme for the decision of the working mode.

5. V-105
   Controlling. Guarantee the oil return. Electric expansion valve controlled by a timer.

6. V-106
   Manual service valve.

7. V-107
   Manual service valve.

8. V-108
   On-off. Open or closed. Used for selection between Discharging mode or Direct AC mode.

3.2.7.2 Liquid level sensors

1. L-101

   Measures the liquid level in the separator. If LSL or LSH are activated the system has to be stopped and a manual reset is required.

2. L-102

   Evaluates the state-of-charge of the CTES unit by measuring the distance with the liquid level of the PCM, which changes due to the expansion of water/ice during phase change. In charging mode, the control system is able to establish the maximum water level (storage fully charged), when the sensor does not change its value for a certain amount of time. The delta level is established in the commissioning phase, so the minimum water level is easily calculated. In discharging mode, the minimum water level (fully discharged) can also be established when the sensor does not change its value for a certain amount of time. When the AHU request the higher load than the storage can provide (>5 V), it means that the storage is fully discharged.

3.2.7.3 Pressure sensors

1. P-101

   Measures the pressure before the CTES unit.

2. P-102

   Measures the pressure in the liquid separator (similar to receiver pressure (p_{rec}) signal in main system).

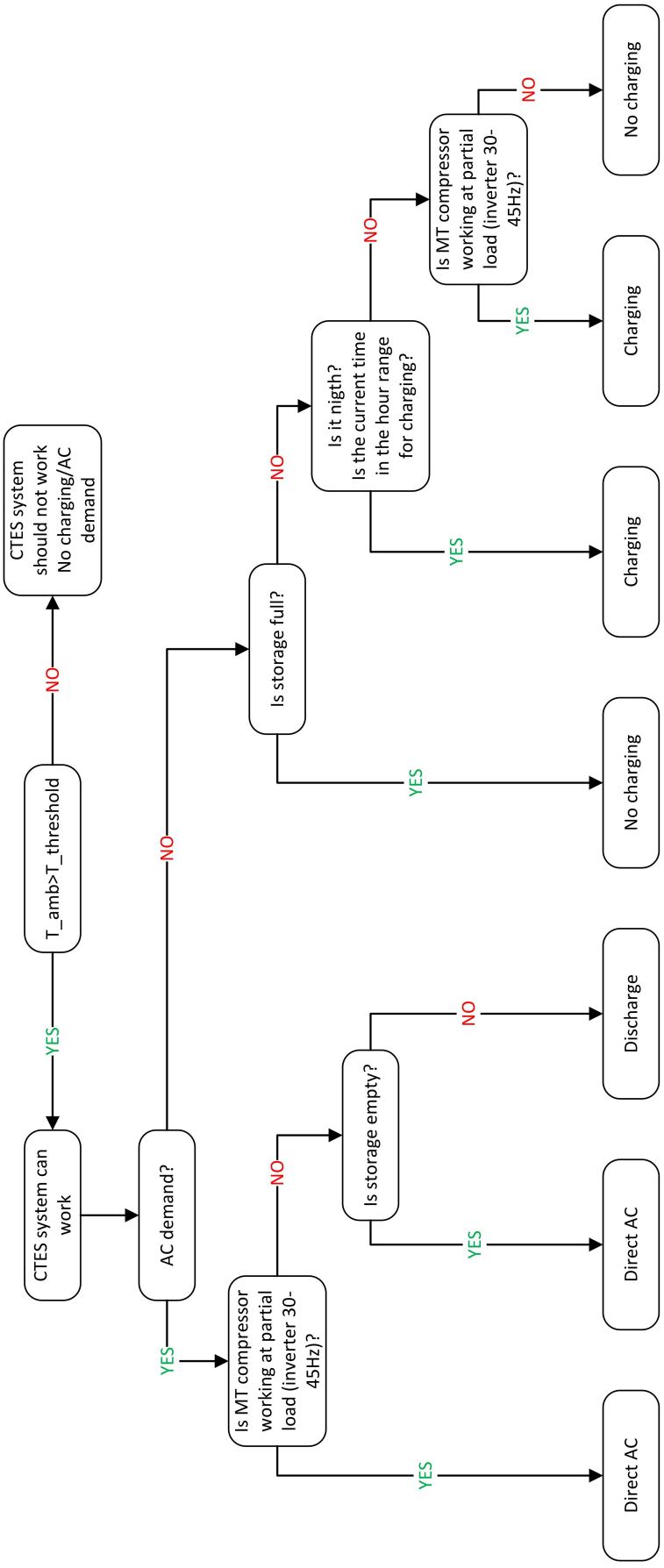

Figure 3.10: Control logic of the TES-AC system

3.3 AHU evaporator coil design

The simulation and design tool HXsim, an internal SINTEF Energy software developed in 2020 by Geir Skaugen, Kjell Kolsaker and Trond Andresen, was employed to design the AHU evaporator coil. Different geometries were investigated taking into account some constraints set by the existing AHU.
The design conditions were established by Aircoil (Årjäng, Sweden) and they are summarized in Table 3.4. It is worth to remember that this coil was added to the pre-existing AHU, thus imposing fixed limitations on the maximum external dimensions. The evaporator coil is required to cool down an air volume flow rate of $15000 m^3/h$ with a relative humidity of 60%, lowering the air temperature from $23°C$ to $19°C$. Therefore, the resulting sensible cooling capacity is approximately 20 kW, calculated by applying the Formula 3.1. It's important to note that the total cooling capacity will be greater due to the additional contribution of latent heat of moisture condensation.

$$Q = \dot{V} \cdot \rho \cdot c_p \cdot (T_i - T_o) \tag{3.1}$$

The CO_2 evaporates at a temperature equal to $5,3°C$ at the evaporator outlet, corresponding to an evaporating pressure of 40 bar. By calculating the pressure drop and the resulting temperature drop, the inlet evaporating temperature can be determined. A vapor quality of $0,8$ at the outlet was selected to ensure an optimal heat transfer coefficient for the refrigerant side throughout the entire heat exchanger.

Air volume flow rate	15000 m^3/h
Air inlet temperature	$23°C$
Air inlet relative humidity	60%
Air inlet specific humidity	$10,52$ g/kg_{air}
Air outlet temperature	$19°C$
Cooling capacity	30 kW
Evaporating outlet temperature	$5,3°C$
Evaporating outlet pressure	40 bar
Outlet vapour quality	$0,8$

Table 3.4: Evaporator design conditions

The heat exchangers had to respect the geometry constrains specified by FACO, which are listed in Table 3.5 and visually represented in Figure 3.11. The number of rows and their circuiting had to be decided.
The software employs the following correlations to calculate the heat transfer

and the pressure drops:

- single phase heat transfer: Gnielinski [57], [58]
- two-phase flow heat transfer: Steiner [57], [59]
- two-phase flow pressure drop: Friedel [60]

Length	2085 mm
Height	1160 mm
Width	300 mm
Tubes per row	26
Tube horizontal pitch	$36,64$ mm
Tube vertical pitch	40 mm
Tube (external diamater x thickness)	$16,5 \times 1$ mm
Finned length	1870 mm
Finned heigth	1080 mm
Fin thickness	$0,2$ mm
Fin spacing	5 mm

Table 3.5: Geometry constrains and choiches of the evaporator

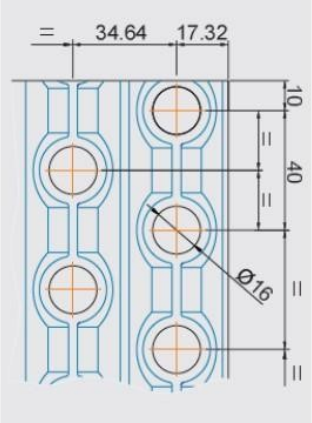

Figure 3.11: Tube geometry configuration

The configurations listed below and shown in Figure 3.12 were investigated:

- 2 rows and 1 circuit (2R-1C)
- 2 rows and 2 circuits (2R-2C)
- 3 rows and 2 circuits (3R-2C)

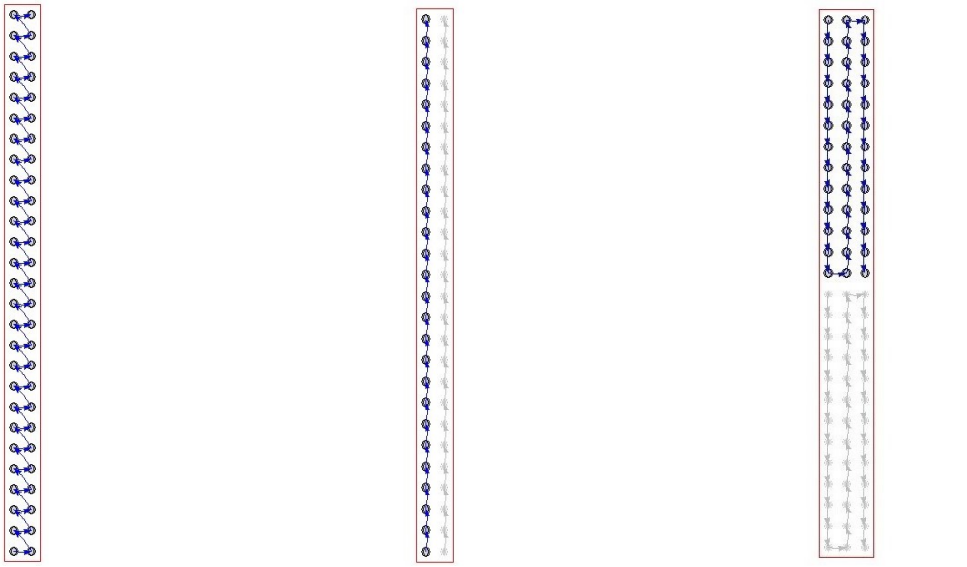

(a) 2 rows - 1 circuit (2R-1C)

(b) 2 rows - 2 circuits (2R-2C)

(c) 3 rows - 2 circuits (3R-2C)

Figure 3.12: Circuitation of the different investigated configuration

3.4 Simulation study

This section describes the development of the simulation models that led to the obtained results. During this thesis work, two distinct simulation models were built to investigate the operation of the TES-AC system and its impact on the refrigeration system. The existing glycol system was also simulated for the purpose of comparison.
The first model for the TES-AC system was used to evaluate the charging and discharging loads, the remained capacity to be integrated and the possibility of total AC load shifting. Instead, the second model was used to investigate the effect of the AC load shifting on the refrigeration system, primarily on the compressors operation. This model was also used to simulate the existing system.

3.4.1 TES-AC system

A dedicated model of the TES-AC system, shown in Figure 3.15, was developed using Dymola to assess whether it can efficiently charge the PCM-CTES during the night and subsequently cover the entirety of the AC load during the day without requiring additional cooling capacity from the primary refrigeration system. In cases where the AC load is not fully covered, the model was used to determine the share it can effectively address.
Two boundary conditions were implemented at the connection point with the liquid separator. One boundary had a pressure of 40 *bar* with the refrigerant assumed as saturated liquid, while the other boundary had a pressure of 28 *bar* with the refrigerant considered as saturated vapor. These boundary conditions served as ideal connections to the refrigeration system.
The PCM-CTES component was developed by Försterling of TLK-Thermo GmbH in collaboration with Selvnes and Sevault of SINTEF Energy. This component was validated [43] relying on the experimental data obtained from the research of Selvnes et al. [31], [42].
The PCM-CTES was modelled based on the geometry described in Section 3.1.1. The discretization involved 9 elements for the refrigerant side and 5 elements for the PCM side, following the approach undertaken by Försterling et al. [43], which demonstrated a good agreement with the results of the experimental tests conducted by Selvnes et al. [31], [42].
The model "Evaporation: Shah Chen / Condensation: Shah / 1-Phase: Gnielinski Dittus Boelter" was used to evaluate the heat transfer coefficient on the

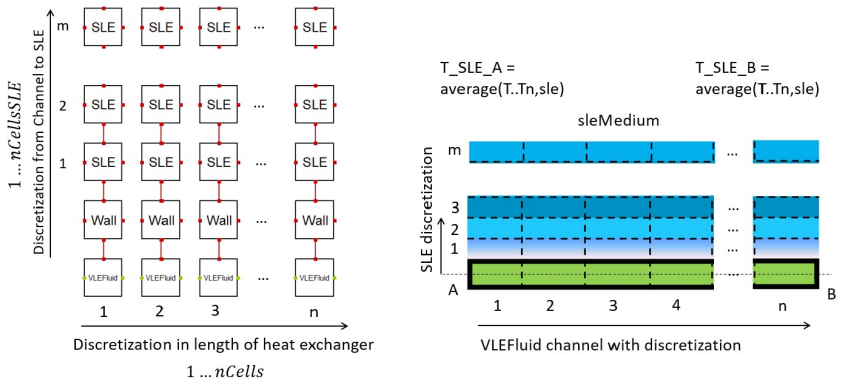

Figure 3.13: Model structure of the PP-HX showing the refrigerant discretization in the refrigerant flow direction and perpendicular in the PCM material [43]

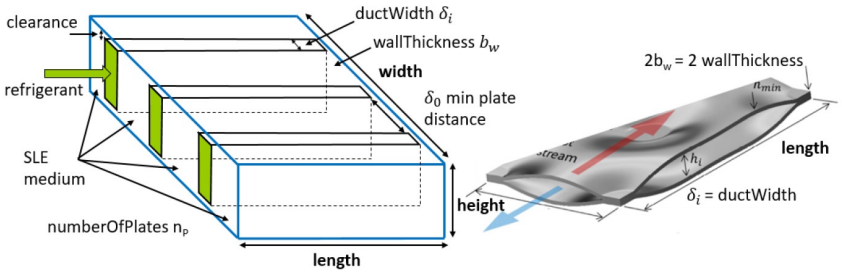

Figure 3.14: Geometry parameters of the PP-HX model [43], [61]

refrigerant side. This model handles three different correlations to describe the heat transfer of two phased mediums. One correlation each is used to describe evaporation, condensation and one-phase mediums. These equations are merged by a linear transition.

For single phase heat transfer, the model "Gnielinski Dittus Boelter" was employed. This model is the implementation of the correlations proposed by Gnielinski, Dittus and Boelter, which describes the heat transfer of a one-phase medium for a variety of tube-like geometries. Corresponding to the properties of the fluid flow, represented by the Reynolds number, three different equations are distinguished. A smooth transition between the equations is achieved by the usage of the smooth transition function.

The model by Shah Chen was used to evaluate the heat transfer coefficient during evaporation. This model is the implementation of the correlations of Shah and Chen, describing the heat transfer during forced convective boiling and evaporation. Since the Froude number compares the inertial and the gravitational forces, it is used to rate the influence of the gravity and, therefore, distinguish between the two approaches. For small Froude numbers (<0,04), the approach from Shah is used, for larger Froude numbers (>0,04), the ap-

proach by Chen is utilized.

The correlation proposed by Shah was adopted for the heat transfer during condensation. This correlation considers horizontal, vertical up-flow and vertical down-flow alignments.

The model of Swamee-Jain, implementing their correlation, was applied to compute the pressure drops inside the pillow plates. Their correlation describes the pressure drop in rough pipes, dependent on the pipe's roughness. Since the pressure drops of laminar flows are mainly influenced by the viscosity of the medium, rather than the pipe's roughness, two different equations, one for laminar flow and one for turbulent flow, are distinguished by the Reynolds number. During the transition area, the two equations are merged linearly. Furthermore, the equation is mirrored at the origin to allow the calculation of the pressure drop for reverse flow problems.

The heat losses to the environment were neglected, since the container is well insulated.

The logic described in Section 3.2 was implemented, except for the additional charging mode during compressors partial load operation. The charging mode is activated between 23:00 (11 p.m.) and 7:00 (7 a.m.) when the supermarket is closed. The status of charging is controlled by the PCM liquid mass. During the charging mode, the pressure is maintained at $28,82\ bar$, corresponding to an evaporation temperature of $-7°C$. When AC cooling is requested, the pressure switches to $39,7\ bar$, equivalent to an evaporation temperature of $5°C$. This increase is allowed by letting some liquid from the main refrigeration system enters the tank. Once the pressure is reached, the filling valve switches its control from the pressure to the liquid level of the TES-AC receiver. The pump activates with a constant volume flow rate only when CTES charging or AC cooling is requested. The volume flow rate is adjusted to ensure complete CTES charging throughout the night, as intended for the demo installation. While in practice, the volume flow rate to the circuit will be dynamically adjusted based on AC demand, facilitated by a diverting valve. However, for the purposes of the model, a constant flow rate was assumed to simplify the system and avoid additional complexity with PI controllers.

Several tests were conducted to examine the charging mode. The volume flow rate of the pump was varied while maintaining a constant value, allowing for an assessment of how the charging time and required capacity change under different conditions. In these tests, the initial temperature of the PCM was set at $1°C$, resulting in a fully discharged PCM-CTES.

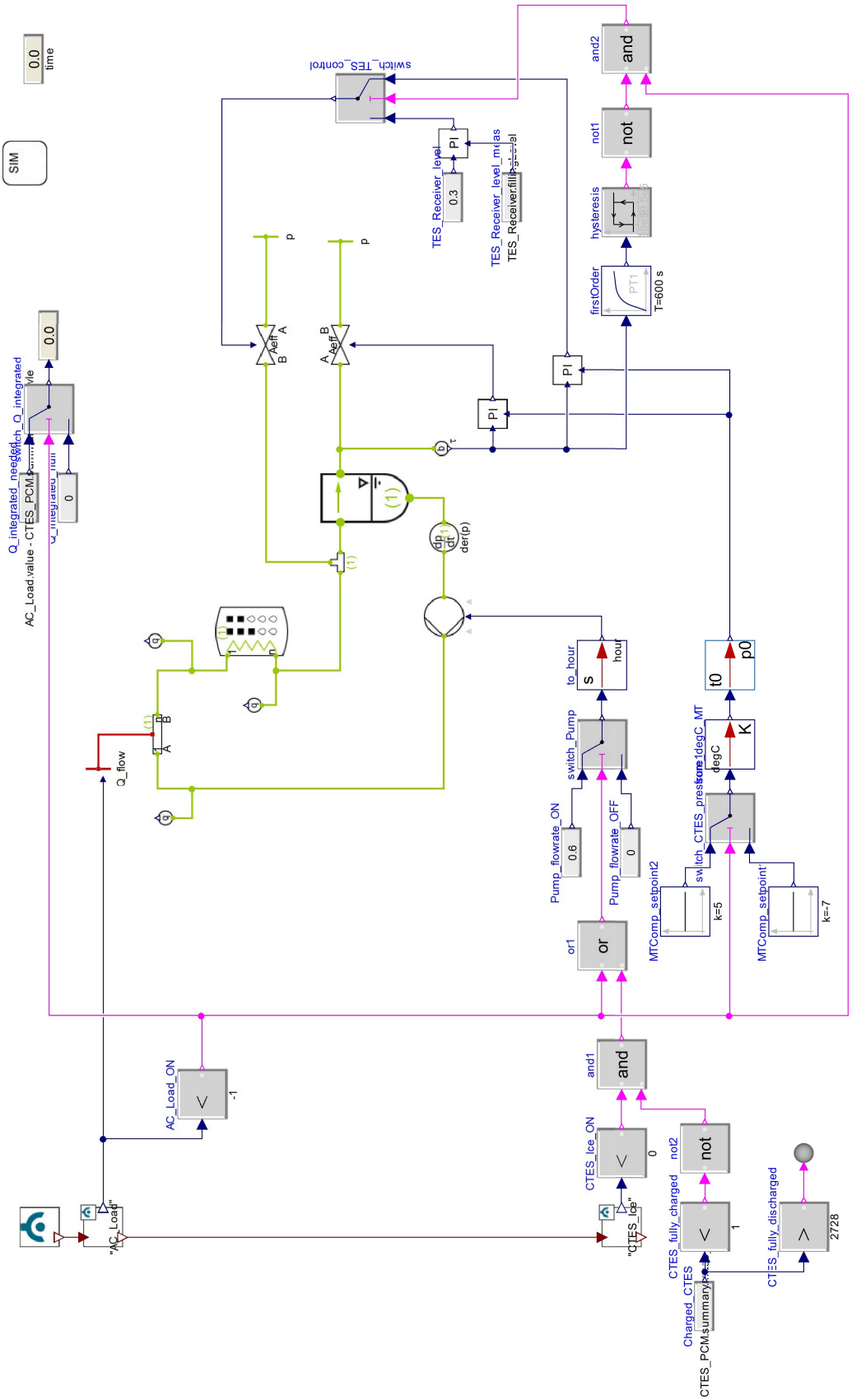

Figure 3.15: Dymola model of the TES-AC system

Furthermore, the model underwent tests in the discharging mode. A constant AC demand of 10, 20, and 30 kW was applied, starting with the PCM-CTES fully charged and an initial temperature of $-1°C$. These evaluations provided insights into the system's behavior and performance in varying operational scenarios.

3.4.1.1 AC load curves

Two daily simulations were conducted, each employing distinct load curves representing an average summer day and the hottest day. Hourly values of the air temperature were obtained from Norsk klimaservicesenter [3], meteorological station of Mjøndalen - Orkidehøgda (SN26790). The 23th of June 2023 was utilized to represent an average day, with a maximum outdoor temperature of $26,7°C$. Additionally, the 16th of June 2023 was selected to represent the hottest day, marked by a peak outdoor air temperature of $31,2°C$.
The cooling load curve, obtained by the linear interpolation of hourly values, was determined using the Formula 3.5, following the AHU scheme installed in REMA 1000 and provided by Aircoil, and considering the listed criteria:

- outdoor temperature of the 16th and 23th of June 2023 for the hottest and average day respectively
- indoor shop temperature = $23°C$. It corresponds to the return air temperature T_{return}.
- constant air volume flow rate $\dot{V} = 15000m^3/h$
- cooling needed when the outdoor temperature is higher than $21°C$
- air recirculation rate $RC_{air} = 50\%$ when the outdoor temperature is higher than the indoor shop temperature. The temperature after the mixing is calculated with Formula 3.2
- efficiency of the wheel heat exchanger for heat recovery $\varepsilon = 0,8$. The fresh air temperature after the recovery is calculated with Formula 3.3
- supply air temperature with decreasing linear trend as the outdoor temperature increases. When the outdoor temperature is $30°C$ and $21°C$, the supply air temperature is $18°C$ and $21°C$, respectively. The line function is shown in Formula 3.4. The supply air temperature was considered to be lower than the real one to take into account the latent heat for de-humidification

[3] `https://klimaservicesenter.no/`

$$T_{mix} = T_{return} \cdot \frac{RC_{air}}{100} + T_{recovery} \cdot \left(1 - \frac{RC_{air}}{100}\right) \tag{3.2}$$

$$T_{recovery} = T_{return} \cdot \varepsilon + T_{amb} \cdot (1 - \varepsilon) \tag{3.3}$$

$$T_{supply} = 28 - \frac{1}{3} \cdot T_{amb} \tag{3.4}$$

$$\dot{Q}_{AC} = \frac{\dot{V}}{3600} \cdot \rho \cdot c_{p,air} \cdot (T_{mix} - T_{supply}) \tag{3.5}$$

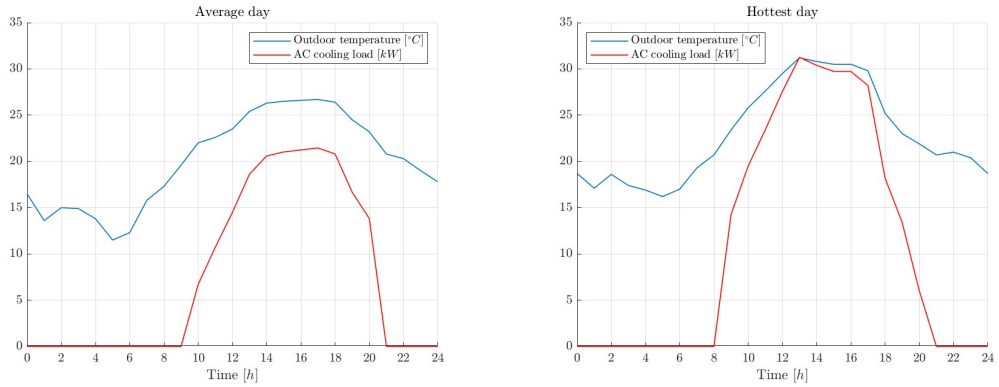

(a) Average day: 23/06/2023 (b) Hottest day: 16/06/2023

Figure 3.16: Outdoor ambient temperature and AC load during the average day and the hottest day

3.4.2 Overall refrigeration system

A simulation model of the entire system was developed in Dymola with certain simplifications, starting from the model of Selvnes et al. (2023) [62]. The TES-AC system was included as an evaporator operating at the MT pressure to simulate the CTES charging process. This simplification is feasible because during the discharging mode, when the AC is requested, the TES-AC system can work independently as a separate system without relying on the refrigeration system's assistance. This CTES evaporator experiences a variable load during the night and has no load (0 kW) during the day. The variable cooling load is obtained from the TES-AC system model during charging mode. The primary aim of this model is to determine the amount of electrical energy required during the day and the compressors' power absorption.
By setting the CTES charging load to 0, the model simulates the existing system. Consequently, the existing system is assessed under identical conditions.

The Dymola model is visible in Figure 3.19 at the end of this section.

3.4.2.1 Compressors

The compressors models were parameterized according to the dimensioning provided by Carrier and based on the correlations from Bitzer's selection software [4].

For the MT level, there are four compressors, with only one 4PTE-7K compressor being variable speed (frequency regulated). The LT level employs a single 2MME-1K compressor, which is also variable speed. The remaining compressors operate as on-off compressors. Key details of the compressors are summarized in Table 3.6.

The LT compressor's speed is regulated through a PI controller to maintain a constant LT pressure corresponding to an evaporation temperature of $-30°C$. Similarly, the speed of the MT compressors is controlled by a PI controller and a compressor controller. Their aim is to ensure a constant MT pressure, corresponding to an evaporation temperature of $-7°C$. The MT compressor controller determines the running compressors based on their maximum power, the presence of frequency regulation, and the valid sets of active compressors shown in Table 3.8. Nominal, minimum, and maximum frequencies for the compressors are provided in Table 3.7.

	Quantity [−]	Application level [−]	Maximum power input $[kW]$	Nominal Displacement (1450 RPM 50Hz) $[m^3/h]$
4KTE-10K	2	MT	12,9	9,6
4PTE-7K	2	MT	8,2	4,3
2MME-1K	1	LT	1,4	1,73

Table 3.6: Compressors general data

	N° of frequency regulated compressors over the total [−]	Nominal frequency $[Hz]$	Minimum frequency $[Hz]$	Maximum frequency $[Hz]$
4KTE-10K	0/2	50	-	-
4PTE-7K	1/2	50	30	70
2MME-1K	1/1	50	40	70

Table 3.7: Variable speed compressors and frequencies

[4] `https://www.bitzer.de/websoftware/`

		4PTE-7K	4PTE-7K	4KTE-10K	4KTE-10K
variable speed		yes	no	no	no
sets	1	false	false	false	false
	2	true	false	false	false
	3	true	true	false	false
	4	true	false	true	false
	5	true	true	true	false
	6	true	true	true	true

Table 3.8: Sets of valid active compressors implemented in the MT compressor controller

The mass flow rate and the power consumption were calculated using Formulas 3.6 and 3.7. In the case of non-frequency-regulated compressors, the correction factors f_m and f_p are equal to 1, otherwise their values are determined using Formulas 3.8 and 3.9. $\dot{m}_{nom}$ and P_{nom} are respectively the mass flow rate and the power consumption at nominal frequency ($n_{nom} = 50\ Hz$) and they are evaluated with Formulas 3.10 and 3.11 in case of transcritical compressor (all the MT compressors), and with Formulas 3.12 and 3.13 in case of subcritical compressor (LT compressor).

The volumetric and isentropic efficiencies are calculated with Formulas 3.14, 3.15, respectively. The efficiency of the electric motor driving the compressor is $\eta_{el} = 0,95$. Table 3.9 shows the correlation coefficients of the different compressor models, meanwhile, the coefficients related to the correction factor due to frequency regulation are displayed in Table 3.10.

$$\dot{m} = \dot{m}_{nom} \cdot \frac{30 \cdot n - 50}{1450} \cdot f_m \tag{3.6}$$

$$P = P_{nom} \cdot \frac{30 \cdot n - 50}{1450} \cdot \frac{f_m}{f_p} \tag{3.7}$$

$$\begin{aligned} f_m = {} & n \cdot \left(x_1 + \frac{p_{disch}}{p_{suct}} \cdot x_2 \right) \\ & + \left(x_3 + \frac{p_{disch}}{p_{suct}} \cdot x_4 \right) \cdot \left(1 + \frac{x_5 \cdot n^2 + x_6 \cdot n + x_7}{100} \right) \\ & + n \cdot (x_8 + T_{evap} \cdot x_9) \\ & + (x_{10} + T_{evap} \cdot x_{11}) \cdot \left(1 + \frac{x_{12} \cdot n^2 + x_{13} \cdot n + x_{14}}{100} \right) \end{aligned} \tag{3.8}$$

Compressor model	4KTE-10K	4PTE-7K	2MME-1K
c_1	9,4379E+02	4,0617E+02	1,1852E+00
c_2	3,1350E+01	1,2453E+01	-9,1308E-03
c_3	-3,2325E+00	-1,7208E+00	-3,1156E-05
c_4	4,1044E-01	1,7893E-01	-1,9148E-01
c_5	-8,8688E-02	-2,0393E-02	6,1915E-03
c_6	-2,8954E-03	3,1430E-03	-1,4123E-05
c_7	7,5339E-04	2,0385E-03	9,7494E-03
c_8	-1,4935E-03	-1,3230E-04	-8,9484E-04
c_9	6,6640E-07	2,7443E-07	6,4073E-06
c_{10}	2,9681E-05	3,4813E-07	0
k_1	-8,8331E+00	-3,8220E+00	5,1888E-02
k_2	-4,4333E-01	-1,5675E-01	3,0142E-02
k_3	3,5929E-01	1,6161E-01	7,7603E-05
k_4	-5,7911E-03	-1,3578E-03	-5,8310E-06
k_5	6,0502E-03	1,8982E-03	-3,4230E-02
k_6	-1,9206E-03	-8,8663E-04	8,7064E-04
k_7	-1,6937E-05	-5,4642E-06	1,1447E-05
k_8	2,0671E-05	-4,0804E-06	-6,5593E-07
k_9	-1,1536E-05	-1,6725E-06	-8,2445E-04
k_{10}	4,7663E-06	2,1889E-06	5,7400E-06
k_{11}	0	0	3,0228E-07
k_{12}	0	0	-1,9697E-08
k_{13}	0	0	-5,2411E-06
k_{14}	0	0	-3,0605E-09
k_{15}	0	0	1,7871E-09
k_{16}	0	0	-2,0361E-10

Table 3.9: Coefficient of the compressors correlations related to the mass flow rate and the power consumption of the three different models considered

x_1	6,5298E-03
x_2	3,1584E-03
x_3	8,3215E-01
x_4	-1,0981E-01
x_5	1,1962E-02
x_6	1,9104E-01
x_7	1,3258E+01
x_8	-5,0370E-03
x_9	3,6175E-05
x_{10}	-1,6738E-02
x_{11}	-4,5199E-05
x_{12}	8,1590E-01
x_{13}	8,5193E-02
x_{14}	1,3260E+01

(a) Coefficients for the mass flow rate correction factor

z_1	2,3634E-04
z_2	6,9372E-03
z_3	9,4123E-01
z_4	-1,7483E-01
z_5	1,5371E-02
z_6	1,1320E+00
z_7	1,3052E+01
z_8	-1,1329E-02
z_9	-9,9241E-05
z_{10}	-2,3117E-02
z_{11}	2,0169E-04
z_{12}	6,9955E-01
z_{13}	-1,3517E-01
z_{14}	1,3257E+01

(b) Coefficients for the power consumption correction factor

Table 3.10: Coefficients of the correction factors related to the frequency regulation for all the compressors

$$\begin{aligned} f_p = n \cdot & \left(z_1 + \frac{p_{disch}}{p_{suct}} \cdot z_2 \right) \\ & + \left(z_3 + \frac{p_{disch}}{p_{suct}} \cdot z_4 \right) \cdot \left(1 + \frac{z_5 \cdot n^2 + z_6 \cdot n + z_7}{100} \right) \\ & + n \cdot (z_8 + T_{evap} \cdot z_9) \\ & + (z_{10} + T_{evap} \cdot z_{11}) \cdot \left(1 + \frac{z_{12} \cdot n^2 + z_{13} \cdot n + z_{14}}{100} \right) \end{aligned} \tag{3.9}$$

$$\begin{aligned} \dot{m}_{nom,transcr} = & (c_1 + c_2 \cdot T_{evap} + c_4 \cdot p_{disch} + c_4 \cdot T_{evap}^2 + c_5 \cdot T_{evap} \cdot p_{disch} \\ & + c_6 \cdot p_{disch}^2 + c_7 \cdot T_{evap}^3 + c_8 \cdot T_{evap}^2 \cdot p_{disch} \\ & + c_9 \cdot T_{evap} \cdot p_{disch}^2 + c_{10} \cdot p_{disch}^3)/3600 \end{aligned} \tag{3.10}$$

$$\begin{aligned} P_{nom,transcr} = & k_1 + k_2 \cdot T_{evap} + k_4 \cdot p_{disch} + k_4 \cdot T_{evap}^2 + k_5 \cdot T_{evap} \cdot p_{disch} \\ & + k_6 \cdot p_{disch}^2 + k_7 \cdot T_{evap}^3 + k_8 \cdot T_{evap}^2 \cdot p_{disch} \\ & + k_9 \cdot T_{evap} \cdot p_{disch}^2 + k_{10} \cdot p_{disch}^3 \end{aligned} \tag{3.11}$$

$$\dot{m}_{nom,subcr} = \Bigg[(c_1 + c_2 \cdot T_{cond} + c_3 \cdot T_{cond}^2) + (c_4 + c_5 \cdot T_{cond} + c_6 \cdot T_{cond}^2) \cdot \frac{p_{disch}}{p_{suct}} + (c_7 + c_8 \cdot T_{cond} + c_9 \cdot T_{cond}^2) \cdot \left(\frac{p_{disch}}{p_{suct}}\right)^2\Bigg] \cdot \rho \cdot V \cdot 50 \tag{3.12}$$

$$\begin{aligned} P_{nom,subcr} = [&(k_1 + k_2 \cdot T_{cond} + k_3 \cdot T_{cond}^2 + k_4 \cdot T_{cond}^3) \\ &+ (k_5 + k_6 \cdot T_{cond} + k_7 \cdot T_{cond}^2 + k_8 \cdot T_{cond}^3) \cdot T_{evap} \\ &+ (k_9 + k_{10} \cdot T_{cond} + k_{11} \cdot T_{cond}^2 + k_{12} \cdot T_{cond}^3) \cdot T_{evap}^2 \\ &+ (k_{13} + k_{14} \cdot T_{cond} + k_{15} \cdot T_{cond}^2 + k_{16} \cdot T_{cond}^3) \cdot T_{evap}^3] \cdot V \cdot 50 \cdot 3600 \end{aligned} \tag{3.13}$$

$$\eta_{vol} = \frac{\dot{m}}{\rho \cdot n \cdot V} \tag{3.14}$$

$$\eta_{is} = \frac{\dot{m}_{nom} \cdot (h_{disch} - h_{suct})}{P_{nom} \cdot \eta_{el}} \tag{3.15}$$

3.4.2.2 Gas cooler

The gas cooler was modelled using a tube equipped with a heat port. A PI controller regulates the heat flux to maintain a temperature approach at the gas cooler outlet (temperature difference between CO_2 outlet and air inlet) of 3 K.

Pressure control was achieved through a HPV, managed by both a PI controller and an high pressure (HP) setpoint controller. This latter component implements equations to determine the optimal discharge pressure based on the gas cooler outlet temperature. The equations implemented are shown in Formulas 3.16, 3.17 and 3.18. The selection criteria for these equations are detailed in Table 3.11. All coefficients relevant to these equations are provided in Table 3.12.

$T_{gc,out} < T_{subcr,max}$	Formula 3.16
$T_{subcr,max} < T_{gc,out} < T_{transcr,min}$	Formula 3.17
$T_{gc,out} > T_{transcr,min}$	Formula 3.18

Table 3.11: Temperature ranges defining the use of the equations for the optimum discharge pressure

$$p_{HP,setpoint} = max(A_2 \cdot (T_{gc,out} + T_{sc})^2 + A_1 \cdot (T_{gc,out} + T_{sc}) + A_0;\ p_{min}) \tag{3.16}$$

$$\begin{aligned} p_{HP,setpoint} = {} & (A_2 \cdot T_{subcr,max}^2 + A_1 \cdot T_{subcr,max} + A_0 + T_{sc}) \\ & + \frac{(T_{gc,out} - T_{subcr,max})}{(T_{transcr,min} - T_{subcr,max})} \cdot (73,77 - (A_2 \cdot T_{subcr,max}^2 \\ & + A_1 \cdot T_{subcr,max} + A_0 + T_{sc}) \end{aligned} \tag{3.17}$$

$$\begin{aligned} p_{HP,setpoint} = {} & min(73,77 - TC_2 \cdot (T_{gc,out} - T_{transcr,min})^2 \\ & + TC_1 \cdot (T_{gc,out} - T_{transcr,min});\ p_{max}) \end{aligned} \tag{3.18}$$

T_{sc}	$1°C$
$T_{subcr,max}$	$24°C$
$T_{transcr,min}$	$29°C$
p_{min}	$50\ bar$
p_{max}	$120\ bar$
TC_1	$2,6\ bar/K$
TC_2	$0\ bar/K^2$
A_0	$35,27573\ bar$
A_1	$0,953944\ bar/K$
A_2	$0,007873\ bar/K^2$

Table 3.12: Parameters, coefficients and their values used on the equations of the HP setpoint controller for the optimum discharge pressure of the gas cooler

3.4.2.3 Ethylene glycol loop evaporator

The evaporator for the mono-ethylene glycol (MEG) loop is modelled using a tube equipped with a heat port. The value of the heat flux depends on the system that is being simulated. For the integrated TES-AC system, the heat flux is set at zero. Conversely, for the MEG circuit system, the heat flux aligns with the AC load values during both average and hottest day, as depicted in Figure 3.16.

The pressure within this evaporator matches that of the liquid receiver, thereby resulting in an evaporation temperature of $5°C$.

3.4.2.4 Liquid receiver

The liquid receiver separates the vapor and liquid fractions after the expansion through the HPV and after the partial evaporation within the MEG circuit evaporator, if operational. A FGBV regulates the pressure within this component. The vapor fraction is flashed to the MT compressors to maintain a constant pressure of 40 *bar*, while the liquid fraction is directed towards the MT and LT evaporators.

3.4.2.5 Internal heat exchanger

The internal heat exchanger (IHX) is modelled using a plate heat exchanger in which the flashed vapor and the liquid, both coming from the liquid receiver, exchange heat. During this process, the liquid undergoes subcooling, while the vapor experiences superheating. To calculate the heat transfer coefficients for both refrigerant sides, the "1-Phase: Gnielinski Dittus Boelter" model, described in Section 3.4.1, was employed. The IHX was discretized into 10 elements for each pathway. Relevant geometric parameters of the IHX are detailed in Table 3.13 and are visually represented in Figure 3.17.

Total number of plates	30
Plate length	250 mm
Plate width	110 mm
Pattern angle	$35°C$
Wall thickness	$0,75$ mm
Pattern amplitude	2 mm
Pattern wave length	$12,6$ mm

Table 3.13: Internal heat exchanger geometry data

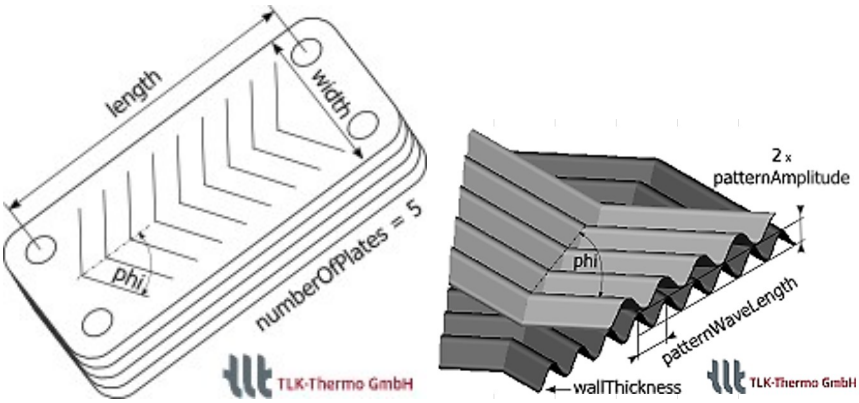

Figure 3.17: Geometry parameters of the internal heat exchanger

3.4.2.6 MT and LT evaporators

The MT and LT evaporators were represented by tubes equipped with heat ports. The values of the MT and LT loads are graphically shown in Figure 3.18. It is worth to remember that the demo supermarket has plug-in freezers, resulting in low LT capacity, needed just for the main cold storage room.
The mass flow rates are regulated through expansion valves controlled according to superheat. The superheating setpoint is equal to 8 K for both the MT and LT evaporators.
In the scenario where the TES-AC system integrated within the booster system is simulated, an additional load is introduced to the MT evaporator. This additional load encompasses the CTES charging load and the capacity required for integration when the storage is either empty or incapable of fully covering the AC load.

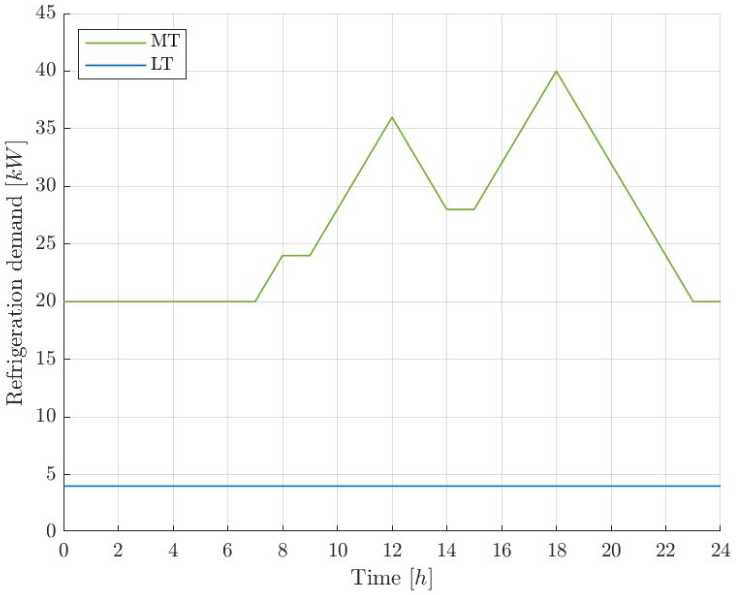

Figure 3.18: MT and LT capacity loads during both the considered days

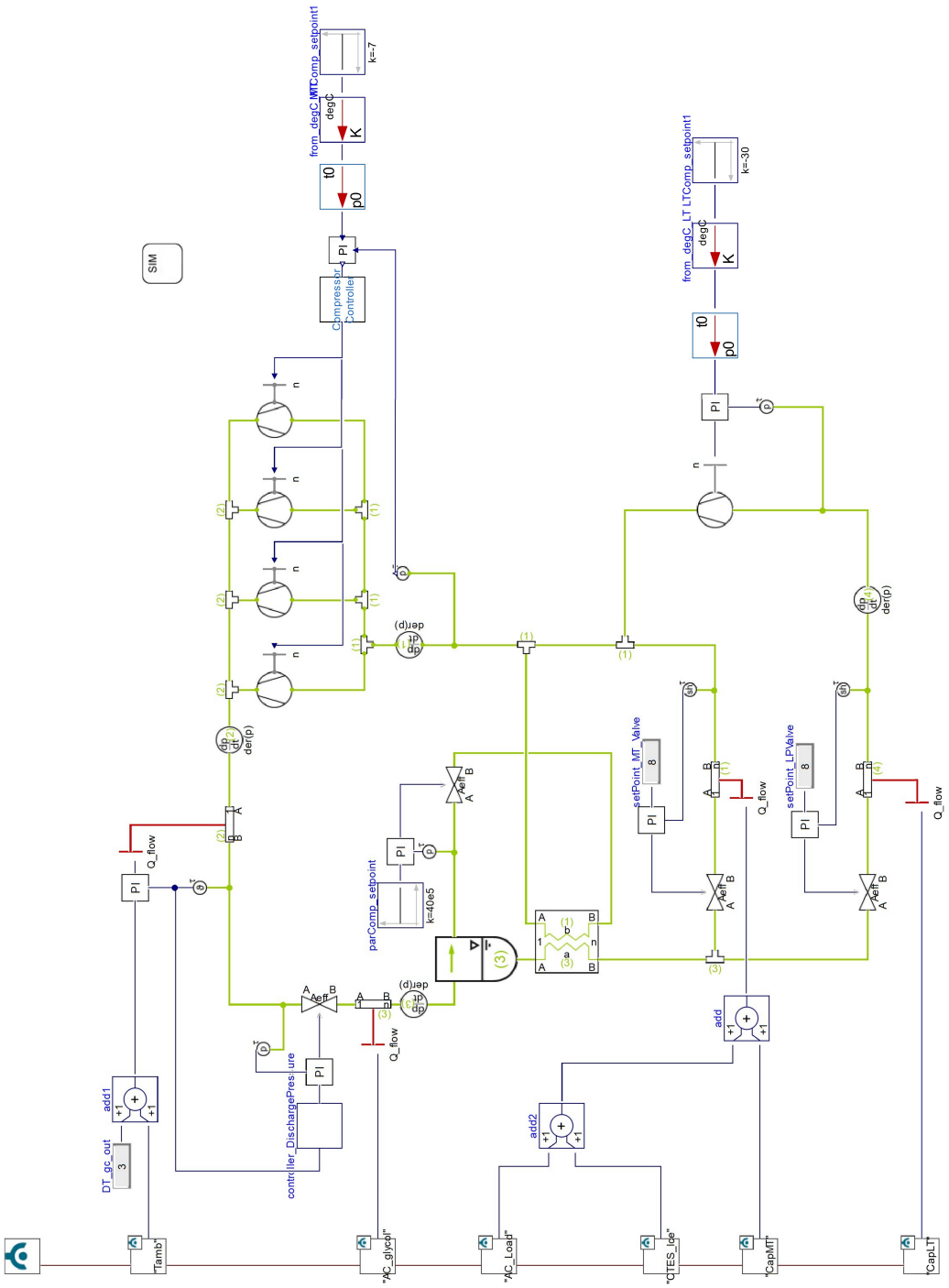

Figure 3.19: Dymola model of the the CO_2 booster system

3.5 Economical analysis

An electricity cost analysis was performed to assess potential cost benefits. Two approaches to electricity pricing were employed: one considering that the supermarket purchases electricity at the market spot price, and the other based on a tariff pricing system.
In the first approach, the hourly electricity prices were taken into account and linearly interpolated. The values of the electricity prices in Oslo during the two considered days were obtained from the Nord Pool database [5]. The resulting price curves for both the average and the hottest day are graphically shown in Figure 3.20.

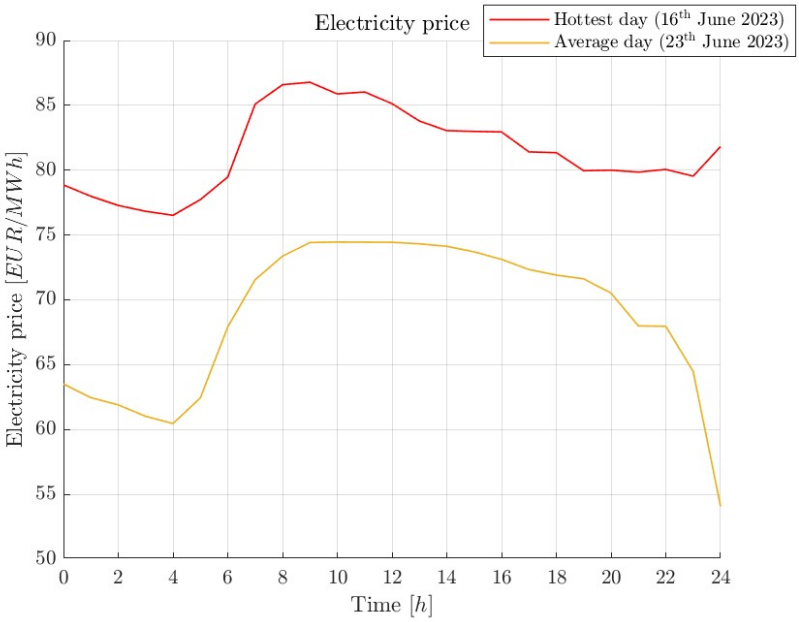

Figure 3.20: Electricity price in the two considered days

In the second approach, the supermarket's electricity purchase was considered within a tariff structure characterized by hourly rates. Three hourly tariff categories were considered as follows:

- −20% on the daily average price during the night time 23:00-7:00
- daily average price during the hours 7:00-8:00 and 19:00-23:00
- +20% on the average price during day time 8:00-19:00

[5] `https://www.nordpoolgroup.com/en/Market-data1/Dayahead/Area-Prices/`

Results

In this chapter, the results are presented. In the "AHU evaporator coil design results" section, the outcomes of the evaporator coil design are shown, and one configuration is selected. The "TES-AC system results" section illustrates and described the simulation results of the TES-AC system. In the final section, "Overall refrigeration system results", the outcomes of the simulations for both the proposed and existing system are displayed and compared.

4.1 AHU evaporator coil design results

The results of the simulations in HXsim are presented in Table 4.1. The volume flow rate of refrigerant is calculated based on saturated liquid conditions at a pressure of 40 *bar* (evaporation temperature $5,3°C$). In these conditions, the density is $894,05\ kg/m^3$.

		2R-1C	2R-2C	3R-2C
outlet air temperature	$[°C]$	19,02	18,93	17,67
outlet relative humidity	[%]	69,65	69,5	71,9
outlet specific humidity	[%]	9,55	9,47	9,05
cooling capacity	$[kW]$	32,74	34,18	45,95
refrigerant mass flow	$[kg/h]$	734,04	684,36	996,48
refrigerant volume flow	$[m^3/h]$	0,821	0,765	1,115
pressure drop	$[bar]$	4,475	0,644	1,716
temperature drop	$[°C]$	4,21	0,63	1,66

Table 4.1: HXsim results related to the three different configuration investigated

The configuration with 2 rows and 2 circuits (2R-2C) was selected to achieve a balanced trade-off between temperature/pressure drop and performance. The 3 rows and 2 circuits configuration (3R-2C) resulted in excessive cooling capacity, indicating over-design. Conversely, the 2 rows and 1 circuit (2R-1C) configuration resulted in an undesirably high temperature/pressure drop.

The designed heat exchanger is able to supply a cooling capacity of $34,18\ kW$ with a corresponding refrigerant mass flow rate of $684,36\ kg/h$, equivalent to a volume flow rate of saturated liquid at the evaporating pressure of 40 *bar* amounting to $0,765\ m^3/h$.
All the geometry parameters of the chosen heat exchanger are listed below:

- 2 circuit
- 2 rows
- 26 tubes per row
- width = 2085 mm
- height = 1160 mm
- length = 300 mm
- tube horizontal pitch = 36,64 mm
- tube vertical pitch = 40 mm
- tube 16,5x1 mm (external diameter x thickness)
- finned length = 1870 mm
- finned height = 1080 mm
- fin spacing = 5 mm

4.2 TES-AC system results

In this section, the results of the simulations of the TES-AC system are shown. They are divided into 4 groups: charging mode, discharging mode, average day and hottest day.

4.2.1 Charging mode

The charging time and the average heat flow rate were evaluated with numerous simulations where the volume flow rate of the pump was varied. It is important to note that, in the Dymola model of the TES-AC system, the pump operates with a constant volume flow rate.
As the refrigerant flow rate increases, the charging time shortens, but a higher heat flow rate is demanded. The relationship between charging time and flow rate shows a distinct hyperbolic trend, whereas the trend in average heat flow rate follows a logarithmic pattern. These trends are visually represented in Figure 4.1.
For a complete charge within a single night (8 hours), the system necessitates a refrigerant volume flow rate higher than $0,6\ m^3/h$ with a minimum average capacity requirement of 30 kW. If a partial charge is required, the system can restore the full charge in less than one night or achieve it within 8 hours using a lower flow rate, thus requiring less capacity.
Employing a volume flow rate of 1 m^3/h allows the CTES to be charged in 6 hours with a capacity of 45 kW. It is important to highlight that the system does not necessarily need to operate at a refrigerant volume flow rate exceeding 1 m^3/h since achieving a complete charge within less than one night is not the primary goal. Additionally, given the use of excess compressor capacity to charge the storage, it is crucial to verify whether the CO_2 refrigeration system is able to supply the required freezing capacity.
The mass of liquid PCM and the discharge status of the CTES are shown in Figure 4.2 with different refrigerant volume flow rates throughout the charging process. The full charging time of the CTES is determined when the mass of liquid PCM reaches zero and thus also the discharge level.
In Figure 4.1, the average heat flow rate was taken into consideration, as it is not a constant factor throughout the charging process. Figure 4.3 shows the requested charging capacity at varying constant refrigerant volume flow rates. Initially, the heat flow rate remains relatively constant, but after a certain period, it rapidly decreases. This decline can be attributed to the

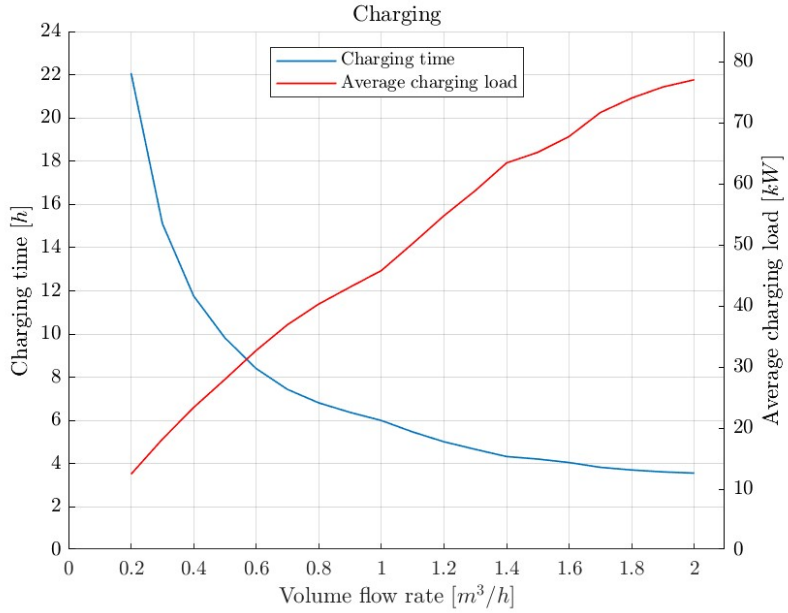

Figure 4.1: Charging time and average heat flow rate vs refrigerant volume flow rate

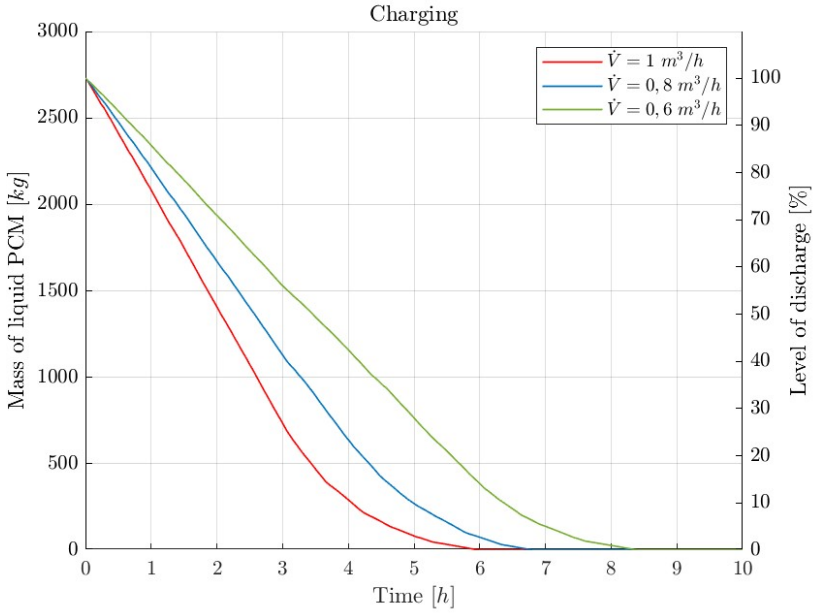

Figure 4.2: Liquid PCM and discharge level vs time varying the refrigerant volume flow rate

thermal conductivity of the PCM and its non-uniform freezing behavior. As depicted in Figure 4.4, the refrigerant is unable to vaporize completely, and this phenomenon leads to a reduction in the average heat transfer coefficient (HTC) on the refrigerant side, as evident in Figure 4.5.

It is worth noting that the vapour quality is typically defined within the range of 0 to 1, but in Figure 4.4 values exceeding 1 are observed. This is not an error,

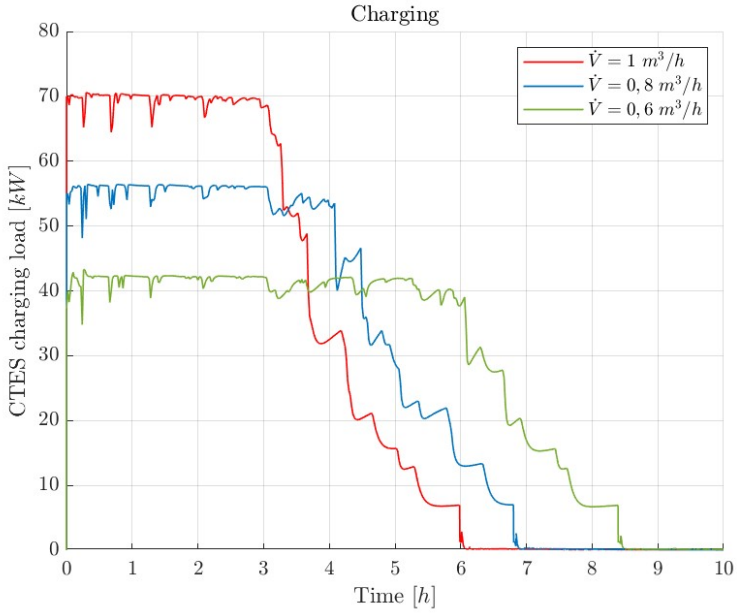

Figure 4.3: Instant CTES charging capacity required during the charging process with different volume flow rates

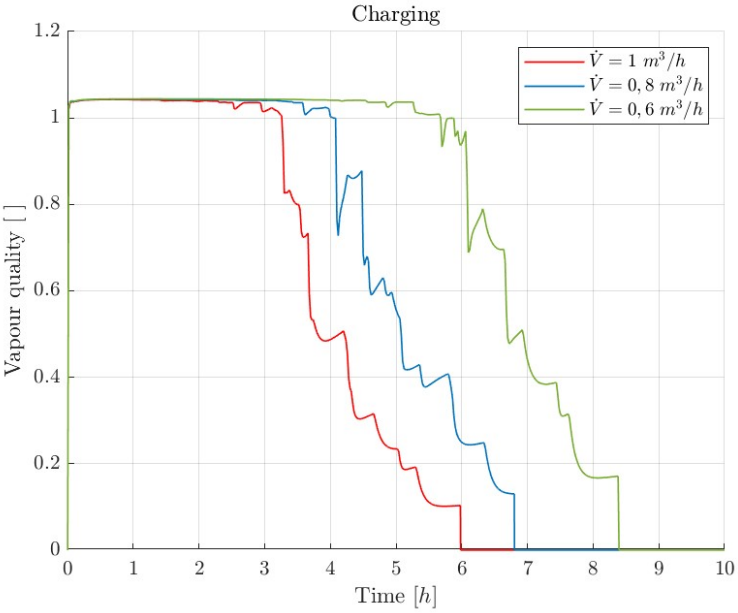

Figure 4.4: Vapour quality of the refrigerant at the PP-HX outlet during the charging process with different volume flow rates

but rather a representation method used by the simulation software to indicate that the vapor is in a superheated state. Indeed, the software calculates the vapour quality with the enthalpies, which can result in values greater than one in such cases.

The average HTC of the refrigerant is displayed in Figure 4.5. It increases with the volume flow rate and decreases as the vapour quality diminishes. The

initial increasing trend is attributed to the nature of average HTC: initially, the refrigerant vaporizes in the first part of the PP-HX, but as freezing progresses and the water in the first section solidifies, vaporization occurs later and the evaporation is prolonged along the path. Same considerations hold true for the decreasing trend when the vapour quality decreases: the refrigerant partially evaporates later in the path due to the presence of frozen water in the initial part of the PP-HX. As a matter of fact, the HTCs of vapour only and liquid only are lower than the one of a two-phase mixture.
The non-uniform freezing of the PCM becomes evident in Figure 4.6. The PCM temperature of the first discretization block along the refrigerant path drops below the freezing point of water ($0°C$) in less than an hour, indicating solidification. Conversely, the PCM in the last discretization block freezes after hours of charging operation.

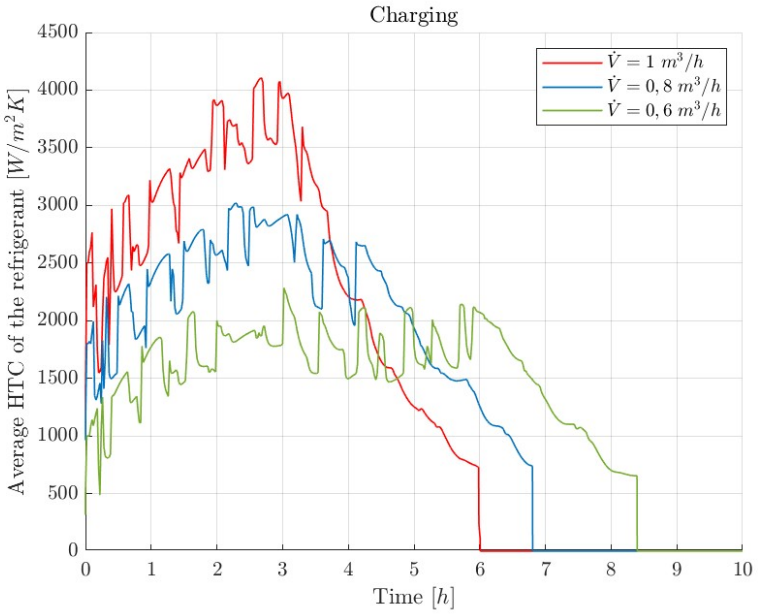

Figure 4.5: Average HTC of the refrigerant side during the charging process with different volume flow rates

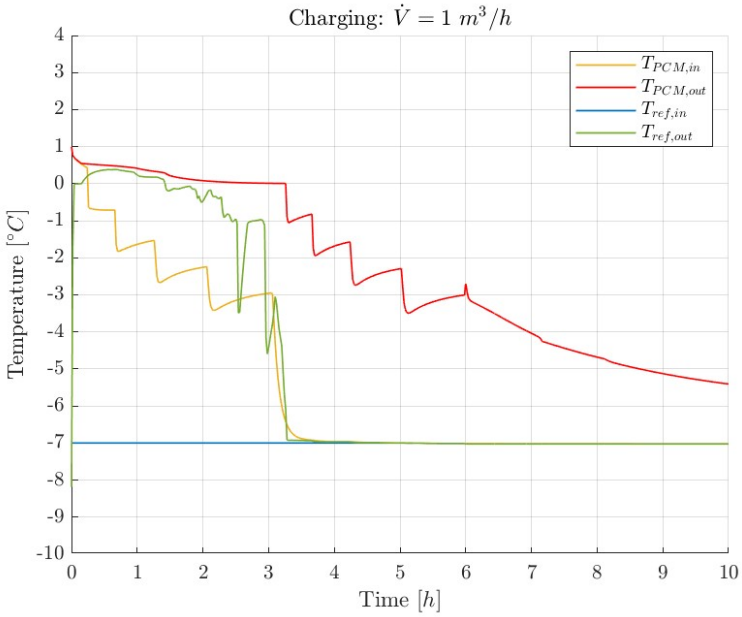

(a) Charging with volume flow rate equal to 1 m^3/h

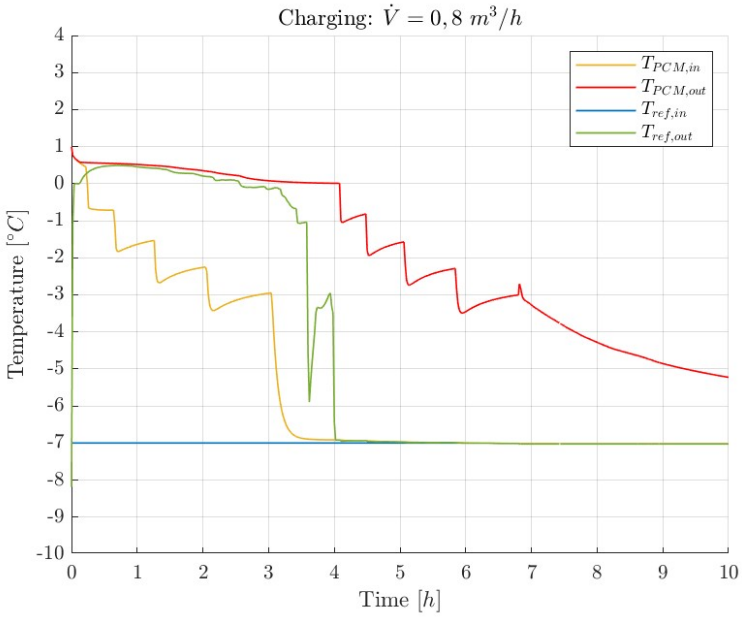

(b) Charging with volume flow rate equal to $0,8\ m^3/h$

Figure 4.6: Temperature of the refrigerant at the inlet and outlet of the PP-HX, and average temperature of the PCM in the first and last discretization block along the refrigerant, during charging

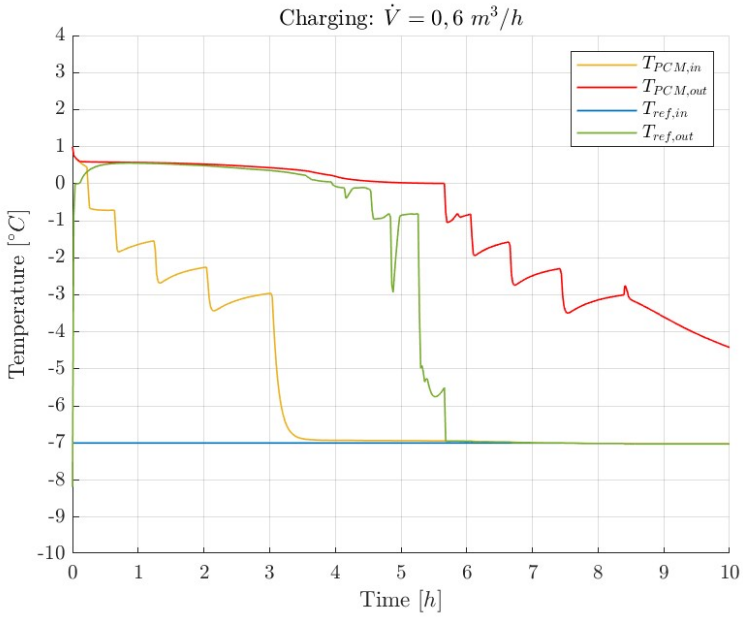

(c) Charging with volume flow rate equal to $0,6\ m^3/h$

Figure 4.6: Temperature of the refrigerant at the inlet and outlet of the PP-HX, and average temperature of the PCM in the first and last discretization block along the refrigerant, during charging

4.2.2 Discharging mode

The mass of liquid PCM and the discharge status of the CTES are presented in Figure 4.7 under different AC loads and refrigerant volume flow rates during the discharging process. The volume flow rate was varied alongside the AC load to maintain constant refrigerant vapor quality at the evaporator outlet, and thus at the inlet of the PP-HX, across the three distinct tests.
The discharge process is considered complete when the mass of liquid PCM equals the total mass, meaning that all the ice has melted. Consequently, this status denotes a discharge level of 100%.

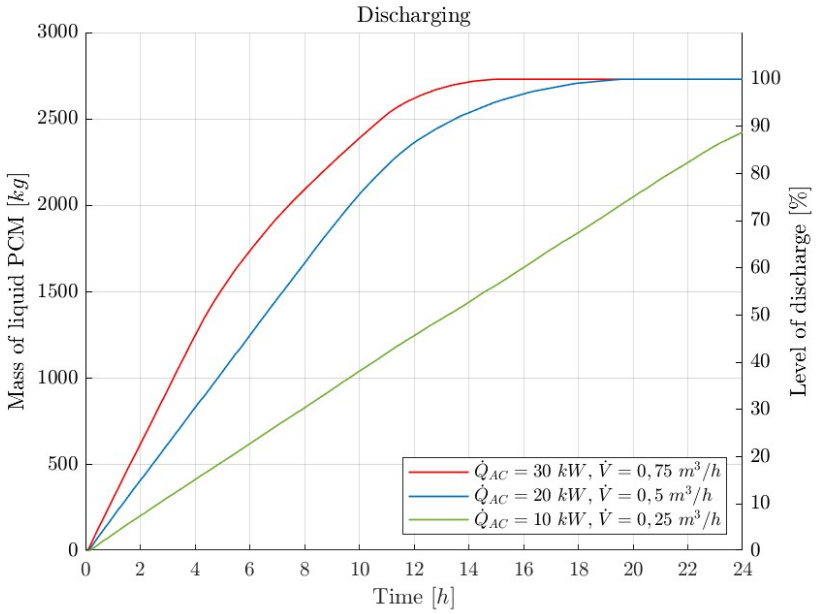

Figure 4.7: Liquid PCM and discharge level vs time varying the AC loadd

The discharge capacity that the CTES can provide during the discharging process under different constant AC loads is shown in Figure 4.8. The CTES is capable of entirely covering a demand of 30 kW for 4 hours, 20 kW for 8 hours and 10 kW for 22 hours. Beyond these durations, the CTES continues to provide capacity but lower than the requested load: for 16 hours with a load of 30 kW, for 21 hours with a load of 20 kW, and for more than a day with a load of 10 kW.
The decreasing trend is attributed to the thermal conductivity of the PCM and its non-uniform melting behavior, as illustrated in Figure 4.12. Therefore, the refrigerant is unable to condense completely, as evident in Figure 4.9.
The average HTC of the refrigerant is shown in Figure 4.10. It increases with the volume flow rate, primarily due to the higher velocity within the channels. Additionally, the HTC grows alongside the vapour quality and the

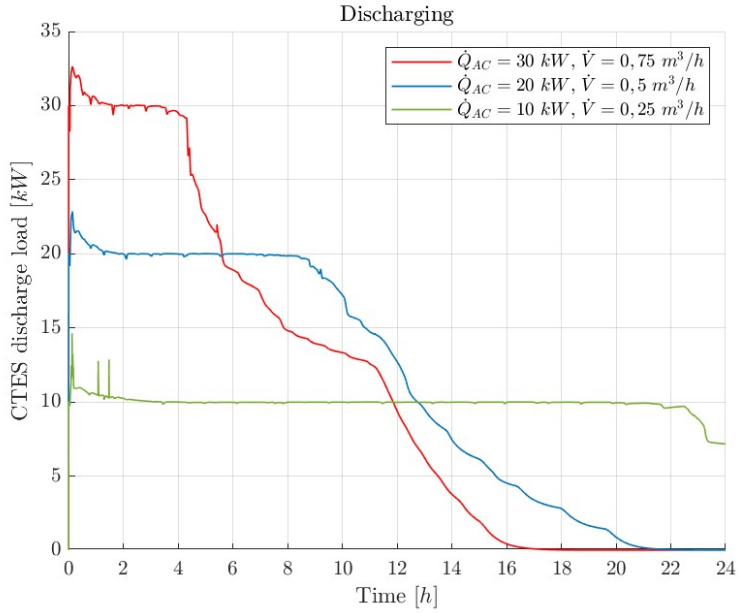

Figure 4.8: Instant CTES discharging capacity supplied during the discharging process with different AC constant loads

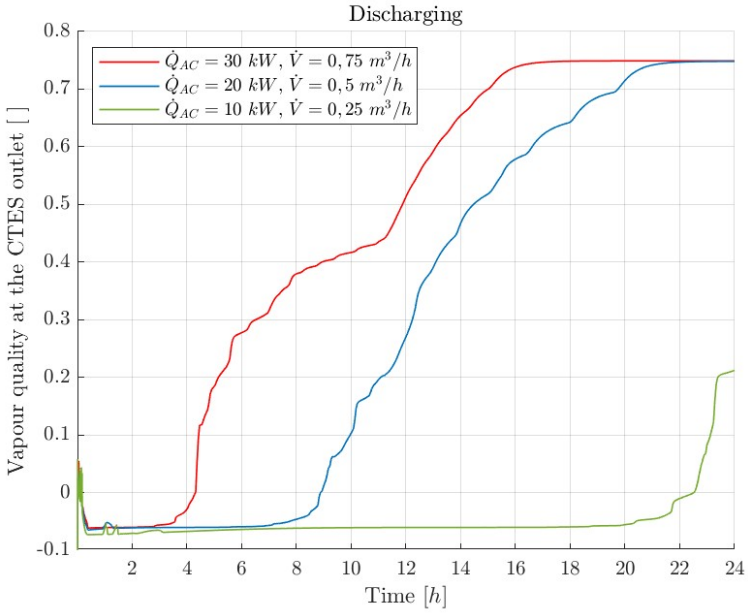

Figure 4.9: Vapour quality of the refrigerant at the PP-HX outlet during the discharging process with different AC constant loads

level of discharge of the CTES. This increasing trend is justified by the fact that the vapour has lower density compared to the liquid phase. Therefore, when operating with constant volume flow rate, the velocity inside the channels increases, resulting in a higher HTC.

As seen in Figure 4.8, the CTES becomes gradually unable to entirely cover the AC load. The remained capacity, which is plotted in Figure 4.11 for various

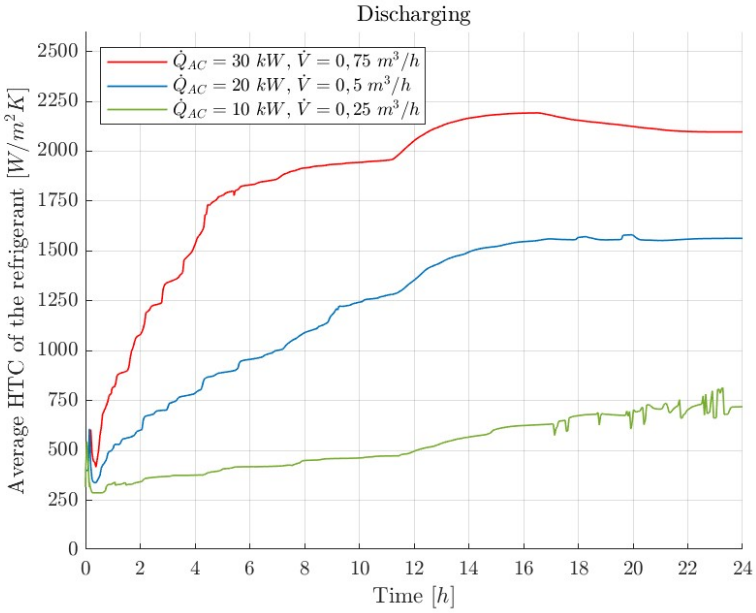

Figure 4.10: Average HTC of the refrigerant side during the discharging process with different AC constant loads

constant AC loads, needs to be integrated by the main refrigeration system by providing additional liquid refrigerant to the TES-AC system.

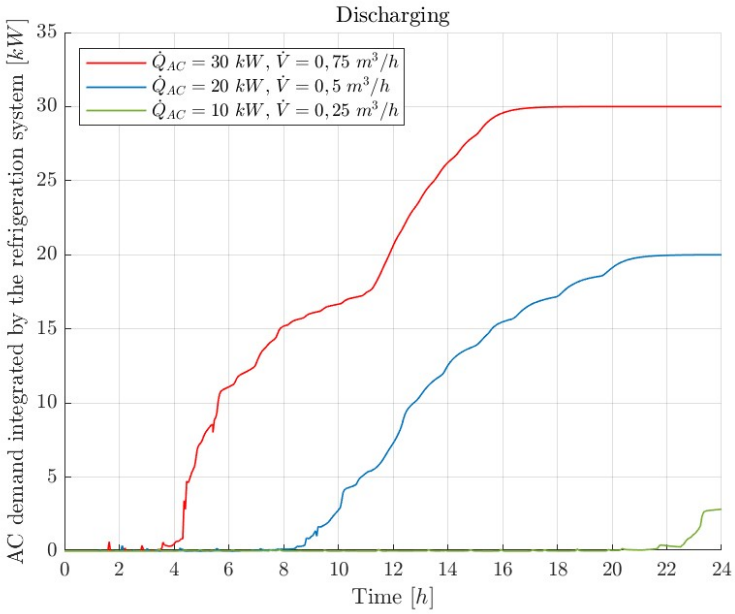

Figure 4.11: Capacity integrated by the main refrigeration system during the discharging process with different AC constant loads

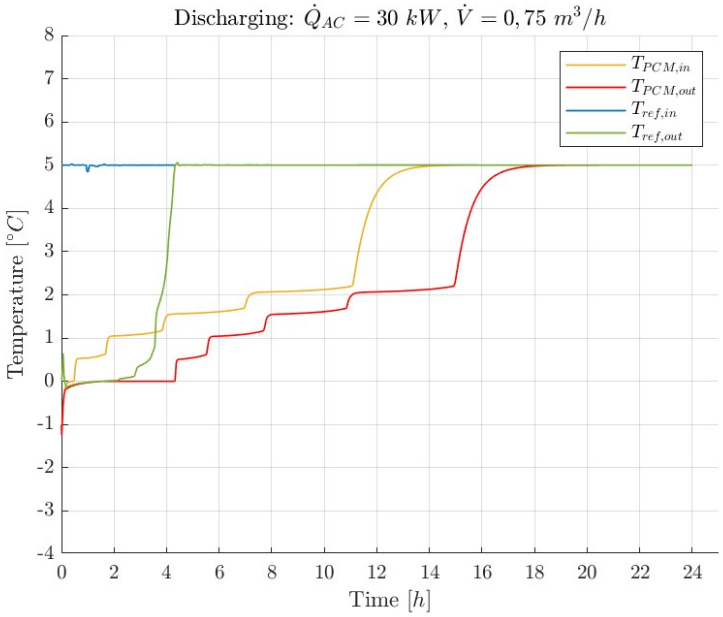

(a) Discharging with AC load equal to 30 kW

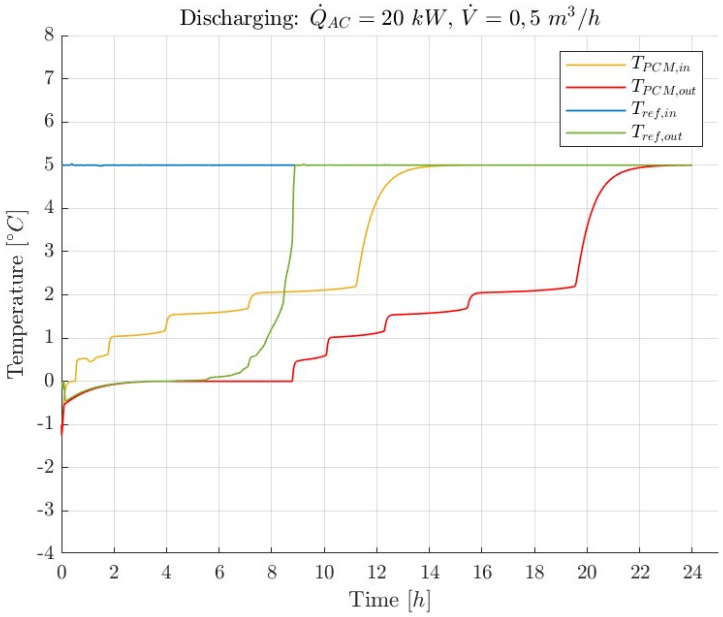

(b) Discharging with AC load equal to 20 kW

Figure 4.12: Temperature of the refrigerant at the inlet and outlet of the PP-HX, and average temperature of the PCM in the first and last discretization block along the refrigerant, during discharging

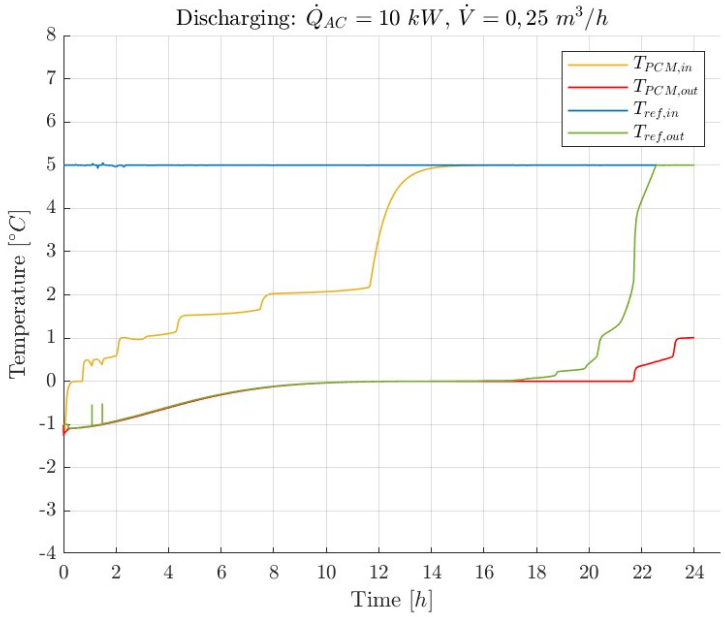

(c) Discharging with AC load equal to 10 kW

Figure 4.12: Temperature of the refrigerant at the inlet and outlet of the PP-HX, and average temperature of the PCM in the first and last discretization block along the refrigerant, during discharging

4.2.3 Average day

During the average day considered, just $71,41\%$ of the PCM experiences the phase change, as indicated in Figure 4.13.
The full charge condition of the CTES is restored during the entire night (8 hours), with the pump working at volume flow rate of $0,35\ m^3/h$.

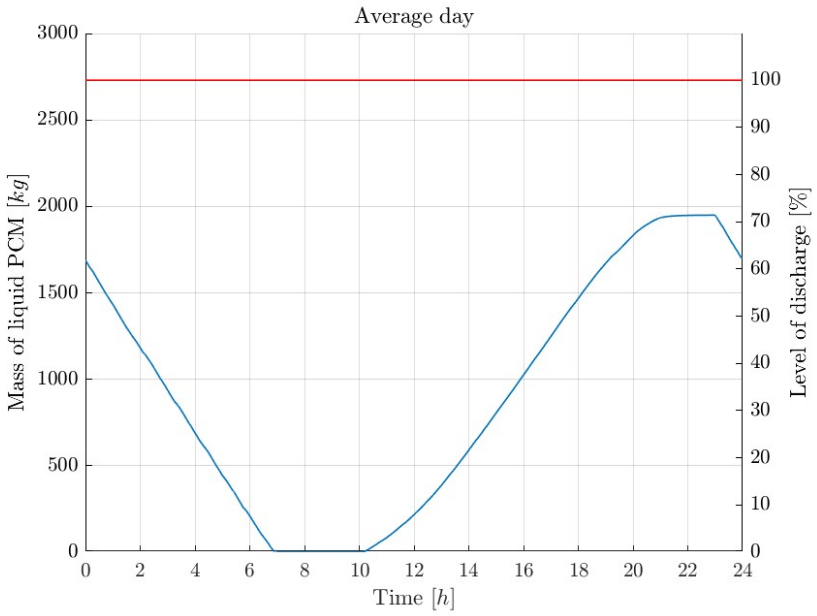

Figure 4.13: Liquid PCM and discharge level during the average day

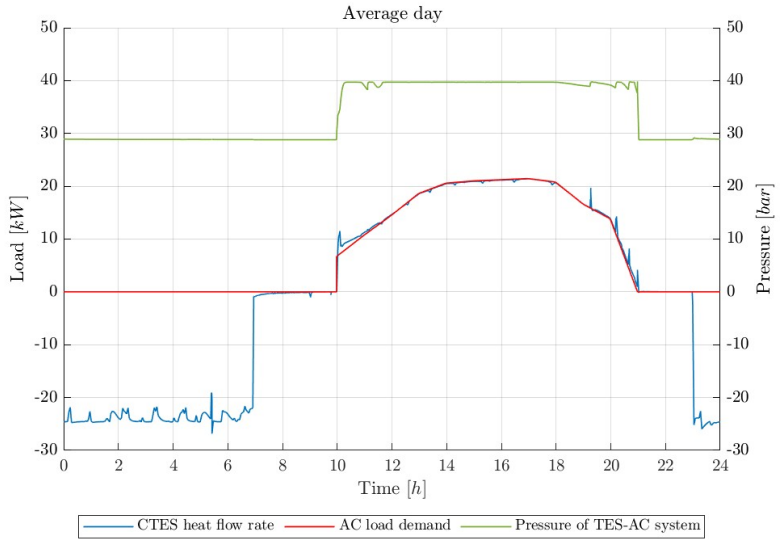

Figure 4.14: Charging and discharging load of the CTES, AC load demand and pressure of the system during the average day

The charging and discharging loads of the CTES are visualized, in terms of CTES heat flow rate throughout the average day, in Figure 4.14. Within

the same graph, the AC load and the pressure of the system are displayed. Remarkably, the AC load is completely supplied by the CTES. Instead, the charging process requires an average capacity of 24 kW.
Since the CTES fully covers the AC load, the TES-AC system can function as a separate system, resulting in the closure of the connection valves with the main system. Moreover, the pressure can be increased, thereby achieving an evaporation temperature of $7 - 9°C$. This adjustment can be reached by initially operating the system in direct AC mode, once the connection valves are fully closed. Consequently, vapor generation inside the circuit leads to a pressure increase. The evaporator can still meet the required AC load since it is operating under a partial load conditions, but the maximum capacity with this refrigerant temperature has to be evaluated. Moreover, the heat exploitation at the CTES is enhanced.

4.2.4 Hottest day

On the hottest day considered, only $90,44\%$ of the PCM undergoes the phase change, as shown in Figure 4.15. This indicates that the system does not fully exploit all the stored energy in the CTES.
The full charge condition of the CTES is restored during the entire night (8 hours), with the pump working at volume flow rate of $0,5\ m^3/h$.

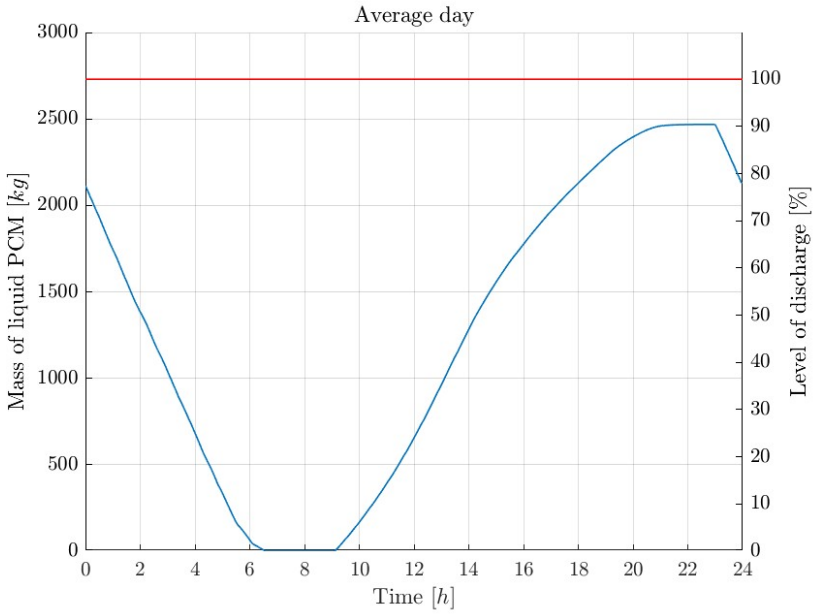

Figure 4.15: Liquid PCM and discharge level during the hottest day

The charging and discharging loads of the CTES are plotted, as CTES heat flow rate throughout the hottest day, in Figure 4.16. In the same graph, the AC load and the pressure of the system are displayed. The CTES is unable to entirely cover the AC load, instead the charging process requires an average capacity of 35 kW. Even though the CTES does not fully meet the AC load, it still manages to supply nearly 60% of it. As a result, the main refrigeration system needs to integrate part of the load by providing liquid refrigerant to the TES-AC system.
The load demand integrated by the main refrigeration system is shown in Figure 4.17, both in terms of capacity $[kW]$ and percentage of load requested [%].

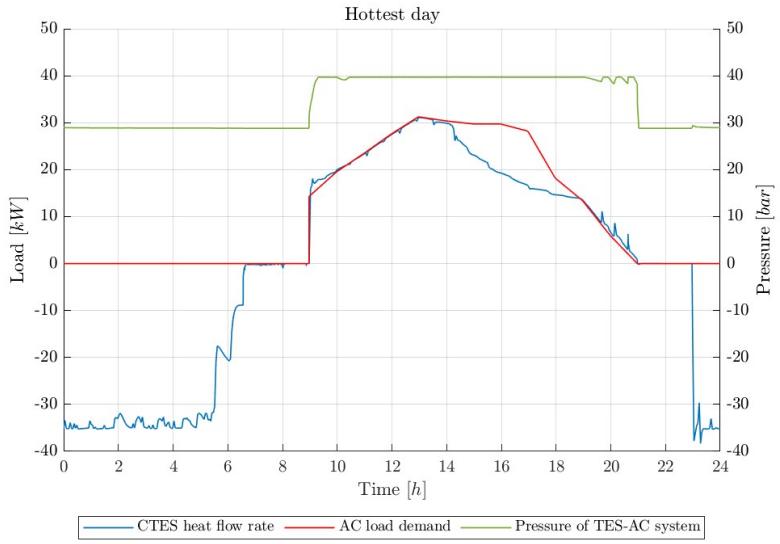

Figure 4.16: Charging and discharging load of the CTES, AC load demand and pressure of the system during the hottest day

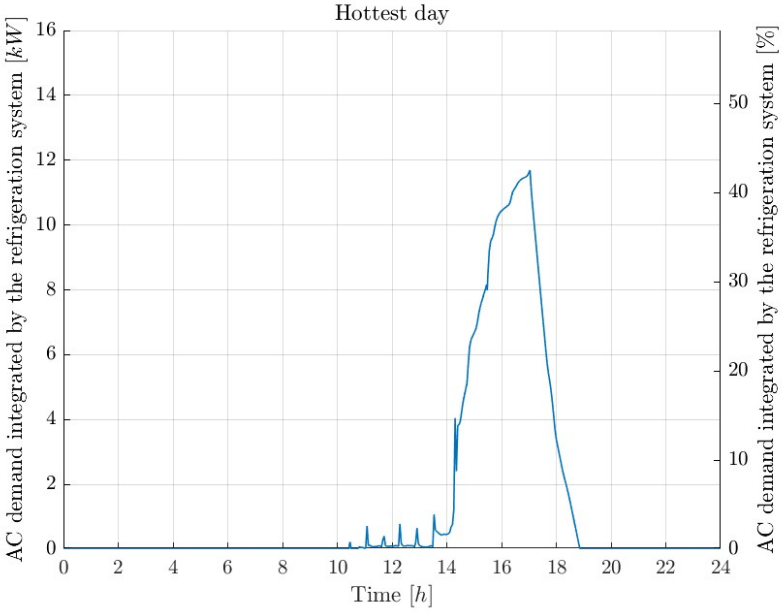

Figure 4.17: AC load demand integrated by the refrigeration system in absolute values on the right axis, and in percentage of load requested on the left axis

4.3 Overall refrigeration system results

In the following section, the results of the simulations for both the existing glycol loop-based system (referred to as the "glycol system") and the proposed system with the CTES (referred to as the "CTES system") are presented and compared. These results are divided into average and hottest day.

4.3.1 Average day

The total load demand, as sum of the MT, LT and AC loads, is shown in Figure 4.18 for both the glycol and CTES system. The CTES system clearly enables load shifting and peak reduction with respect to the instantaneous AC production of the glycol system. Specifically, the maximum load demand of the glycol system is $68,78\ kW$, while the CTES system presents a lower value of $47,79\ kW$, leading to a significant reduction of $30,52\%$ in peak load demand. However, these concepts need to be further examined taking into account the systems performances.

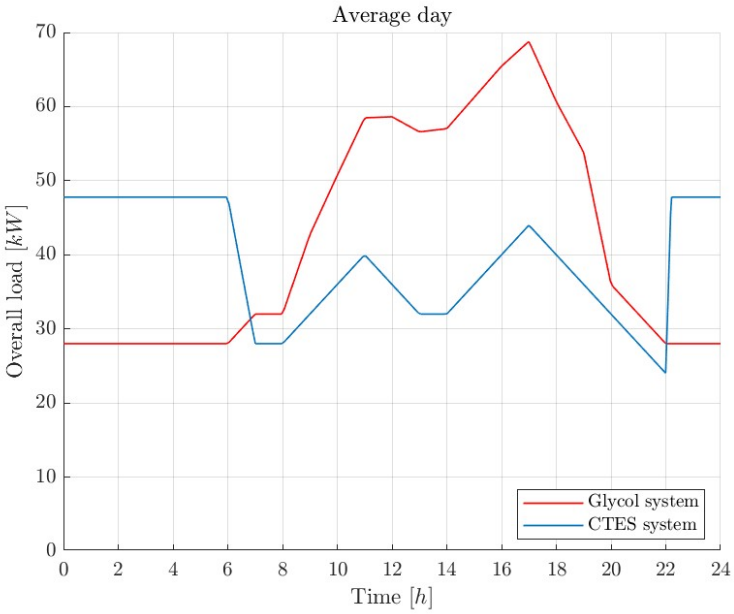

Figure 4.18: Total load demand of the glycol and CTES systems during the average day

The COP of the systems is visible in Figure 4.19. In general, the CTES system demonstrates a higher COP than the glycol system during the night, but slightly lower COP during the day.
The increase in the COP during the night is attributed to the compressor operating at full load with enhanced efficiency in comparison to the glycol

system. Conversely, the decrease in the COP is observed during the daytime as the CTES system operates at partial load in warm outdoor conditions. Instead, the glycol system displays better performance during daytime, given that the compressors operate at higher loads, resulting in improved efficiencies. Compressors efficiencies are reported in Figure F.1 in Appendix F.

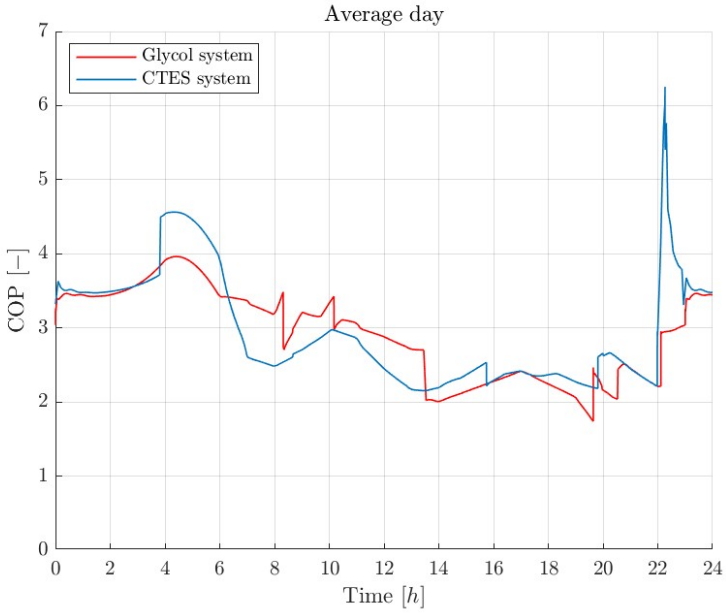

Figure 4.19: Coefficient of performance of the glycol and CTES systems during the average day

The power absorption of the compressors in the two investigated systems is compared in Figure 4.20. The CTES system achieves significant peak shaving, with a clear reduction of the peak power absorption by $30,93\%$. In absolute terms, it is reduced from $28,72\ kW$ with the glycol system to $19,83\ kW$ with the CTES system. Load shifting is also accomplished, with an increase in electrical consumption during the night by $74,75\%$ and a reduction during the day by $22,94\%$. During the night, electrical consumption represents $31,06\%$ of the overall daily consumption with the CTES, compared to $16,57\%$ with the glycol system. This is visible in Figure 4.21, which displays the cumulative power consumption of the two systems over the entire day. The CTES system exhibits a much more linear consumption profile. Conversely, the glycol system experiences an increase in consumption during the daytime due to the instantaneous AC production. Energy savings are achieved by producing and storing the energy required for the AC demand during the night when the system benefits from a higher COP due to lower outdoor temperatures. For the average day considered, the energy saving amounts to $6,75\%$.

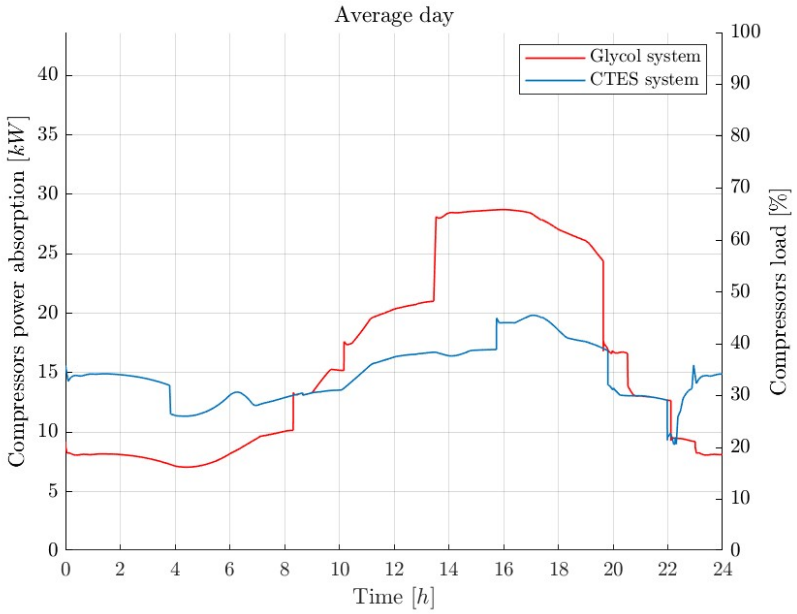

Figure 4.20: Compressors power absorption of the glycol and CTES systems during the average day

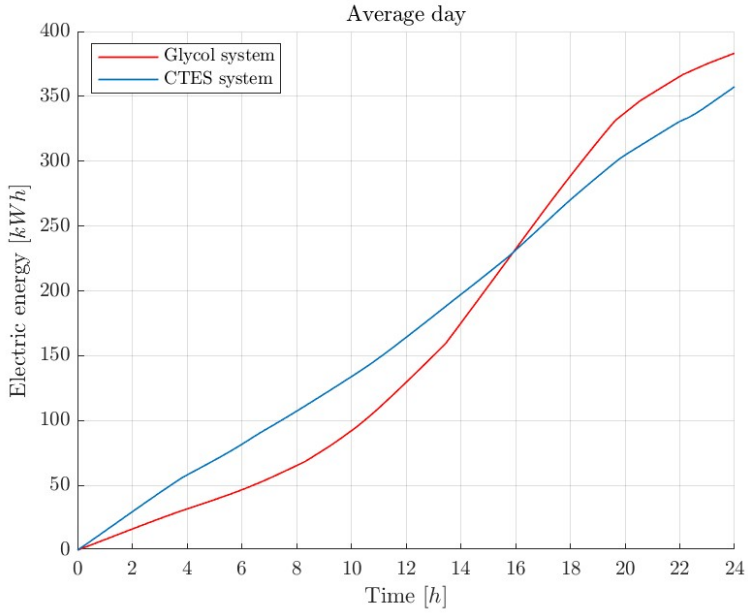

Figure 4.21: Cumulated electrical consumption of the glycol and CTES systems during the average day

Since the peak shaving and load shifting are successfully achieved in the average day, one of the compressors 4KTE-10K no longer contributes to the operation, as shown in Figure 4.22, where the compressor frequency is plotted [1].
The frequencies of the compressors are reported in Figure E.1 in Appendix E.

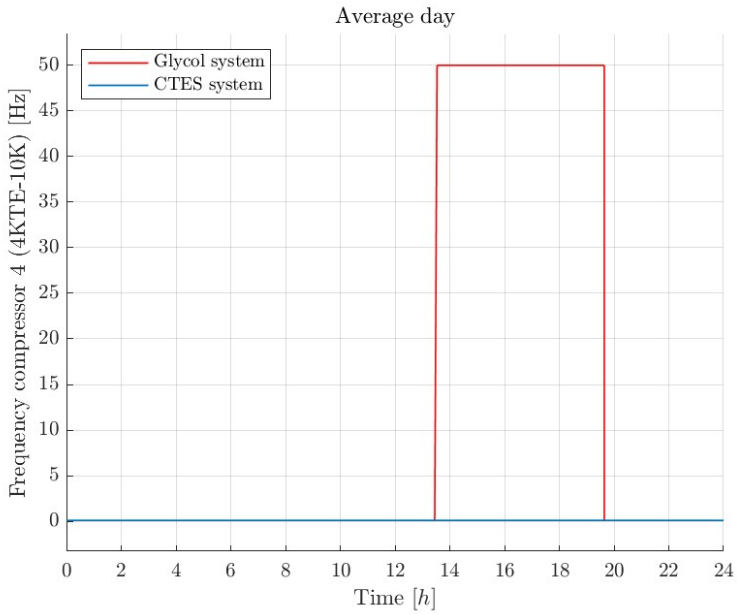

Figure 4.22: Frequency of the compressor n.4 (4KTE-10K) during the average day

[1] frequency equal to 0 Hz means that the compressor is turned off

4.3.2 Hottest day

The total load demand, as sum of the MT, LT and AC loads, is shown in Figure 4.23 for both the glycol and CTES system. The CTES system clearly enables for load shifting and peak reduction compared to the instantaneous AC production of the glycol system. Specifically, the maximum load demand of the glycol system is $76,72\ kW$, while the CTES system presents a lower value of $58,34\ kW$, leading to a significant reduction of $23,97\%$ in peak load demand. However, these concepts need to be further examined taking into account the systems performances.

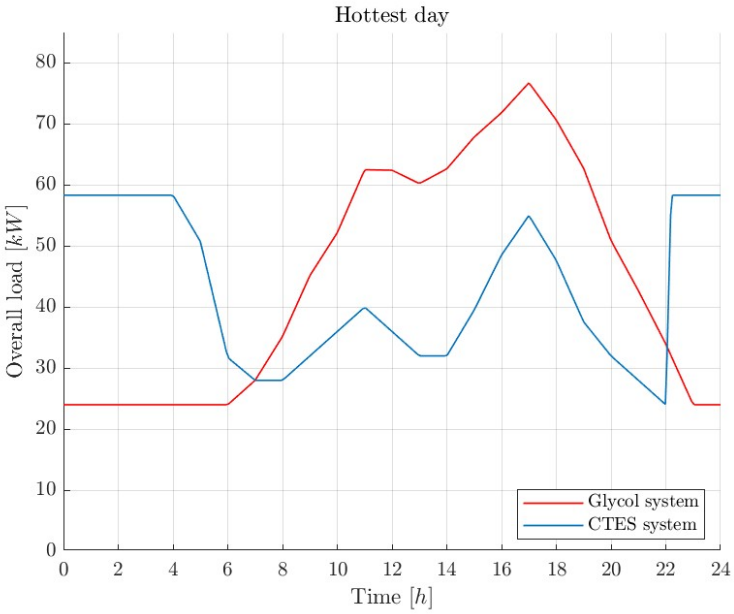

Figure 4.23: Total load demand of the glycol and CTES systems during the hottest day

The COP of the systems is visible in Figure 4.24. Generally, the CTES system demonstrates a higher COP than the glycol system during the night, but slightly lower COP during the day.
The increase in the COP during the night is attributed to the compressor operating at full load with enhanced efficiency in comparison to the glycol system. Conversely, the decrease in the COP is observed during the daytime as the CTES system operates at partial load in warm outdoor conditions. Instead, the glycol system displays better performance during daytime, given that the compressors operate at higher loads, resulting in improved efficiencies. Compressors efficiencies are reported in Figure F.2 in Appendix F.
The power absorption of the compressors in the two investigated systems is compared in Figure 4.25. The CTES system achieves significant peak shaving,

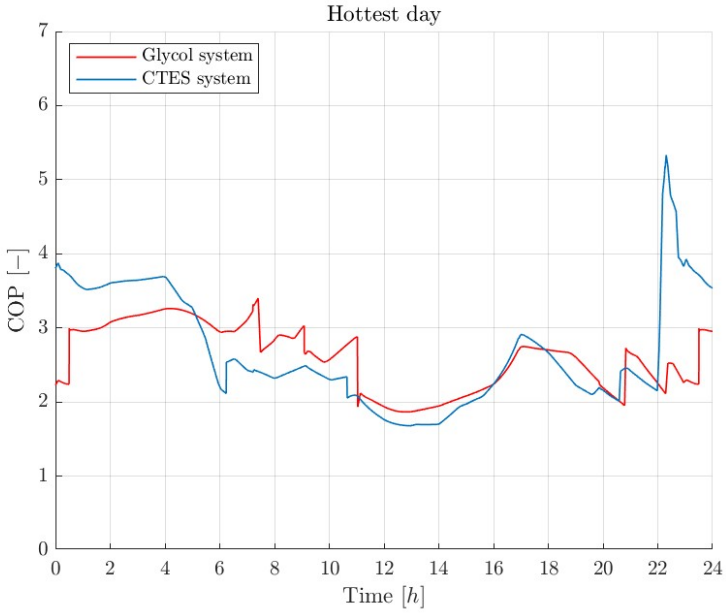

Figure 4.24: Coefficient of performance of the glycol and CTES systems during the hottest day

with a clear reduction of the peak power absorption by $32,33\%$. In absolute terms, it is reduced from $34,87\ kW$ with the glycol system to $23,6\ kW$ with the CTES system. Load shifting is also accomplished, with an increase in electrical consumption during the night by $72,27\%$ and a reduction during the day by $28,03\%$. During the night, electrical consumption represents $31,53\%$ of the overall daily consumption with the CTES, compared to $16,14\%$ with the glycol system. This is visible in Figure 4.26, which displays the cumulative power consumption of the two systems over the entire day. The CTES system exhibits a much more linear consumption profile. Conversely, the glycol system experiences an increase in consumption during the daytime due to the instantaneous AC production. Energy savings are achieved by producing and storing the energy required for the AC demand during the night when the system benefits from a higher COP due to lower outdoor temperatures. For the hottest day considered, the energy saving amounts to $11,84\%$.

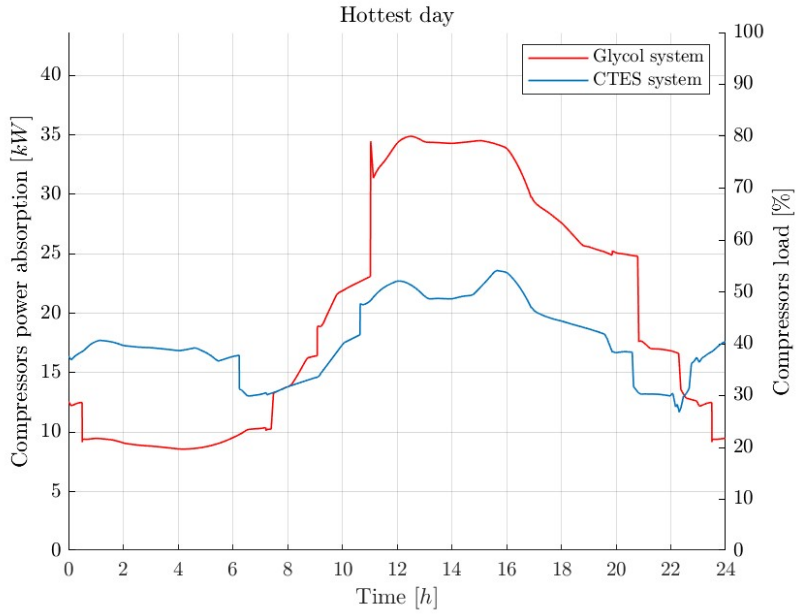

Figure 4.25: Compressors power absorption of the glycol and CTES systems during the hottest day

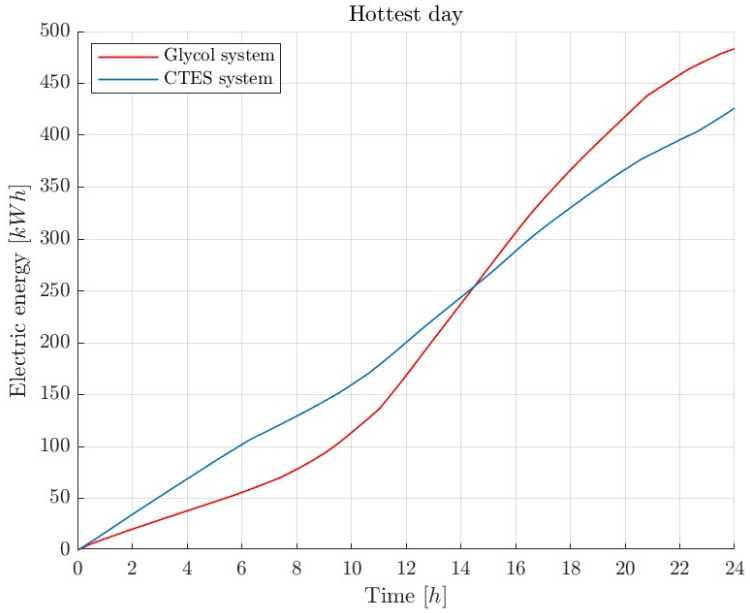

Figure 4.26: Cumulated electrical consumption of the glycol and CTES systems during the hottest day

Since the peak shaving and load shifting are successfully achieved in the hottest day, one of the compressors 4KTE-10K no longer contributes to the operation, as shown in Figure 4.27, where the compressor frequency is plotted [2].
The frequencies of the compressors are reported in Figure E.2 in Appendix E.

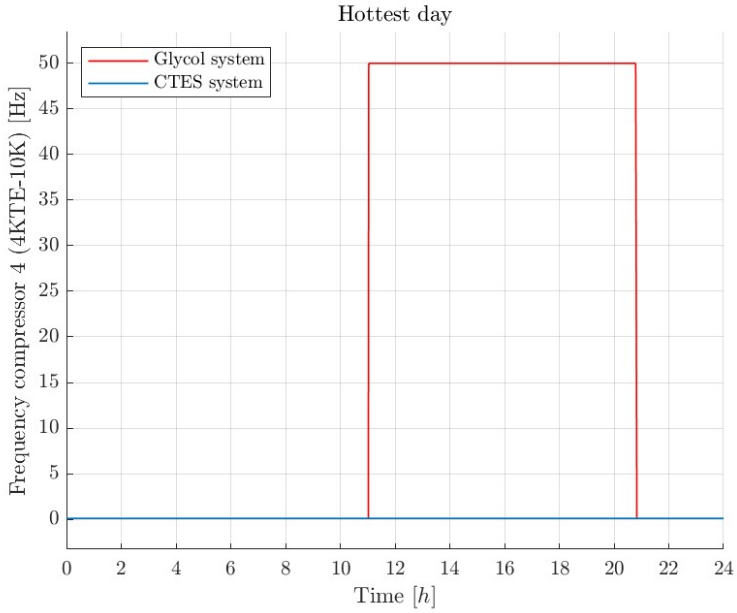

Figure 4.27: Frequency of the compressor n.4 (4KTE-10K) during the hottest day

[2] frequency equal to 0 Hz means that the compressor is turned off

4.4 Economical analysis results

The comparison of the electricity costs on the average and hottest day, considering the spot pricing system, is shown in Table 4.2. Additionally, the comparison taking into account the tariff pricing system is shown in Table 4.3. An electricity cost reduction is achieved in all scenarios. On the hottest day, the reduction is more pronounced compared to the average day, owing to the increased energy demand for AC in both of the evaluated pricing systems. If the supermarket purchases electricity under the assumed tariff scheme, there is an increase in both the absolute and percentage reduction, making the system much more economically advantageous.

	CTES system	Glycol system	Difference	Reduction
	[€]	[€]	[€]	[%]
Average day	24,84	27,20	2,36	8,67
Hottest day	34,78	39,78	5,00	12,56

Table 4.2: Electricity cost comparison in the two simulated days, considering the spot pricing system

	CTES system	Glycol system	Difference	Reduction
	[€]	[€]	[€]	[%]
Average day	25,77	29,15	3,38	11,60
Hottest day	36,12	43,23	7,11	16,45

Table 4.3: Electricity cost comparison in the two simulated days, considering the tariff pricing system

Discussion

The system performs exceptionally well on both considered days, achieving load shifting and peak shaving of the compressors power, as demonstrated in Figures 4.20 and 4.20. The charging process is consistently completed within a single night (8 hours). Additionally, the system achieves some energy savings, although it is not the primary objective of this project.

The COP of the CTES system is generally higher than the glycol system during the night, but slightly lower during the day. Similar result was obtained by Selvnes et al. (2023) in their study [62].

On an average day, the CTES sufficiently covers the AC load demand, enabling the TES-AC system to operate independently by completely closing the connection valves with the refrigeration system. However, on the hottest days, achieving this level of independence becomes challenging, though such conditions occur only for a week throughout the summer. The AC is typically required for only 1-2 months during the entire summer, depending on the year. As a result, the system remains turned off for most of the year.

Since not all the PCM experiences melting, the CTES can be downsized. This concept must be deeply evaluated to see if this reduction affects the operation of the compressors, e.g. the possibility of removing one of them.

The peak reduction was evaluated $30,93\%$ and $32,33\%$ on the average and hottest day, respectively. Comparable results were obtained by Selvnes et al. (2023) [62] when evaluating a similar CO_2 booster system for total AC load shifting. They achieved a peak reduction of 16% in Oslo, and even higher values could be expected for a more representative week of a Norwegian summer, as they pointed out. Sevault et al. (2021) [63], studying a 200 kWh PCM heat storage integrated into a heating system of a building, found a peak reduction of up to 42%. D'Agaro et al. (2021) [64] investigated an ice-CTES for AC purposes in a CO_2 booster refrigerating unit, revealing an AC peak load reduction from 70 kW to 40 kW, but without evaluating its effect on

the compressors operation. The peak reduction varies a lot depending on the system, the dimensions of the PCM storage, and the outdoor temperature. This is why such different results are obtained in similar studies.

A critical observation regarding this system is its inability to charge the CTES when the AC is required 24/7, due to the simultaneous impossibility of charging and supplying AC. The system can only charge the CTES during periods when AC is not continuously required throughout the day. This situation is more common in warmer countries like Italy. In periods with 24/7 of AC demand, the system operates in direct AC mode. This concept needs further investigation by simulating a supermarket in a warmer climate to determine the number of days when charging is allowed and if the system remains economically viable.

For optimal utilization of the system, it is advantageous that the AC is requested as frequently as possible, but only during the day and not at night. Under such conditions, the system becomes more economically convenient.

With the successful achievement of the project goals, one of the compressors can be removed, as shown in Figures 4.22 and 4.27, to recover the cost of the pump. The mono-ethylene glycol (MEG) loop can also be eliminated, recouping the cost of the TES-AC system pipes. By removing the cooling coil and evaporator of the MEG circuit, the cost of the CO_2 evaporator in the AHU can also be recovered. However, the costs of the liquid separator and the CTES (including the PP-HX and container) are not recoverable.

Furthermore, the analysis does not consider the benefits of reducing the peak power demand. Decreasing the maximum peak power required by the supermarket directly influences the consumption tariff paid to the grid operator. Additionally, many grid operators offer larger customers a reduction in the consumption tariff if they can provide flexibility in power demand on short notice. Integrating CTES technology into refrigeration systems allows system owners to decouple refrigeration supply and demand, enabling adaptation to the future electricity market [62].

The calculated electricity cost savings are $8,67\%$ and $12,56\%$ considering the spot pricing system, and $11,6\%$ and $16,45\%$ considering the tariff pricing system, on the average and hottest day, respectively. Selvnes et al. (2023) [62] reported cost savings of $7,3\%$ in Oslo considering a tariff pricing system, but even greater results can be achieved by considering a warmer week, as they suggested. In their study, when considering the spot pricing system, the cost savings are found to be lower than 2%. This is primarily attributed to the in-

vestigated period, during which the electricity prices are not consistently lower during the night, as pointed out by them. Coccia et al. (2019) [65] analyzed a CTES for refrigeration demand in a CO_2 supermarket system in Genoa, Italy, revealing yearly electricity cost saving of $25,4\%$.

Implementing a smart control system based on price prediction and weather forecast can lead to even greater savings. With such an advanced control strategy, the system can optimize its charging operation by taking advantage of lower electricity prices during low temperature periods. This intelligent approach allows for reducing electricity expenses.

However, despite the potential for significant savings, the payback time might still be too long, especially in regions with a short AC season. The limited duration of AC demand affects the overall cost-effectiveness of the technology. The economic attractiveness of the system is heavily influenced by factors such as electricity price and peak power tax. Additionally, the length of the AC season plays a crucial role in determining the feasibility of the system as a cost-saving solution.

During the winter when the AC demand is non-existent, the CTES can be efficiently employed for refrigeration purposes. A proposed utilization for the winter period involves repurposing the system to refrigerate display cabinets for salad/vegetables or beverage cabinets that require a temperature of 7-8°C. By adapting the system to serve vegetables or beverage cabinets throughout the winter, its operational benefits extend beyond the traditional cooling season, making it a versatile and economically viable solution. This proposed approach ensures that the CTES remains active throughout the entire year, helping to optimize its usage and economic benefits.

Conclusions

6.1 Conclusions

In conclusion, this study presents a comprehensive analysis of the simulation results of the TES-AC system, divided into four main categories: charging mode, discharging mode, average day, and hottest day.

During the charging mode, the system performance was evaluated by varying the volume flow rate of the pump. It was observed that increasing the refrigerant flow rate reduced the charging time while increasing the average heat flow rate. The charging time exhibited a hyperbolic trend, while the average heat flow rate showed a logarithmic trend. The system successfully completed a full charge in one night (8 hours) with a refrigerant volume flow rate higher than $0,6\ m^3/h$, requiring a minimum average capacity of 30 kW. For partial charges, a lower refrigerant flow rate and capacity were sufficient. The CTES did not require a refrigerant volume flow rate higher than 1 m^3/h since a full charge in less than one night was not needed, and the excess compressors capacity was used to charge the storage.

The discharge process was evaluated under different AC loads and refrigerant volume flow rates. The CTES fully covers a requested load of 30 kW for 4 hours, 20 kW for 8 hours, and 10 kW for 22 hours, and for other more hours is able to partially cover the requested load. The discharge capacity decreases due to the thermal conductivity of the PCM and its non-uniform melting, resulting in incomplete condensation of the refrigerant.

The system performance during the average day demonstrated successful load shifting and peak shaving, efficiently covering the AC load demand and operating independently from the refrigeration system. On the hottest day, while the CTES was not able to fully cover the AC load after hours of operation, it still supplied around 60% of the required capacity. The system effectively shifted the load, allowing the refrigeration system to integrate the remaining

load.
Comparisons between the glycol and CTES systems highlighted the CTES benefits, achieving load shifting and peak shaving of the compressors power consumption. The CTES system resulted in reduced peak power absorption, up to $32,33\%$, and more linear electricity consumption. Moreover, energy savings, up to $11,84\%$, were achieved by producing and storing energy for AC demand during the night when the system performance was enhanced by lower outdoor temperatures.
The CTES system showed an electricity cost reduction under both the considered pricing systems, for both the average and hottest day. The economic advantage could be further improved when considering a smart control system based on price prediction and weather forecast.
While the CTES system presented promising results, the payback period remained a concern, particularly in regions with a short AC season. The economic attractiveness of the technology heavily relies on factors such as electricity pricing, peak power tax, and the length of the AC season.
To maximize the CTES system utilization and economic advantage, a proposed utilization for the winter involves repurposing the system for refrigerating salad/vegetables or beverage cabinets. By doing so, the CTES remains actively employed throughout the entire year, extending its operational benefits beyond the conventional cooling season and enhancing its overall cost-effectiveness.
In conclusion, the TES-AC system has shown considerable potential for load shifting, peak shaving, and energy savings. However, further investigation and optimization are required to address specific challenges and adapt the system to different climatic and pricing conditions. With continued research and advancements in smart control strategies, the CTES system could become a valuable and sustainable solution for energy-efficient refrigeration and air conditioning applications.

6.2 Future works

In order to further advance the understanding and applicability of the TES-AC system, several opportunities for future research and development have been identified:

- More realistic simulation: the current study provided valuable insights into the TES-AC system performance. However, the two Dymola models can be merged into a single one to obtain a single model more similar

to the reality. The complete model of the refrigeration system with the TES-AC system, as shown in Figure I.1 in Appendix I, serves as the foundation for such advanced investigations, but some parameters have to be tuned to avoid being in conflict with each other.

- Testing and comparison (summer 2024): experimental testing of the TES-AC system and monitoring its performance will be undertaken during the summer of 2024, to validate the simulation results and demonstrate its real-world performance. Testing the system under controlled conditions and comparing the results with the simulation data will ensure the accuracy and reliability of the developed models.
- Winter utilization: the proposed winter utilization of the CTES involves adapting the system to refrigerate display fridge cabinets that require a temperature of 7-8°C, such as those used for storing salad, vegetables, or beverages. This strategic application aims to extend the operational benefits of the system beyond the traditional AC season and maximize its economic advantages.
- Supermarket building performance simulation: to gather more precise and accurate results, it is essential to conduct a building performance simulation of the shop in exam, over the AC season. By doing so, it is possible to obtain a more accurate load curve and determine the exact number of hours with AC demand in a reference year. Simulating, during the overall AC season, the presented Dymola models with the obtained hourly AC load demand and the outdoor temperature, the number of hours for effective load shifting is evaluated, helping in the investigation of the system performance.
- Investigation in warmer climates: the TES-AC system performance in warmer climates, where AC demand may be more persistent and intense, should be carefully investigated. Conducting simulations and experiments in regions with higher average temperatures can reveal the system behavior under more challenging conditions. This investigation will shed light on the system adaptability and potential for widespread implementation in different climates.
- In-depth economic analysis: to assess the economic feasibility of the TES-AC system and return on investment, a comprehensive economic analysis is essential. The cost recovery by dismissing the existing MEG circuit has to be taken into account, as all the aspects related to the energy contract

of the considered supermarket. Different analyses aimed at evaluating the system cost-effectiveness, under various electricity pricing schemes, peak power tax rates, and seasonal AC demand patterns, will help in identifying the most economically advantageous scenarios and regions for the implementation of such a system.

By addressing these research directions, the TES-AC system can be further optimized, leading to increased energy efficiency, cost-effectiveness, and environmental sustainability. Moreover, the knowledge gained from these investigations will contribute to the advancement of thermal energy storage technologies and their integration with air conditioning and refrigeration systems, paving the way for a more sustainable and energy-efficient future.

References

[1] International Energy Agency. *The Future of Cooling*. 2018. URL: https://www.iea.org/reports/the-future-of-cooling.

[2] Á. Pardiñas Á., Contiero L., Hafner A., et al. *Attaining a higher flexibility degree in CO_2 compressor racks.* 14th IIR-Gustav Lorentzen Conference on Natural Refrigerants (GL2020). Proceedings. Kyoto, Japon, December 7-9th 2020. Dec. 7, 2020. DOI: 10.18462/iir.gl.2020.1123. URL: https://iifiir.org/en/fridoc/attaining-a-higher-flexibility-degree-in-co-lt-sub-gt-2-lt-sub-gt-compressor-racks-142984.

[3] Michal Haida, Krzysztof Banasiak, Jacek Smolka, et al. "Experimental analysis of the R744 vapour compression rack equipped with the multi-ejector expansion work recovery module". In: *International Journal of Refrigeration* 64 (Apr. 1, 2016), pp. 93–107. ISSN: 0140-7007. DOI: 10.1016/j.ijrefrig.2016.01.017. URL: https://www.sciencedirect.com/science/article/pii/S0140700716000232.

[4] Contiero L., Á. Pardiñas Á., and Hafner A. *Multi ejector and pivoting-supported R744 application with AC for supermarkets.* 9th IIR Conference on Ammonia and CO_2 Refrigeration Technologies. Proceedings: Ohrid, North Macedonia, 16-17 September, 2021. Sept. 16, 2021. DOI: 10.18462/iir.nh3-co2.2021.0019. URL: https://iifiir.org/en/fridoc/multi-ejector-and-pivoting-supported-r744-application-with-ac-for-144325.

[5] Á. Pardiñas Á., Fabris F., Contiero L., et al. *Ejector for the world: simplified ejector-supported CO_2 refrigeration systems for all climates.* 15th IIR-Gustav Lorentzen Conference on Natural Refrigerants (GL2022). Proceedings. Trondheim, Norway, June 13-15th 2022. June 13, 2022. DOI: 10.18462/iir.gl2022.0062. URL: https://iifiir.org/en/fridoc/ejector-for-the-world-simplified-ejector-supported-co-lt-sub-gt-2-lt-sub-gt-145324.

[6] Manescu R. I., Allouche Y., Larrañaga Janeiro A., et al. *Experimental investigation on the integration of cold energy storage into a R744 refrigeration system.* Proceedings of the 25th IIR International Congress of Refrigeration: Montréal , Canada, August 24-30, 2019. Aug. 24, 2019. DOI: 10.18462/iir.icr.2019.1861. URL: https://iifiir.org/en/fridoc/experimental-investigation-on-the-integration-of-cold-energy-storage-34897.

[7] Bernard Nagengast and ASHRAE. *Air Conditioning and Refrigeration Timeline.* 2020. URL: https://www.ashrae.org/about/mission-and-vision/ashrae-industry-history/air-conditioning-and-refrigeration-timeline.

[8] Mark O. McLinden and Marcia L. Huber. "(R)Evolution of Refrigerants". In: *Journal of Chemical & Engineering Data* 65.9 (2020), pp. 4176–4193. DOI: 10.1021/acs.jced.0c00338. URL: https://doi.org/10.1021/acs.jced.0c00338.

[9] Pinklesh Arora, Ajay Tyagi, and Geetha Seshadri. "Fourth Generation Refrigerant: HFO 1234 yf'. In: *Current science* 115 (Oct. 2018), p. 1497. DOI: 10.18520/cs/v115/i8/1497-1503. URL: https://www.researchgate.net/publication/328494214_Fourth_Generation_Refrigerant_HFO_1234_yf.

[10] T.J. Wallington, M. Andersen, and Ole Nielsen. "Atmospheric chemistry of short-chain haloolefins: Photochemical ozone creation potentials (POCPs), global warming potentials (GWPs), and ozone depletion potentials (ODPs)". In: *Chemosphere* 129 (2015), pp. 135–141. ISSN: 0045-6535. DOI: 10.1016/j.chemosphere.2014.06.092. URL: https://www.sciencedirect.com/science/article/pii/S0045653514008492.

[11] Gustav Lorentzen. "Revival of carbon dioxide as a refrigerant". In: *International Journal of Refrigeration* 17.5 (1994), pp. 292–301. ISSN: 0140-7007. DOI: https://doi.org/10.1016/0140-7007(94)90059-0. URL: https://www.sciencedirect.com/science/article/pii/0140700794900590.

[12] Ilana Koegelenberg. *World Guide to Transcritical CO_2 Refrigeration.* 2020. URL: https://issuu.com/shecco/docs/r744-guide.

[13] Michael Eckert, Michael Kauffeld, and Volker Siegismund. *Natural Refrigerants: Applications and Practical Guidelines.* VDE VERLAG, 2022.

[14] Danfoss. *Learn about CO_2 as a natural refrigerant*. URL: https://www.danfoss.com/en/about-danfoss/our-businesses/cooling/refrigerants-and-energy-efficiency/refrigerants-for-lowering-the-gwp/carbon-dioxide-co2/.

[15] Jørn Stene. "Residential CO2 heat pump system for combined space heating and hot water heating". In: *International Journal of Refrigeration* 28.8 (2005). CO2 as Working Fluid - Theory and Applications, pp. 1259–1265. ISSN: 0140-7007. DOI: https://doi.org/10.1016/j.ijrefrig.2005.07.006. URL: https://www.sciencedirect.com/science/article/pii/S0140700705001775.

[16] Ángel Á. Pardiñas, Håkon Selvnes, Krzysztof Banasiak, et al. "Next generation of ejector-supported R744 booster systems for commercial refrigeration at all climates". In: *International Journal of Refrigeration* 148 (2023), pp. 168–178. ISSN: 0140-7007. DOI: https://doi.org/10.1016/j.ijrefrig.2022.10.027. URL: https://www.sciencedirect.com/science/article/pii/S0140700722003966.

[17] Marco Azzolin, Gianluca Cattelan, Simone Dugaria, et al. "Integrated CO2 systems for supermarkets: Field measurements and assessment for alternative solutions in hot climate". In: *Applied Thermal Engineering* 187 (2021), p. 116560. ISSN: 1359-4311. DOI: https://doi.org/10.1016/j.applthermaleng.2021.116560. URL: https://www.sciencedirect.com/science/article/pii/S135943112100017X.

[18] Ángel Á. Pardiñas, Hanne Kauko, Mihir Mouchum Hazarika, et al. "Two-stage evaporator for R744 heat pumps using greywater as heat source". In: *Energy and Buildings* 289 (2023), p. 113047. ISSN: 0378-7788. DOI: https://doi.org/10.1016/j.enbuild.2023.113047. URL: https://www.sciencedirect.com/science/article/pii/S0378778823002773.

[19] Rodrigo Llopis, Laura Nebot-Andrés, Daniel Sánchez, et al. "Subcooling methods for CO2 refrigeration cycles: A review". In: *International Journal of Refrigeration* 93 (2018), pp. 85–107. ISSN: 0140-7007. DOI: https://doi.org/10.1016/j.ijrefrig.2018.06.010. URL: https://www.sciencedirect.com/science/article/pii/S0140700718302160.

[20] Jacek Smolka, Michal Palacz, Jakub Bodys, et al. "Performance comparison of fixed- and controllable-geometry ejectors in a CO2 refrigeration system". In: *International Journal of Refrigeration* 65 (2016), pp. 172–182. ISSN: 0140-7007. DOI: https://doi.org/10.1016/j.ijrefrig.

2016.01.025. URL: https://www.sciencedirect.com/science/article/pii/S0140700716000311.

[21] Armin Hafner, Sven Försterling, and Krzysztof Banasiak. "Multi-ejector concept for R-744 supermarket refrigeration". In: *International Journal of Refrigeration* 43 (2014), pp. 1–13. ISSN: 0140-7007. DOI: https://doi.org/10.1016/j.ijrefrig.2013.10.015. URL: https://www.sciencedirect.com/science/article/pii/S0140700714000668.

[22] Engin Söylemez, Armin Hafner, Christian Schlemminger, et al. "The Performance Analysis of an Integrated CO2 Refrigeration System with Multi-Ejectors Installed in a Supermarket". In: *Energies* 15.9 (2022). ISSN: 1996-1073. DOI: 10.3390/en15093142. URL: https://www.mdpi.com/1996-1073/15/9/3142.

[23] Ángel Á. Pardiñas, Michael Jokiel, Christian Schlemminger, et al. "Modeling of a CO_2-based integrated refrigeration system for supermarkets". In: *Energies* 14.21 (2021). DOI: 10.3390/en14216926. URL: https://ntnuopen.ntnu.no/ntnu-xmlui/handle/11250/2827505.

[24] Ali H. Abedin and Marc A. Rosen. "A Critical Review of Thermochemical Energy Storage Systems". In: *The Open Renewable Energy Journal* 4.1 (2011). URL: https://benthamopen.com/ABSTRACT/TOREJ-4-42.

[25] Håkon Selvnes, Yosr Allouche, Raluca Iolanda Manescu, et al. "Review on cold thermal energy storage applied to refrigeration systems using phase change materials". In: *Thermal Science and Engineering Progress* 22 (2021), p. 100807. ISSN: 2451-9049. DOI: https://doi.org/10.1016/j.tsep.2020.100807. URL: https://www.sciencedirect.com/science/article/pii/S2451904920303279.

[26] M. Alparslan Zehir and Mustafa Bagriyanik. "Demand Side Management by controlling refrigerators and its effects on consumers". In: *Energy Conversion and Management* 64 (2012). IREC 2011, The International Renewable Energy Congress, pp. 238–244. ISSN: 0196-8904. DOI: https://doi.org/10.1016/j.enconman.2012.05.012. URL: https://www.sciencedirect.com/science/article/pii/S019689041200218X.

[27] Mahmood Mastani Joybari, Fariborz Haghighat, Jeff Moffat, et al. "Heat and cold storage using phase change materials in domestic refrigeration systems: The state-of-the-art review". In: *Energy and Buildings* 106 (2015). SI: IEA-ECES Annex 31 Special Issue on Thermal Energy Storage, pp. 111–124. ISSN: 0378-7788. DOI: https://doi.org/10.1016/

j.enbuild.2015.06.016. URL: https://www.sciencedirect.com/science/article/pii/S0378778815300463.

[28] Jay Taneja, Ken Lutz, and David Culler. "Flexible loads in future energy networks". In: *Proceedings of the fourth international conference on Future energy systems*. 2013, pp. 285–286. DOI: 10.1145/2487166.2487209. URL: https://www.researchgate.net/publication/262395195_Flexible_loads_in_future_energy_networks.

[29] Jay Taneja, Ken Lutz, and David Culler. "The impact of flexible loads in increasingly renewable grids". In: *2013 IEEE International Conference on Smart Grid Communications (SmartGridComm)*. IEEE. 2013, pp. 265–270. URL: https://ieeexplore.ieee.org/document/6687968.

[30] T. Korth, F. Loistl, and C. Schweigler. "Novel integration of latent heat storage in multisplit air conditioning systems". In: *25th IIR International Congress of Refrigeration Proceedings, International Institute of Refrigeration*. 2019. URL: https://iifiir.org/fr/fridoc/integration-innovante-du-stockage-de-chaleur-latente-dans-un-systeme-de-34873.

[31] Håkon Selvnes, Yosr Allouche, Armin Hafner, et al. "Cold thermal energy storage for industrial CO2 refrigeration systems using phase change material: An experimental study". In: *Applied Thermal Engineering* 212 (2022), p. 118543. ISSN: 1359-4311. DOI: https://doi.org/10.1016/j.applthermaleng.2022.118543. URL: https://www.sciencedirect.com/science/article/pii/S135943112200494X.

[32] Tanathep Leungtongkum, Denis Flick, Hong Minh Hoang, et al. "Insulated box and refrigerated equipment with PCM for food preservation: State of the art". In: *Journal of Food Engineering* 317 (2022), p. 110874. ISSN: 0260-8774. DOI: 10.1016/j.jfoodeng.2021.110874. URL: https://www.sciencedirect.com/science/article/pii/S0260877421004003.

[33] B. Gin, M. M. Farid, and P. K. Bansal. "Effect of door opening and defrost cycle on a freezer with phase change panels". In: *Energy Conversion and Management* 51.12 (2010), pp. 2698–2706. ISSN: 0196-8904. DOI: 10.1016/j.enconman.2010.06.005. URL: https://www.sciencedirect.com/science/article/pii/S0196890410002153.

[34] Benjamin Gin and Mohammed M. Farid. "The use of PCM panels to improve storage condition of frozen food". In: *Journal of Food Engineering* 100.2 (2010), pp. 372–376. ISSN: 0260-8774. DOI: 10.1016/j.jfoodeng.2010.04.016. URL: https://www.sciencedirect.com/science/article/pii/S0260877410002013.

[35] Armin Ghodrati, Rahim Zahedi, and Abolfazl Ahmadi. "Analysis of cold thermal energy storage using phase change materials in freezers". In: *Journal of Energy Storage* 51 (2022), p. 104433. ISSN: 2352-152X. DOI: https://doi.org/10.1016/j.est.2022.104433. URL: https://www.sciencedirect.com/science/article/pii/S2352152X2200456X.

[36] R. Elarem, S. Mellouli, E. Abhilash, et al. "Performance analysis of a household refrigerator integrating a PCM heat exchanger". In: *Applied Thermal Engineering* 125 (2017), pp. 1320–1333. ISSN: 1359-4311. DOI: https://doi.org/10.1016/j.applthermaleng.2017.07.113. URL: https://www.sciencedirect.com/science/article/pii/S1359431117307895.

[37] Subhanjan Bista, Seyed Ehsan Hosseini, Evan Owens, et al. "Performance improvement and energy consumption reduction in refrigeration systems using phase change material (PCM)". In: *Applied Thermal Engineering* 142 (2018), pp. 723–735. ISSN: 1359-4311. DOI: 10.1016/j.applthermaleng.2018.07.068. URL: https://www.sciencedirect.com/science/article/pii/S1359431118322439.

[38] Shuang-Fei Li, Zhen-hua Liu, and Xue-Jiao Wang. "A comprehensive review on positive cold energy storage technologies and applications in air conditioning with phase change materials". In: *Applied Energy* 255 (2019), p. 113667. ISSN: 0306-2619. DOI: https://doi.org/10.1016/j.apenergy.2019.113667. URL: https://www.sciencedirect.com/science/article/pii/S0306261919313546.

[39] Guanghai Liu, Qingting Li, Junzhang Wu, et al. "Improving system performance of the refrigeration unit using phase change material (PCM) for transport refrigerated vehicles: An experimental investigation in South China". In: *Journal of Energy Storage* 51 (2022), p. 104435. ISSN: 2352-152X. DOI: https://doi.org/10.1016/j.est.2022.104435. URL: https://www.sciencedirect.com/science/article/pii/S2352152X22004583.

[40] Andrea Fragnito, Nicola Bianco, Marcello Iasiello, et al. "Experimental and numerical analysis of a phase change material-based shell-and-tube

heat exchanger for cold thermal energy storage". In: *Journal of Energy Storage* 56 (2022), p. 105975. ISSN: 2352-152X. DOI: https://doi.org/10.1016/j.est.2022.105975. URL: https://www.sciencedirect.com/science/article/pii/S2352152X22019636.

[41] Minghan Xu, Yuguo Gao, Fu Fang, et al. "Experimental and unified mathematical frameworks of water-ice phase change for cold thermal energy storage". In: *International Journal of Heat and Mass Transfer* 187 (2022), p. 122536. ISSN: 0017-9310. DOI: https://doi.org/10.1016/j.ijheatmasstransfer.2022.122536. URL: https://www.sciencedirect.com/science/article/pii/S0017931022000187.

[42] Håkon Selvnes, Yosr Allouche, and Armin Hafner. "Experimental characterisation of a cold thermal energy storage unit with a pillow-plate heat exchanger design". In: *Applied Thermal Engineering* 199 (2021), p. 117507. ISSN: 1359-4311. DOI: https://doi.org/10.1016/j.applthermaleng.2021.117507. URL: https://www.sciencedirect.com/science/article/pii/S135943112100939X.

[43] Sven Försterling, Håkon Selvnes, and Alexis Sevault. *Validation of a Modelica numerical model for pillow plate heat exchangers using phase change material*. IIR, 2022. ISBN: 978-2-36215-045-6. URL: https://sintef.brage.unit.no/sintef-xmlui/handle/11250/3029923.

[44] Lizhong Yang, Uver Villalobos, Bakytzhan Akhmetov, et al. "A comprehensive review on sub-zero temperature cold thermal energy storage materials, technologies, and applications: State of the art and recent developments". In: *Applied Energy* 288 (2021), p. 116555. ISSN: 0306-2619. DOI: https://doi.org/10.1016/j.apenergy.2021.116555. URL: https://www.sciencedirect.com/science/article/pii/S0306261921001033.

[45] Armin Hafner, Tom Ståle Nordtvedt, and Ingrid Rumpf. "Energy saving potential in freezing applications by applying cold thermal energy storage with solid carbon dioxide". In: *Procedia Food Science* 1 (2011). 11th International Congress on Engineering and Food (ICEF11), pp. 448–454. ISSN: 2211-601X. DOI: https://doi.org/10.1016/j.profoo.2011.09.069. URL: https://www.sciencedirect.com/science/article/pii/S2211601X11000708.

[46] Mahmood Mastani Joybari, Håkon Selvnes, Erling Vingelsgård, et al. "Parametric study of low-temperature thermal energy storage using car-

bon dioxide as the phase change material in pillow plate heat exchangers". In: *Applied Thermal Engineering* 221 (2023), p. 119796. ISSN: 1359-4311. DOI: https://doi.org/10.1016/j.applthermaleng.2022.119796. URL: https://www.sciencedirect.com/science/article/pii/S1359431122017264.

[47] T.R. Whiffen and S.B. Riffat. "A review of PCM technology for thermal energy storage in the built environment: Part I". In: *International Journal of Low-Carbon Technologies* 8.3 (May 2012), pp. 147–158. ISSN: 1748-1317. DOI: 10.1093/ijlct/cts021. eprint: https://academic.oup.com/ijlct/article-pdf/8/3/147/1948791/cts021.pdf. URL: https://doi.org/10.1093/ijlct/cts021.

[48] Harald Mehling and Luisa F Cabeza. "Heat and cold storage with PCM". In: *Heat and mass transfer* (2008), pp. 11–55. DOI: 10.1007/978-3-540-68557-9. URL: https://www.researchgate.net/publication/259267440_Heat_and_Cold_Storage_with_PCM_An_Up_to_Date_Introduction_Into_Basics_and_Applications.

[49] L. F. Cabeza. "3.07 - Thermal Energy Storage". In: *Comprehensive Renewable Energy*. Ed. by Ali Sayigh. Oxford: Elsevier, 2012, pp. 211–253. ISBN: 978-0-08-087873-7. DOI: 10.1016/B978-0-08-087872-0.00307-3. URL: https://www.sciencedirect.com/science/article/pii/B9780080878720003073.

[50] Belen Zalba, Jose Ma Marin, Luisa F Cabeza, et al. "Review on thermal energy storage with phase change: materials, heat transfer analysis and applications". In: *Applied thermal engineering* 23.3 (2003), pp. 251–283. DOI: https://doi.org/10.1016/S1359-4311(02)00192-8. URL: https://www.sciencedirect.com/science/article/abs/pii/S1359431102001928.

[51] Luisa F Cabeza, Ingrid Martorell, Laia Miró, et al. "Introduction to thermal energy storage systems". In: *Advances in Thermal Energy Storage Systems*. Elsevier, 2021, pp. 1–33. DOI: https://doi.org/10.1016/B978-0-12-819885-8.00001-2. URL: https://www.sciencedirect.com/science/article/abs/pii/B9780128198858000012.

[52] D. Zhou, C. Y. Zhao, and Y. Tian. "Review on thermal energy storage with phase change materials (PCMs) in building applications". In: *Applied Energy* 92 (2012), pp. 593–605. ISSN: 0306-2619. DOI: 10.1016/

j.apenergy.2011.08.025. URL: https://www.sciencedirect.com/science/article/pii/S0306261911005216.

[53] Yousef M.F. El Hasadi. "Numerical simulation of the melting process of nanostructured based colloidal suspensions phase change materials including the effect of the transport of the particles". In: *Journal of Molecular Liquids* 287 (2019), p. 110886. ISSN: 0167-7322. DOI: https://doi.org/10.1016/j.molliq.2019.110886. URL: https://www.sciencedirect.com/science/article/pii/S0167732218362470.

[54] W.Q. Li, Z.G. Qu, Y.L. He, et al. "Experimental and numerical studies on melting phase change heat transfer in open-cell metallic foams filled with paraffin". In: *Applied Thermal Engineering* 37 (2012), pp. 1–9. ISSN: 1359-4311. DOI: https://doi.org/10.1016/j.applthermaleng.2011.11.001. URL: https://www.sciencedirect.com/science/article/pii/S1359431111006181.

[55] C.Y. Zhao, W. Lu, and Y. Tian. "Heat transfer enhancement for thermal energy storage using metal foams embedded within phase change materials (PCMs)". In: *Solar Energy* 84.8 (2010), pp. 1402–1412. ISSN: 0038-092X. DOI: https://doi.org/10.1016/j.solener.2010.04.022. URL: https://www.sciencedirect.com/science/article/pii/S0038092X10001817.

[56] Zhirong Liao, Chao Xu, Yunxiu Ren, et al. "A novel effective thermal conductivity correlation of the PCM melting in spherical PCM encapsulation for the packed bed TES system". In: *Applied Thermal Engineering* 135 (2018), pp. 116–122. ISSN: 1359-4311. DOI: https://doi.org/10.1016/j.applthermaleng.2018.02.048. URL: https://www.sciencedirect.com/science/article/pii/S1359431117367741.

[57] John H. Lienhard IV and John H. Lienhard V. *A Heat Transfer Textbook, 5th edition*. Massachusetts Institute of Technology, 2020. URL: https://ahtt.mit.edu/.

[58] V. Gnielinski. "New equations for heat and mass transfer in turbulent pipe and channel flow". In: *Int. Chem. Eng* 16.2 (1976), pp. 359–368. URL: https://archive.org/details/sim_international-chemical-engineering_1976-04_16_2/mode/2up.

[59] Steiner D. and J. Taborek. "Flow Boiling Heat Transfer in Vertical Tubes Correlated by an Asymptotic Model". In: *Heat Transfer Engineering* 13.2

(1992), pp. 43–69. DOI: 10.1080/01457639208939774. URL: https://doi.org/10.1080/01457639208939774.

[60] Michael R. King, Stéphane Colin, Srinivas Garimella, et al. *Heat Transfer and Fluid Flow in Minichannels and Microchannels*. Butterworth-Heinemann, 2013.

[61] M. Piper, A. Olenberg, J.M. Tran, et al. "Determination of the geometric design parameters of pillow-plate heat exchangers". In: *Applied Thermal Engineering* 91 (2015), pp. 1168–1175. ISSN: 1359-4311. DOI: https://doi.org/10.1016/j.applthermaleng.2015.08.097. URL: https://www.sciencedirect.com/science/article/pii/S1359431115008947.

[62] Selvnes H., Á. Pardiñas Á., and Hafner A. *Cold thermal energy storage for air conditioning in a supermarket CO_2 booster refrigeration system.* 10th IIR Conference on Ammonia and CO_2 Refrigeration Technologies. Apr. 27, 2023. DOI: 10.18462/iir.nh3-co2.2023.0021. URL: https://iifiir.org/en/fridoc/cold-thermal-energy-storage-for-air-conditioning-in-a-supermarket-146984.

[63] Sevault A., Salgado-Beceiro J., and Pires Bjorgen K. O. *200-kWh latent heat storage unit using a pillow-plate heat exchanger: demonstration in an office building.* 15th IIR-Gustav Lorentzen Conference on Natural Refrigerants (GL2022). Proceedings. Trondheim, Norway, June 13-15th 2022. June 13, 2022. DOI: 10.18462/iir.gl2022.0063. URL: https://iifiir.org/en/fridoc/200-kwh-latent-heat-storage-unit-using-a-pillow-plate-heat-exchanger-145325.

[64] D'agaro P., Libralato M., Toffoletti G., et al. *Ice thermal energy storage for electricity peak shaving in a commercial refrigeration/HVAC unit.* 6th IIR Conference on Thermophysical Properties and Transfer Processes of Refrigerants. Sept. 1, 2021. DOI: 10.18462/iir.TPTPR.2021.2038. URL: https://iifiir.org/en/fridoc/ice-thermal-energy-storage-for-electricity-peak-shaving-in-a-144291.

[65] Coccia G., Arteconi A., D'agaro P., et al. *Demand side management of a commercial refrigeration system with cold thermal energy storage.* Proceedings of the 25th IIR International Congress of Refrigeration: Montréal , Canada. Aug. 24, 2019. DOI: 10.18462/iir.icr.2019.1088. URL: https://iifiir.org/en/fridoc/demand-side-management-of-a-commercial-refrigeration-system-with-cold-35179.

Appendix

List of appendices:

A - NKM2023 poster of the project

B - Cycle on the p-h diagram

C - Pressures in the different parts of the systems

D - Temperatures in the different parts of the systems

E - Frequencies of the MT compressors

F - Efficiencies of the MT compressors

G - Refrigerant temperature along the evaporator

H - Refrigerant heat transfer coefficient along the evaporator

I - Complete Dymola simulation model proposed as further work

A - NKM2023 poster of the project

Cold thermal energy storage for supermarket application

NTNU
Norwegian University of Science and Technology

Davide Tommasini
Student at Department of Energy and Process Engineering (EPT), NTNU, 7491 Trondheim

Background

There is a large transition in supermarket refrigeration with a strong focus on reducing the energy demand and the installation cost. Highly efficient system configurations with R744 are introduced in various locations throughout Europe; however, further improvements are necessary and possible, for example with the use of ejector-based expansion work recovery, pivoting compressor arrangements, and the implementation of local cold thermal energy storages (CTES), etc.

The implementation of local cold thermal energy storages in combination with the R744 refrigeration system can have economic benefits which enables an implementation in the market. CTES devices reduce the peak load demand and allow for load shifting to periods with: low electricity cost, high electricity production with renewables (e.g. PV panels), free cooling capacity from the rack. These units can also lead to a radical downsizing of the compressor packs and make it possible to remove the frequency controlling device of the MT compressors.

Project

The project consists in an integration of a PCM-CTES (Cold Thermal Energy Storage with Phase Change Material) into an existing refrigeration system of a REMA 1000 supermarket, which purpose is to provide the cooling required by the AHU (Air Handling Unit) for the AC (Air Conditioning).
The work will inlude:

- Operation and implementation architectures for the CTES
- Apply a simulation model representing supermarket units
- Investigation of various strategies for peak shavings, constant compressor power operation and load/demand adaption via active CTES units
- Evaluation of investment costs and how the implementation of CTES within the display cabinets will affect it
- Data processing and analysis of the modelling and experimental results

The existing refrigeration system, installed in REMA 1000 supermarket, is a booster CO_2 system able to provide air conditioning through a glicole-base loop (figure 1).

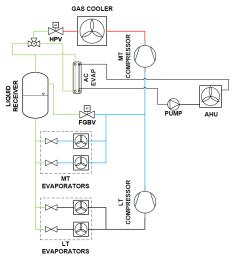

Figure 1: P&ID of the actual refrigeration system in REMA 1000 supermarkets

The PCM used is water, thus the energy will be stored and provided using the latent heat of a source at 0°C. The heat exchange is obtained through a pillow plate heat exchanger submerged in the water.
A liquid separator is installed, in that way it is possible to use a pump to make the refrigerant flow inside the circuit (figure 3).
Three valves connects the liquid separator to the main refrigeration circuit (figure 3): one valve has to maintain the level inside the separator to guarantee that inside the circuit there is always liquid; an other one controls the pressure inside the circuit releasing the refrigerant vapor to the main refrigeration circuit; a third valve is required to guarantee the oil return.

The system is able to work in three different modes by changing the position of the valves: charging, discharging or direct AC.

CHARGING
The system charges the CTES during the night or when the MT compressor is working at partial load. The refrigerant evaporates inside the pillow plate heat exchanger of the CTES, freezing the water. To achieve the greater cooling capacity, the lowest temperature is required, and so the lowest achievable pressure. Thus the system works at the MT pressure (T_{evap}≈-7°C; p≈29 bar).

DISCHARGING
Whenever the cooling is needed, the CTES is discharged (figure 2): the refrigerant evaporates into the AHU and recondenses into the CTES. The working pressure is the one of the liquid receiver of the main refrigerant circuit (T_{evap}≈5°C; p≈40 bar) to avoid frost formation on the cooling coil of the AHU and to guarantee a good heat exchange between the CO_2 and the PCM.

DIRECT AC
The direct AC mode is governed by a valve that by-pass the CTES when it is fully discharged.

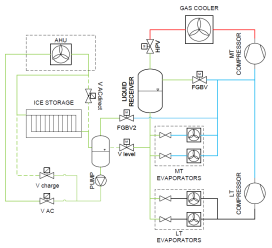

Figure 2: P&ID of the overall system in discharging mode

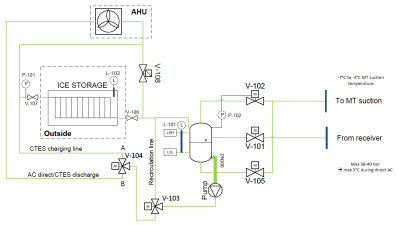

Figure 3: Detailed P&ID of the CTES system providing cooling for AC

About me

- 23 y.o. student from Italy
- February-July 2023: Exchange student at NTNU, Trondheim
- 2021-2023: Master's degree in Energy Engineering at the University of Padua
- 2018-2021: Bachelor's degree in Energy Engineering at the University of Padua

My LinkedIn profile:

- E-mail: davidetom99@gmail.com
- Phone: +39 3317354302

Norsk Kjøleteknisk Forening

NTNU

Figure A.1: Poster presented at the Norsk Kjøleteknisk Møte 2023 conference (NKM2023) held in Trondheim on May 23th-24th

B - Cycle on the p-h diagram

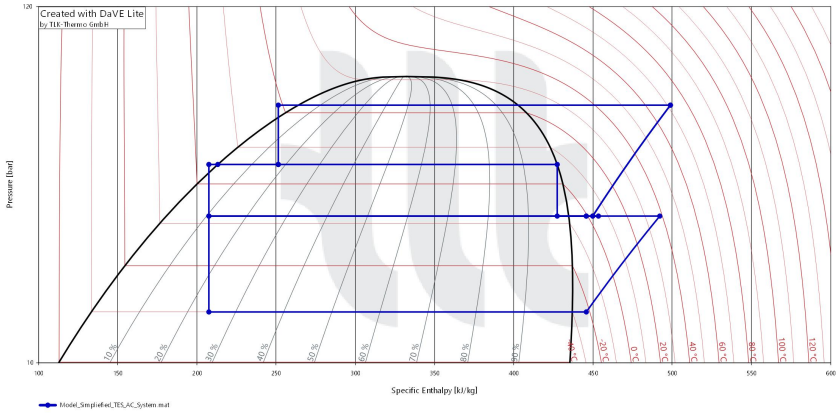

(a) R744 booster cycle in subcritical operation

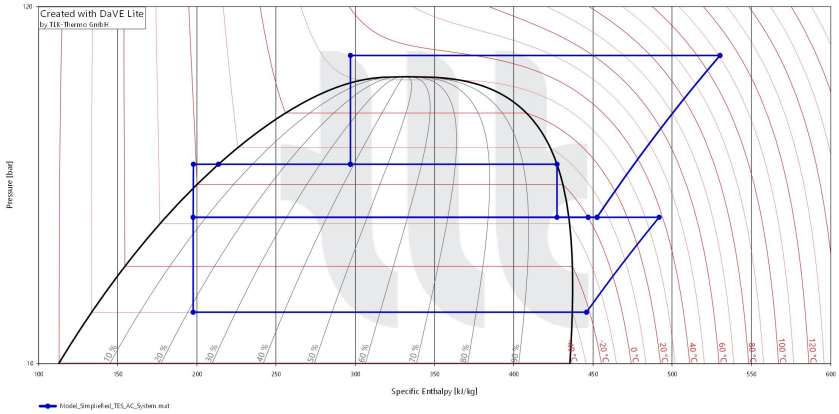

(b) R744 booster cycle in transcritical operation

Figure B.1: R744 booster cycle in subcritical and transcritical operations, obtained by Dymola simulation and plotted with DaVE Lite [1] (TLK-Thermo GmbH, Braunschweig, Germany)

[1] `https://www.tlk-thermo.com/index.php/en/dave`

C - Pressures in the different parts of the systems

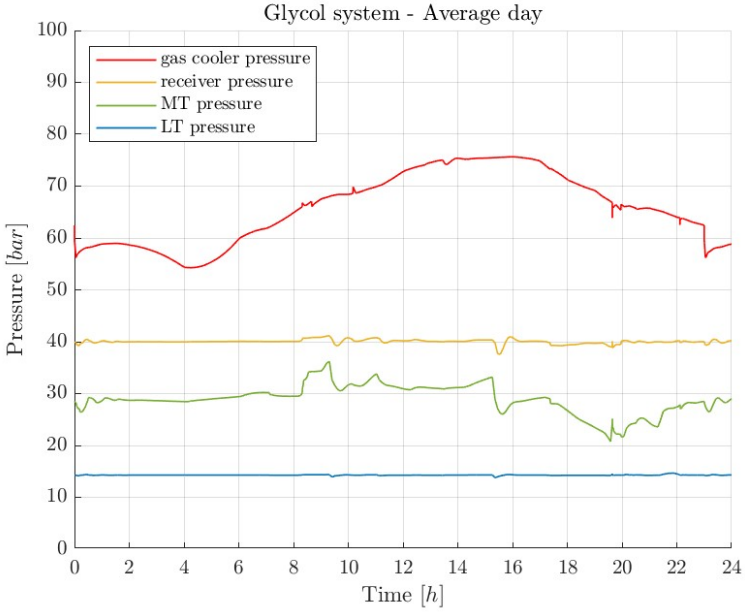

(a) Pressures in the glycol system during the average day

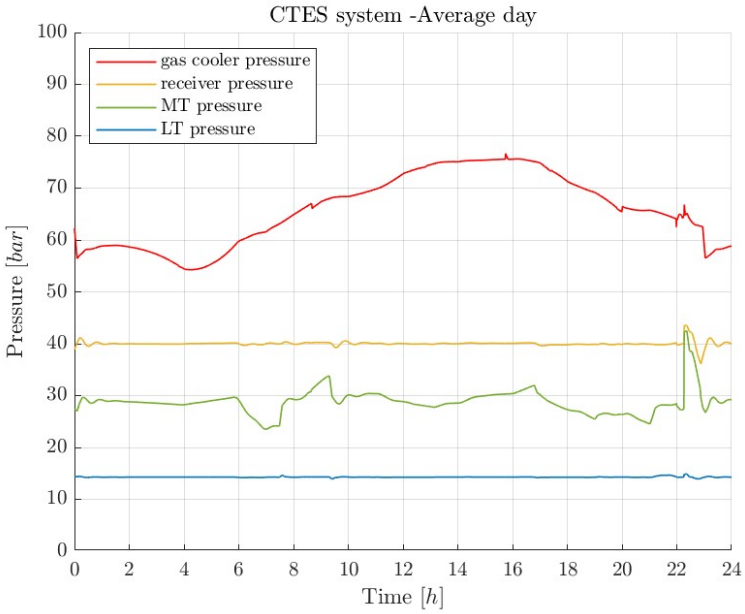

(b) Pressures in the CTES system during the average day

Figure C.1: Pressures in both the CTES and glycol systems during the average and hottest day

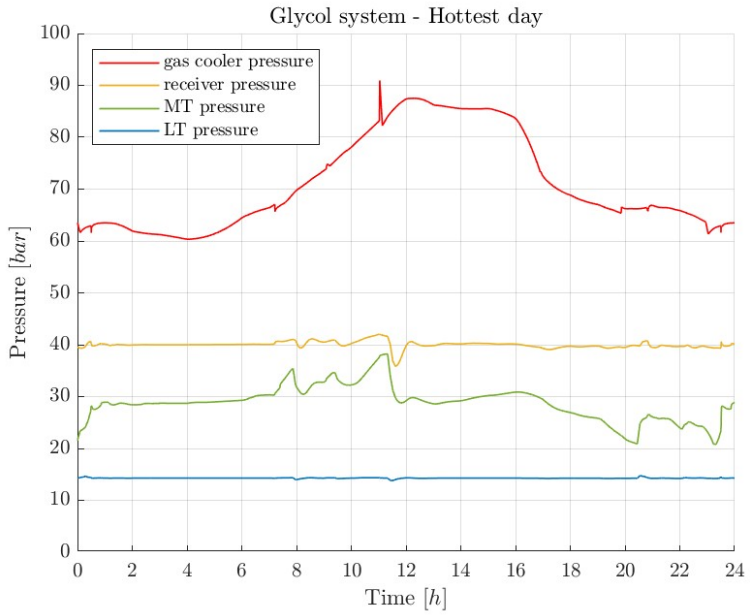

(c) Pressures in the glycol system during the hottest day

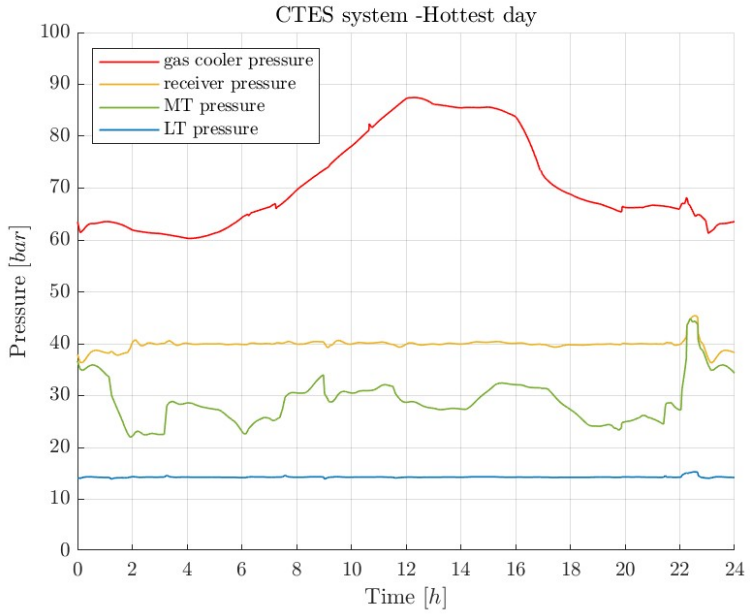

(d) Pressures in the CTES system during the hottest day

Figure C.1: Pressures in both the CTES and glycol systems during the average and hottest day

D - Temperatures in the different parts of the systems

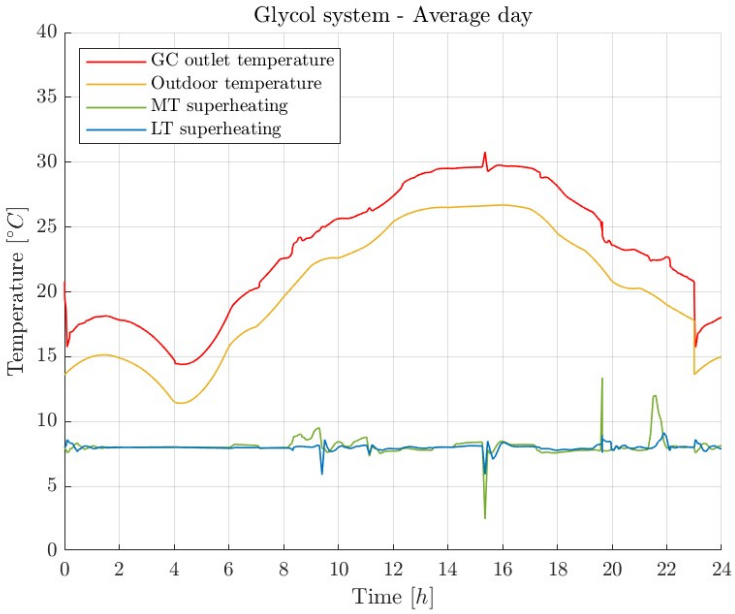

(a) Temperatures in the glycol system during the average day

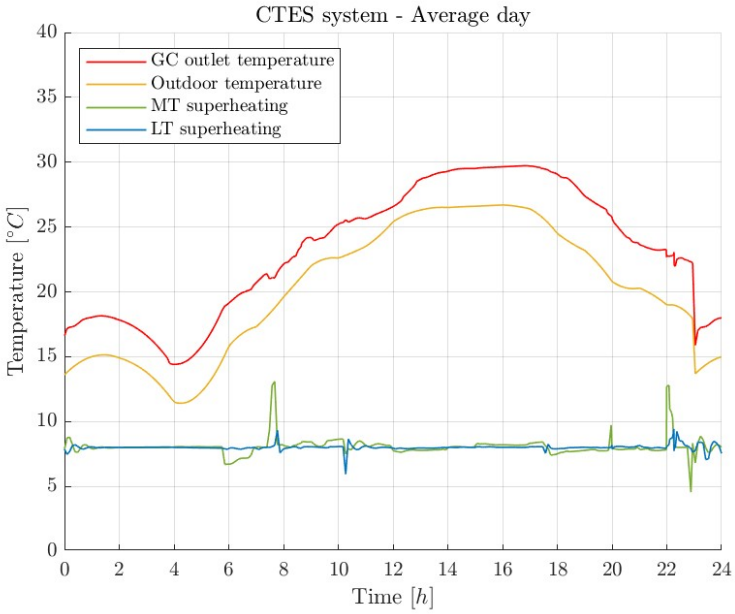

(b) Temperatures in the CTES system during the average day

Figure D.1: Temperatures in both the CTES and glycol systems during the average and hottest day

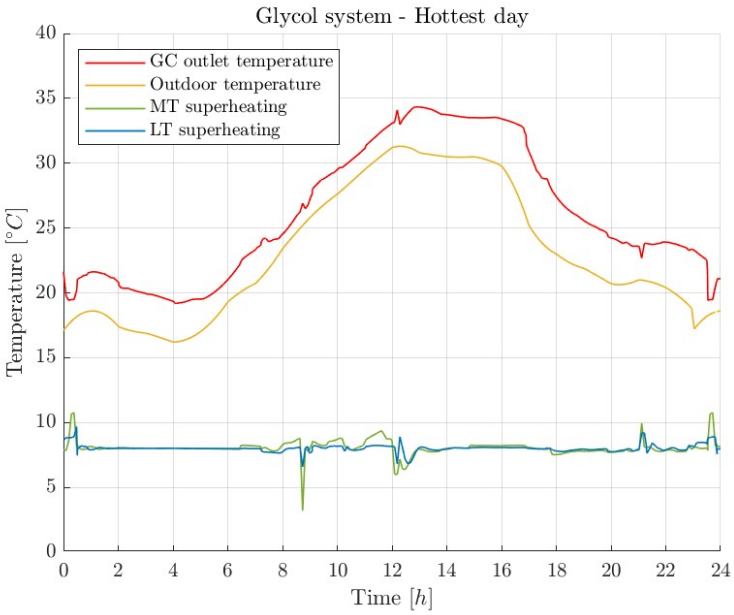

(c) Temperatures in the glycol system during the hottest day

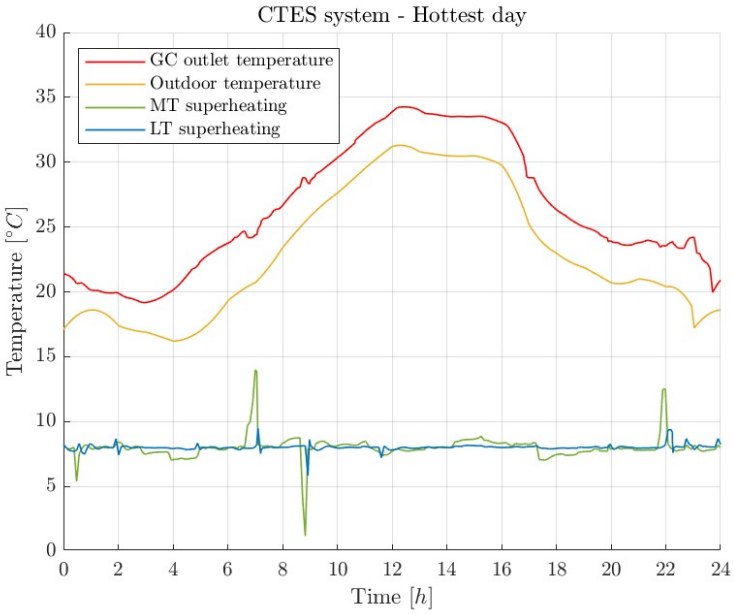

(d) Temperatures in the CTES system during the hottest day

Figure D.1: Temperatures in both the CTES and glycol systems during the average and hottest day

E - Frequencies of the MT compressors

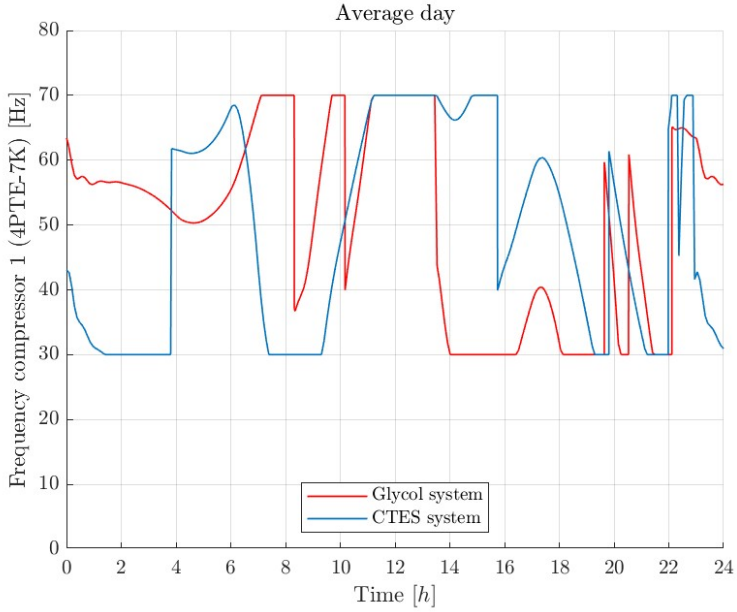

(a) Frequency of the compressor n. 1 (4PTE-7K) during the average day

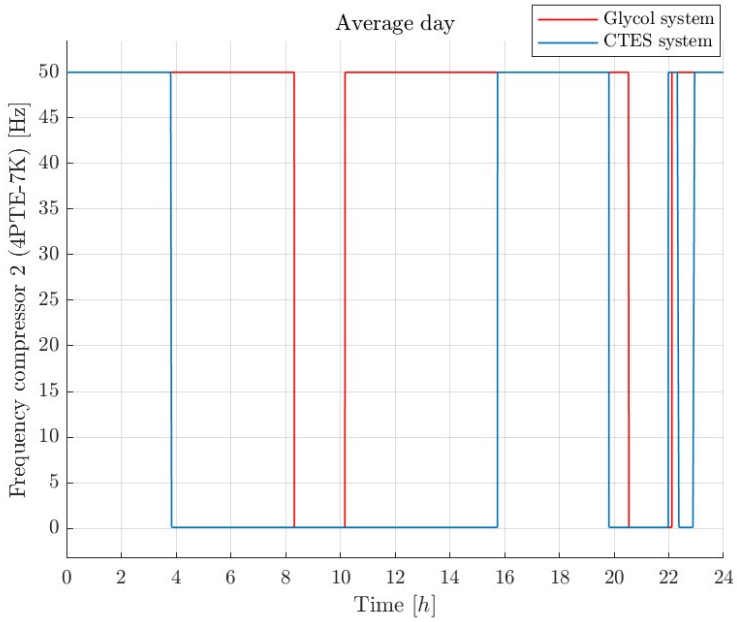

(b) Frequency of the compressor n. 2 (4PTE-7K) during the average day

Figure E.1: Frequencies of all the MT compressors during the average day

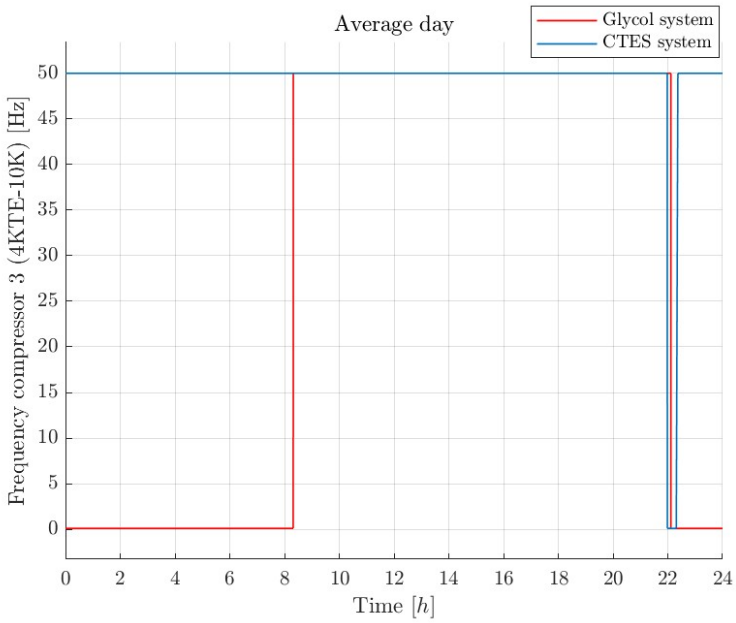

(c) Frequency of the compressor n. 3 (4KTE-10K) during the average day

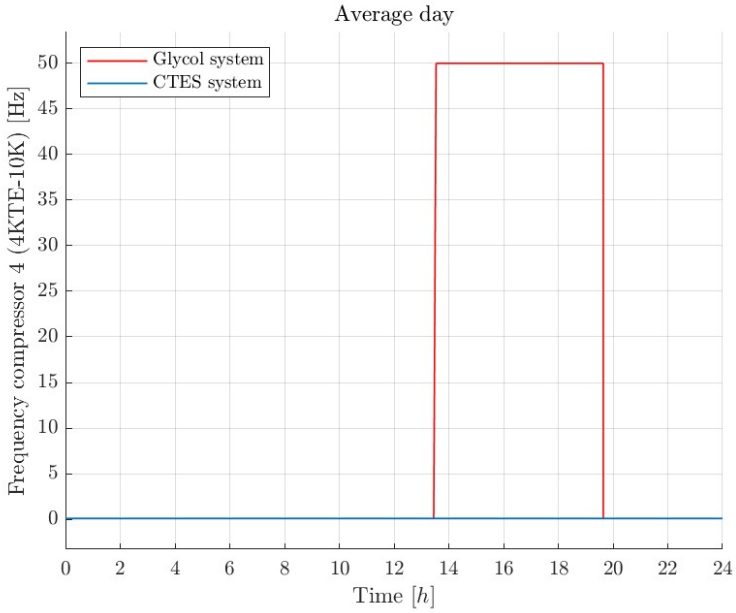

(d) Frequency of the compressor n. 4 (4KTE-10K) during the average day

Figure E.1: Frequencies of all the MT compressors during the average day

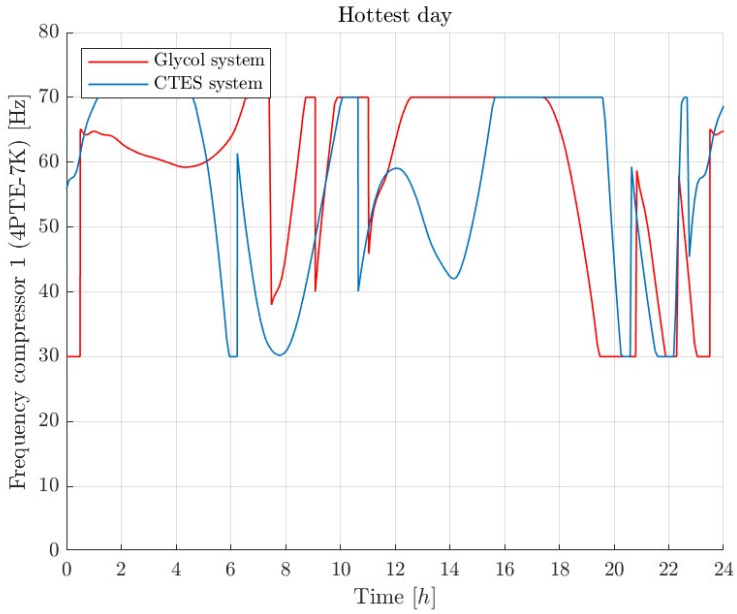

(a) Frequency of the compressor n. 1 (4PTE-7K) during the hottest day

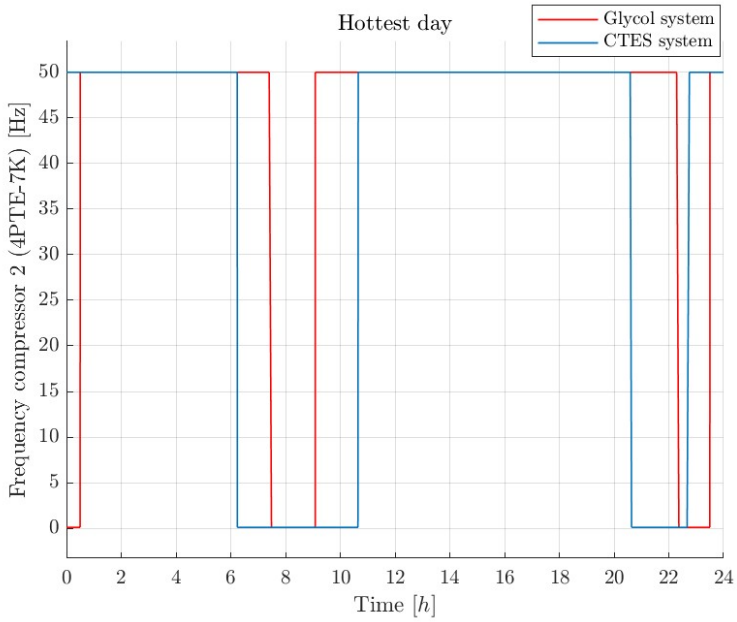

(b) Frequency of the compressor n. 2 (4PTE-7K) during the hottest day

Figure E.2: Frequencies of all the MT compressors during the hottest day

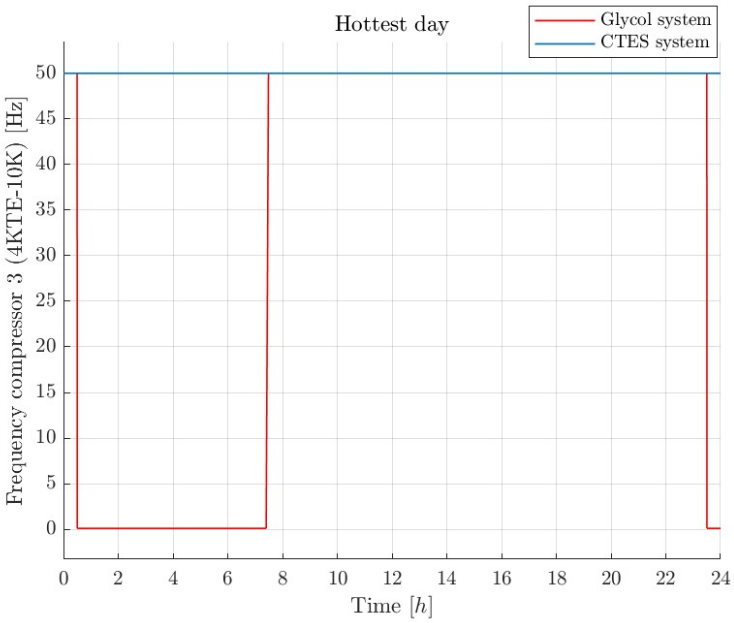

(c) Frequency of the compressor n. 3 (4KTE-10K) during the hottest day

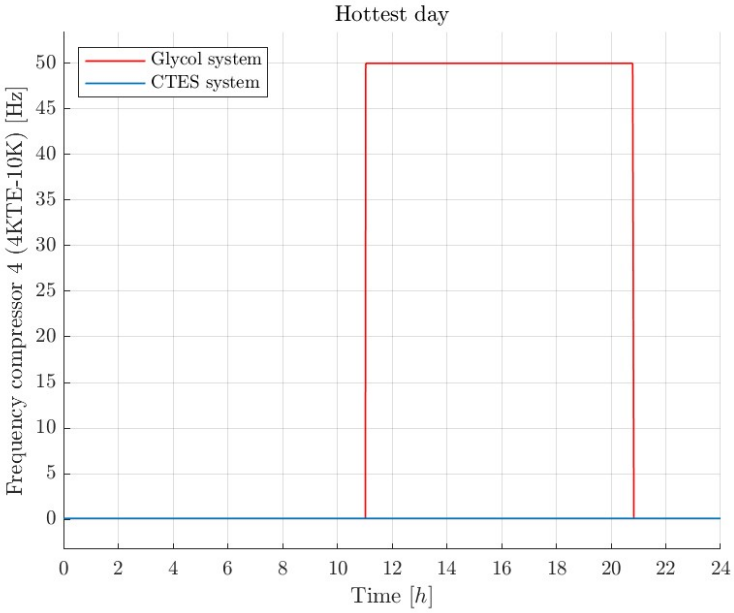

(d) Frequency of the compressor n. 4 (4KTE-10K) during the hottest day

Figure E.2: Frequencies of all the MT compressors during the hottest day

F - Efficiencies of the MT compressors

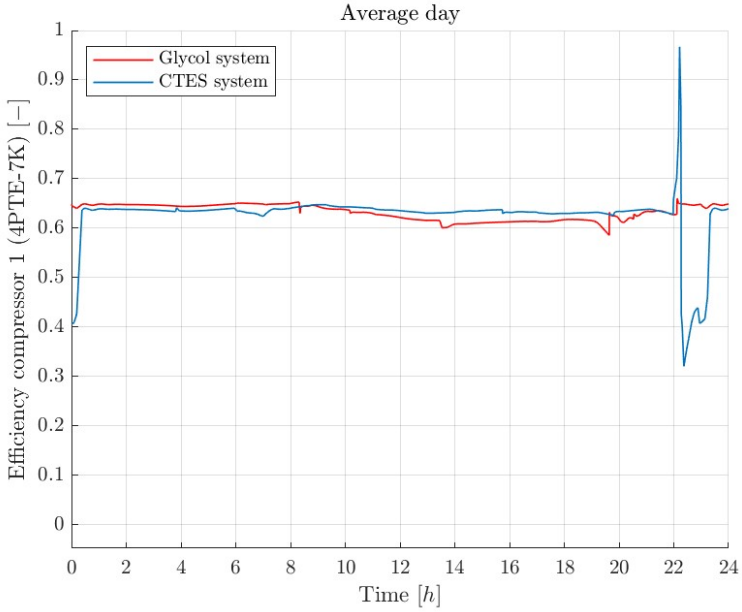

(a) Efficiency of the compressor n. 1 (4PTE-7K) during the average day

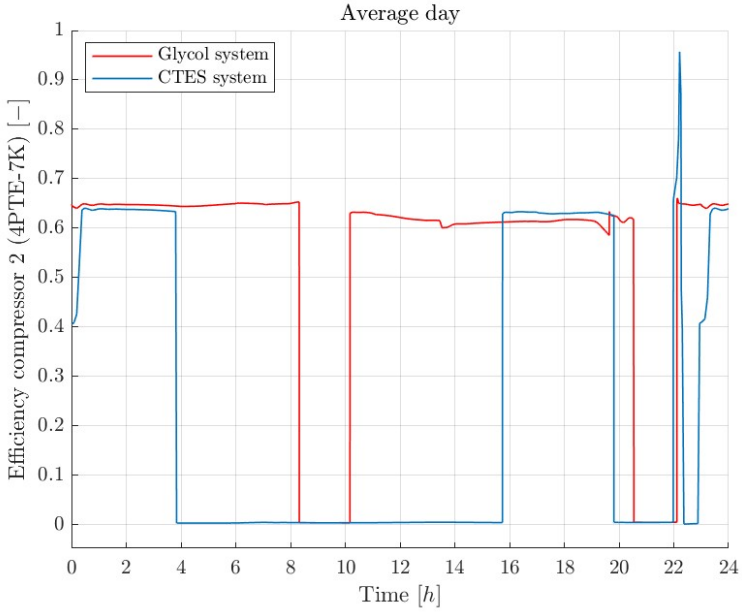

(b) Efficiency of the compressor n. 2 (4PTE-7K) during the average day

Figure F.1: Efficiencies of all the MT compressors during the average day

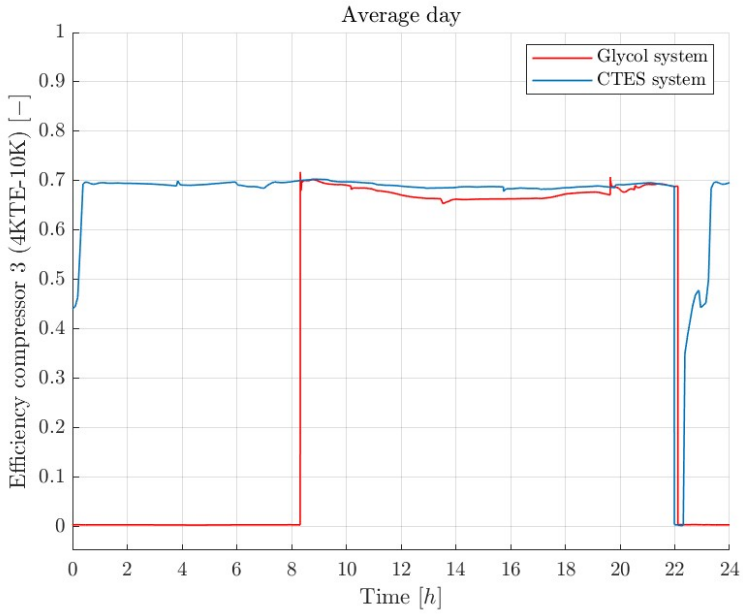

(c) Efficiency of the compressor n. 3 (4KTE-10K) during the average day

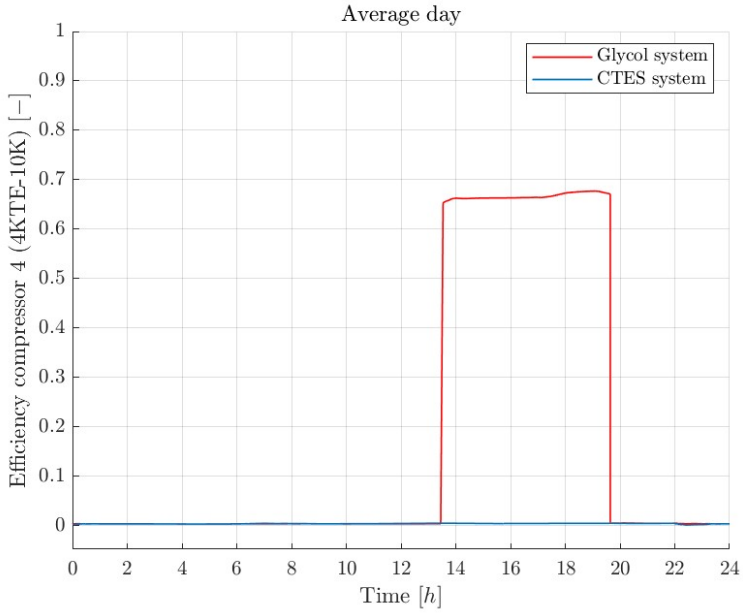

(d) Efficiency of the compressor n. 4 (4KTE-10K) during the average day

Figure F.1: Efficiencies of all the MT compressors during the average day

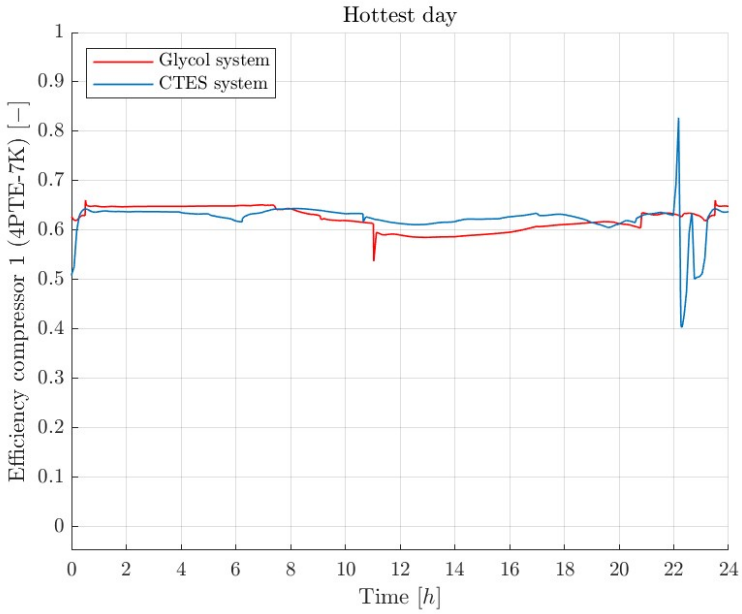

(a) Efficiency of the compressor n. 1 (4PTE-7K) during the hottest day

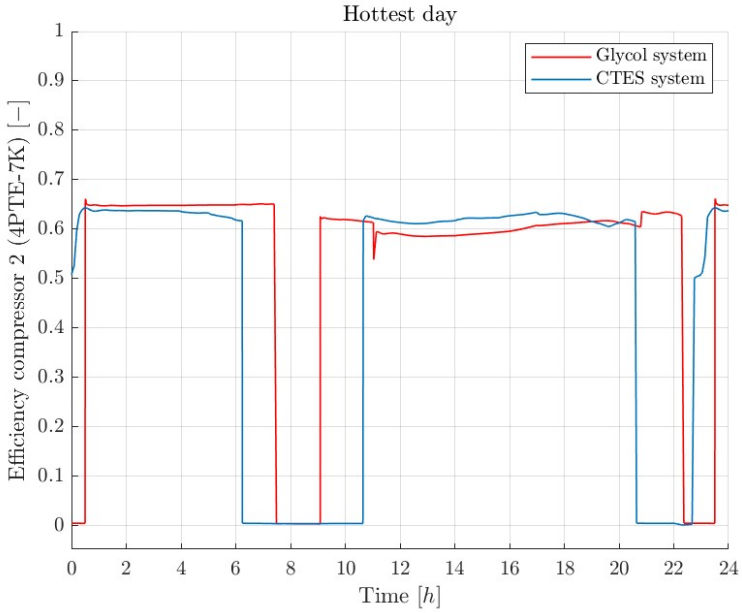

(b) Efficiency of the compressor n. 2 (4PTE-7K) during the hottest day

Figure F.2: Efficiencies of all the MT compressors during the hottest day

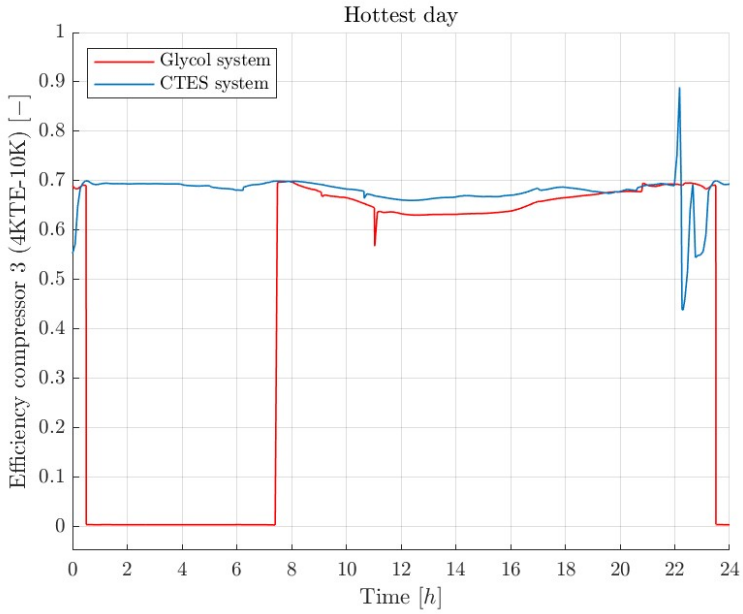

(c) Efficiency of the compressor n. 3 (4KTE-10K) during the hottest day

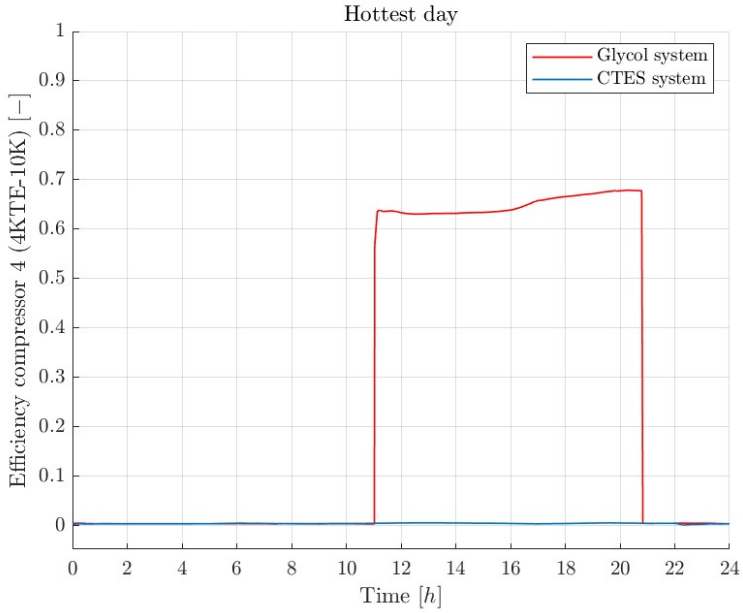

(d) Efficiency of the compressor n. 4 (4KTE-10K) during the hottest day

Figure F.2: Efficiencies of all the MT compressors during the hottest day

G - Refrigerant temperature along the evaporator

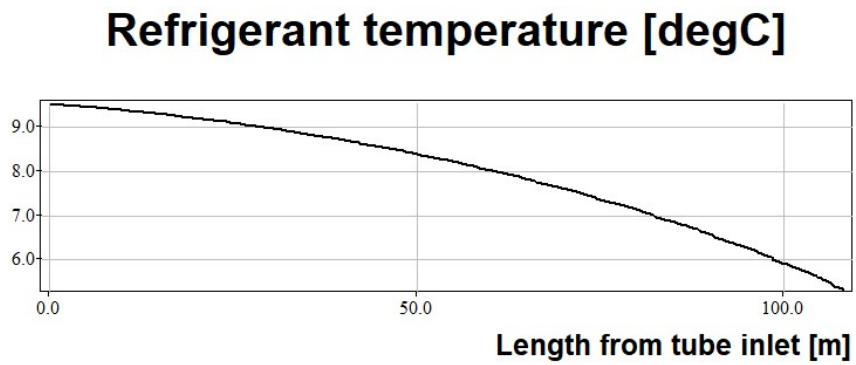

(a) Configuration 2R-1C: refrigerant temperature along the evaporator

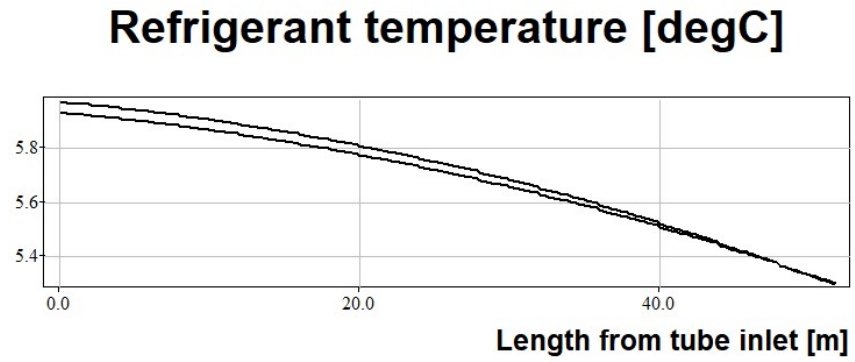

(b) Configuration 2R-2C: refrigerant temperature along the evaporator

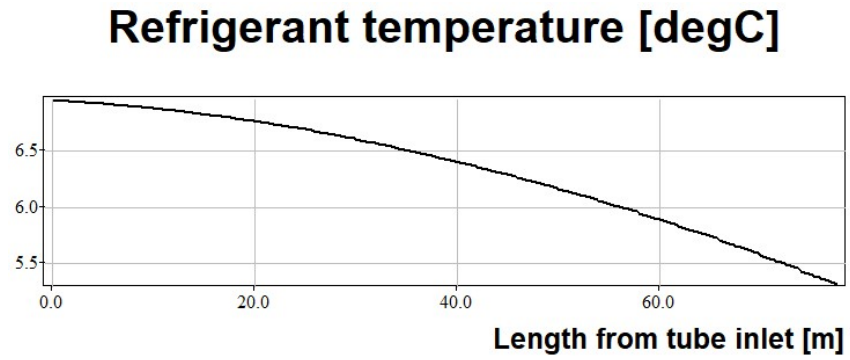

(c) Configuration 3R-2C: refrigerant temperature along the evaporator

Figure G.1: Refrigerant temperature along the evaporator of the different investigated configurations

H - Refrigerant heat transfer coefficient along the evaporator

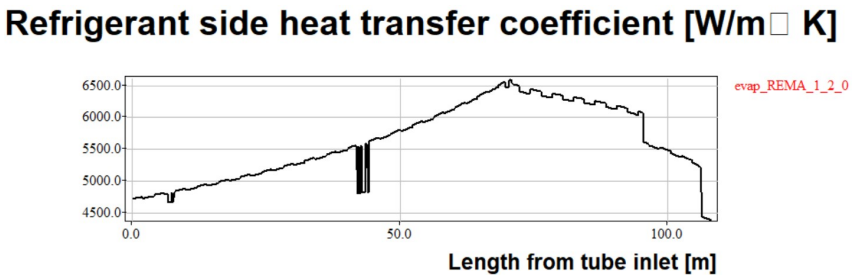

(a) Configuration 2R-1C: refrigerant heat transfer coefficient along the evaporator

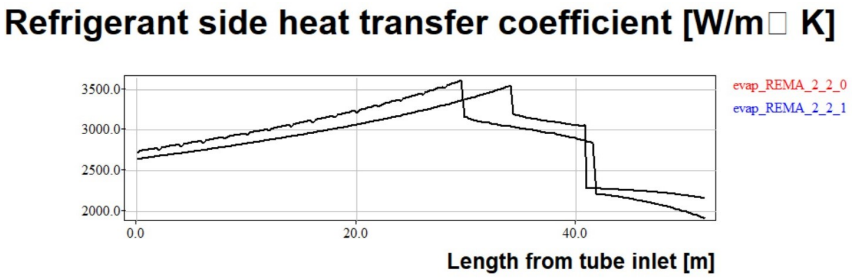

(b) Configuration 2R-2C: refrigerant heat transfer coefficient along the evaporator

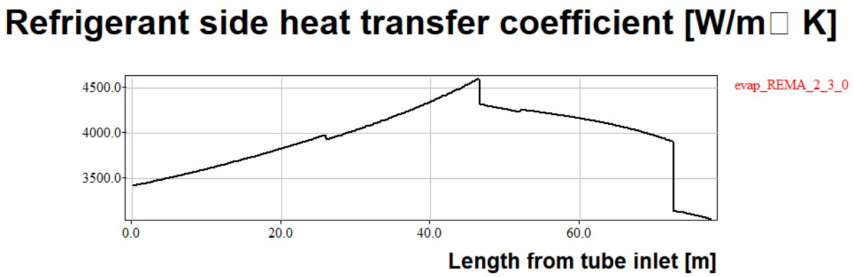

(c) Configuration 3R-2C: refrigerant heat transfer coefficient along the evaporator

Figure H.1: Refrigerant heat transfer coefficient along the evaporator of the different investigated configurations

I - Complete Dymola simulation model proposed as further work

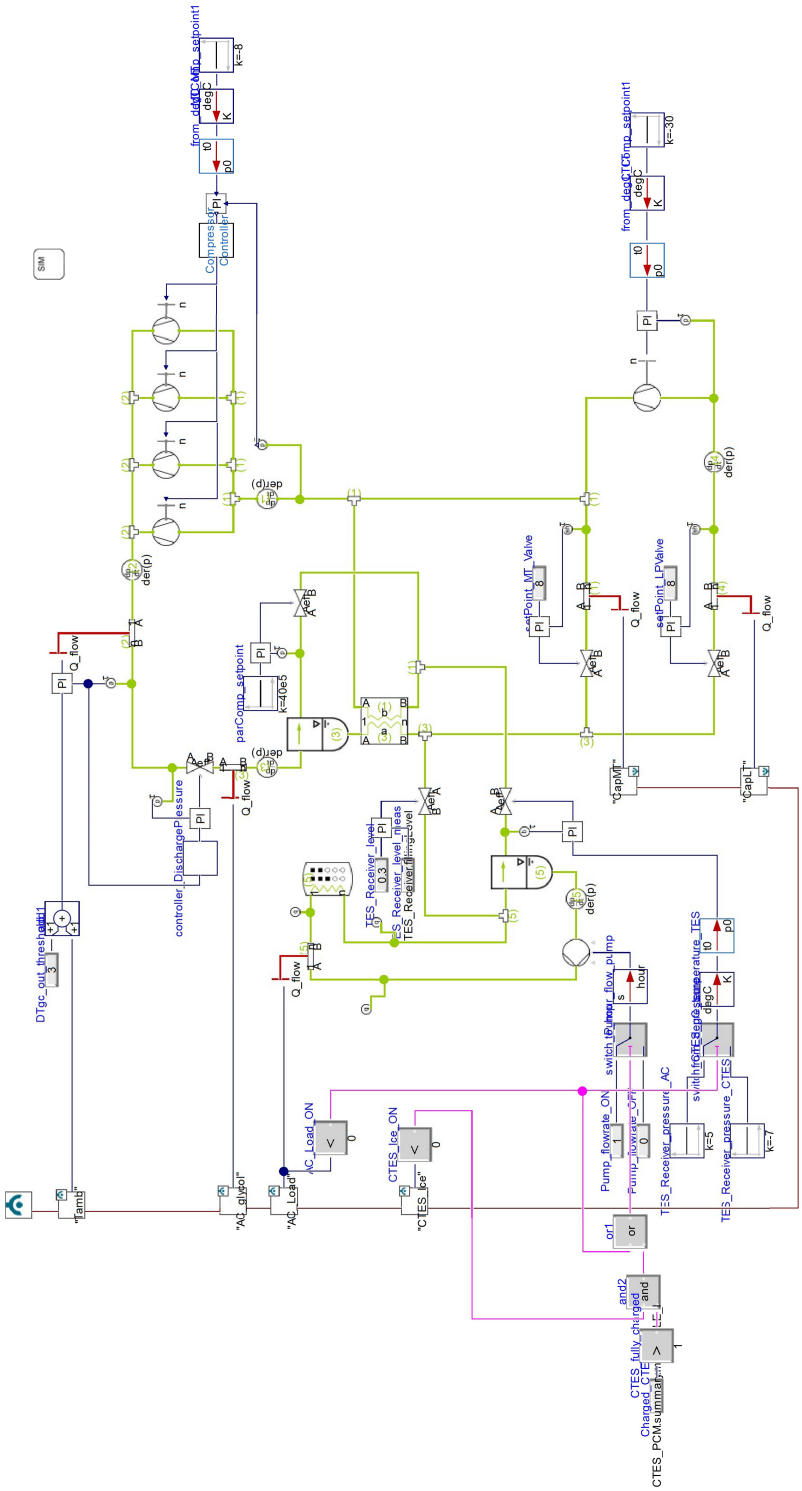

Figure I.1: Complete Dymola simulation model proposed as further work, obtained by merging the two simulation models presented in the thesis